

## 6.0 STRUCTURAL/SEISMIC CONSIDERATIONS

### 6.1 Introduction

This section considers the structural adequacy of the new Spent Fuel Pool (SFP) maximum density spent fuel racks under all loadings postulated for normal, seismic, and accident conditions at the Virgil C. Summer Nuclear Station (VCSNS). The module layout is illustrated in Figure 1.1.1, along with the X and Y coordinate axes used to identify displacement orientation.

The analyses undertaken to confirm the structural integrity of the racks, are performed in compliance with the USNRC Standard Review Plan [6.1.1] and the OT Position Paper [6.1.2]. An abstract of the methodology, modeling assumptions, key results, and summary of the parametric evaluation is presented. Delineation of the relevant criteria is discussed in the text associated with each analysis.

### 6.2 Overview of Rack Structural Analysis Methodology

The response of a free-standing rack module to seismic inputs is highly nonlinear and involves a complex combination of motions (sliding, rocking, twisting, and turning), resulting in potential impacts and friction effects. Some of the unique attributes of the rack dynamic behavior include a large fraction of the total structural mass in a confined rattling motion, friction support of rack pedestals against lateral motion, and large fluid coupling effects due to deep submergence and independent motion of closely spaced adjacent structures.

Linear methods, such as modal analysis and response spectrum techniques, cannot accurately simulate the structural response of such a highly nonlinear structure to seismic excitation. An accurate simulation is obtained only by direct integration of the nonlinear equations of motion with the three pool slab acceleration time-histories applied as the forcing functions acting simultaneously.

Whole Pool Multi-Rack (WPMR) analysis is the vehicle utilized in this project to simulate the dynamic behavior of the complex storage rack structures. The following sections provide the basis for this selection and discussion on the development of the methodology.

### 6.2.1 Background of Analysis Methodology

Reliable assessment of the stress field and kinematic behavior of the rack modules calls for a conservative dynamic model incorporating all *key attributes* of the actual structure. This means that the model must feature the ability to execute the concurrent motion forms compatible with the free-standing installation of the modules.

The model must possess the capability to effect momentum transfers which occur due to rattling of fuel assemblies inside storage cells and the capability to simulate lift-off and subsequent impact of support pedestals with the pool liner (or bearing pad). The contribution of the water mass in the interstitial spaces around the rack modules and within the storage cells must be modeled in an accurate manner, since erring in quantification of fluid coupling on either side of the actual value is no guarantee of conservatism.

The Coulomb friction coefficient at the pedestal-to-pool liner (or bearing pad) interface may lie in a rather wide range and a conservative value of friction cannot be prescribed *a priori*. In fact, a perusal of results of rack dynamic analyses in numerous docket (Table 6.2.1) indicates that an upper bound value of the coefficient of friction often maximizes the computed rack displacements as well as the equivalent elastostatic stresses.

In short, there are a large number of parameters with potential influence on the rack kinematics. The comprehensive structural evaluation must deal with all of these without sacrificing conservatism.

The three-dimensional single rack dynamic model introduced by Holtec International in the Enrico Fermi Unit 2 rack project (ca. 1980) and used in some 50 rerack projects since that time (Table 6.2.1) addresses most of the abovementioned array of parameters. The details of this methodology are also published in the permanent literature [6.2.1]. Despite the versatility of the 3-D seismic model, the accuracy of the single rack simulations has been suspect due to one key element; namely, hydrodynamic participation of water around the racks. During dynamic rack motion, hydraulic energy is either drawn from or added to the moving rack, modifying its submerged motion in a significant manner. Therefore, the dynamics of one rack affects the motion of all others in the pool.

A dynamic simulation, which treats only one rack, or a small grouping of racks, is intrinsically inadequate to predict the motion of rack modules with any quantifiable level of accuracy. Three-dimensional Whole Pool Multi-Rack analyses carried out on several previous plants demonstrate that single rack simulations may under predict rack displacement during seismic responses [6.2.2].

Briefly, the 3-D rack model dynamic simulation, involving one or more spent fuel racks, handles the array of variables as follows:

Interface Coefficient of Friction Parametric runs are made with upper bound and lower bound values of the coefficient of friction. The limiting values are based on experimental data which have been found to be bounded by the values 0.2 and 0.8. Simulations are also performed with the array of pedestals having randomly chosen coefficients of friction in a Gaussian distribution with a mean of 0.5 and lower and upper limits of 0.2 and 0.8, respectively. In the fuel rack simulations, the Coulomb friction interface between rack support pedestal and liner is simulated by piecewise linear (friction) elements. These elements function only when the pedestal is physically in contact with the pool liner or bearing pad.

Rack Beam Behavior Rack elasticity, relative to the rack base, is included in the model by introducing linear springs to represent the elastic bending action, twisting, and extensions.

Impact Phenomena Compression-only gap elements are used to provide for opening and closing of interfaces such as the pedestal-to-bearing pad interface, and the fuel assembly-to-cell wall interface. These interface gaps are modeled using nonlinear spring elements. The term "nonlinear spring" is a generic term used to denote the mathematical representation of the condition where a restoring force is not linearly proportional to displacement.

Fuel Loading Scenarios The fuel assemblies are conservatively assumed to rattle in unison which exaggerates the contribution of impact against the cell wall.

Fluid Coupling Holtec International extended Fritz's classical two-body fluid coupling model to multiple bodies and utilized it to perform the first two-dimensional multi-rack analysis (Diablo Canyon, ca. 1987). Subsequently, laboratory experiments were conducted to validate the multi-rack fluid

coupling theory. This technology was incorporated in the computer code DYNARACK [6.2.4] which handles simultaneous simulation of all racks in the pool as a Whole Pool Multi-Rack 3-D analysis. This development was first utilized in Chinshan, Oyster Creek, and Shearon Harris plants [6.2.1, 6.2.3] and, subsequently, in numerous other rerack projects. The WPMR analyses have corroborated the accuracy of the single rack 3-D solutions in predicting the maximum structural stresses, and also serve to improve predictions of rack kinematics.

For closely spaced racks, demonstration of kinematic compliance is verified by including all modules in one comprehensive simulation using a WPMR model. Additional more conservative single rack analyses are performed to confirm kinematic stability under the most adverse conditions such as fuel loading eccentricities and interim reracking configurations. In WPMR analysis, all rack modules are modeled simultaneously and the coupling effect due to this multi-body motion is included in the analysis. Due to the superiority of this technique in predicting the dynamic behavior of closely spaced submerged storage racks, the Whole Pool Multi-Rack analysis methodology is used for this project.

### 6.3 Description of Racks

The new high density storage racks are analyzed for installation as follows:

#### RACK WEIGHT DATA

Rack #/Module I.D.	Cells/Module	Array Size	Empty Rack Dry Weight (lbs)
1/A1	156	13x12	23,314
2/A2	156	13x12	23,314
3/B1	144	12x12	21,601
4/B2	144	12x12	21,153
5/A3	156	13x12	23,321
6/A4	156	13x12	23,321
7/B3	144	12x12	21,608
8/C1	100	10x10	25,279
9/A5	156	13x12	22,836
10/A6	156	13x12	22,836
11/B4	144	12x12	21,162
12/C2	100	10x10	24,895

For the purpose of modeling, the racks are numbered, 1 through 12. Rack #1 is module A1 in the northwest corner of the pool. The numbering progresses west to east, so that module B2, in the northeast corner is Rack #4 and module C2 in the southeast corner is Rack #12.

Rack material is defined in Table 6.3.1.

The cartesian coordinate system utilized within the rack dynamic model has the following nomenclature:

- x = Horizontal axis along plant North
- y = Horizontal axis along plant West
- z = Vertical axis upward from the rack base

## 6.4 Synthetic Time-Histories

The synthetic time-histories in three orthogonal directions (N-S, E-W, and vertical) are generated in accordance with the provisions of SRP [6.1.2], Section 3.7.1. In order to prepare an acceptable set of acceleration time-histories, Holtec International's proprietary code GENEQ [6.4.1] is utilized.

A preferred criterion for the synthetic time-histories in SRP 3.7.1 calls for both the response spectrum and the power spectral density corresponding to the generated acceleration time-history to envelope their target (design basis) counterparts with only finite enveloping infractions. The time-histories for the pools have been generated to satisfy this preferred criterion. The seismic files also satisfy the requirements of statistical independence mandated by SRP 3.7.1.

Figures 6.4.1 through 6.4.3 provide plots of the time-history accelerograms which were generated over a 20 second duration for the SSE event. Figures 6.4.4 through 6.4.6 provide plots of the time-history accelerograms which were generated over a 20 second duration for the OBE event. These artificial time-histories are used in all non-linear dynamic simulations of the racks.

Results of the correlation function of the three time-histories are given in Table 6.4.1. Absolute values of the correlation coefficients are shown to be less than 0.15, indicating that the desired statistical independence of the three data sets has been met.

## 6.5 WPMR Methodology

Recognizing that the analytical work effort must deal with both stress and displacement criteria, the sequence of model development and analysis steps that are undertaken are summarized in the following:

- a. Prepare 3-D dynamic models suitable for a time-history analysis of the new maximum density racks. These models include the assemblage of all rack modules in each pool. Include all fluid coupling interactions and mechanical coupling appropriate to performing an accurate non-linear simulation. This 3-D simulation is referred to as a Whole Pool Multi-Rack model.

- b. Perform 3-D dynamic analyses on various physical conditions (such as coefficient of friction and extent of cells containing fuel assemblies). Archive appropriate displacement and load outputs from the dynamic model for post-processing.
- c. Perform stress analysis of high stress areas for the limiting case of all the rack dynamic analyses. Demonstrate compliance with ASME Code Section III, Subsection NF limits on stress and displacement.

#### 6.5.1 Model Details for Spent Fuel Racks

The dynamic modeling of the rack structure is prepared with special consideration of all nonlinearities and parametric variations. Particulars of modeling details and assumptions for the Whole Pool Multi-Rack analysis of racks are given in the following:

##### 6.5.1.1 Assumptions

- a. The fuel rack structure motion is captured by modeling the rack as a 12 degree-of-freedom structure. Movement of the rack cross-section at any height is described by six degrees-of-freedom of the rack base and six degrees-of-freedom at the rack top. In this manner, the response of the module, relative to the base-plate, is captured in the dynamic analyses once suitable springs are introduced to couple the rack degrees-of-freedom and simulate rack stiffness.
- b. Rattling fuel assemblies within the rack are modeled by five lumped masses located at H, .75H, .5H, .25H, and at the rack base (H is the rack height measured above the base-plate). Each lumped fuel mass has two horizontal displacement degrees-of-freedom. Vertical motion of the fuel assembly mass is assumed equal to rack vertical motion at the base-plate level. The centroid of each fuel assembly mass can be located off-center, relative to the rack structure centroid at that level, to simulate a partially loaded rack.
- c. Seismic motion of a fuel rack is characterized by random rattling of fuel assemblies in their individual storage locations. All fuel assemblies are assumed to move in-phase within a rack. This exaggerates computed dynamic loading on the rack structure and, therefore, yields conservative results.
- d. Fluid coupling between the rack and fuel assemblies, and between the rack and wall, is simulated by appropriate inertial coupling in the system kinetic energy. Inclusion of these effects uses the methods of [6.5.2, 6.5.3] for rack/assembly coupling and for rack-to-rack coupling.
- e. Fluid damping and form drag are conservatively neglected.

- f. Sloshing is found to be negligible at the top of the rack and is, therefore, neglected in the analysis of the rack.
- g. Potential impacts between the cell walls of the new racks and the contained fuel assemblies are accounted for by appropriate compression-only gap elements between masses involved. The possible incidence of rack-to-wall or rack-to-rack impact is simulated by gap elements at the top and bottom of the rack in two horizontal directions. Bottom gap elements are located at the base-plate elevation. The initial gaps reflect the presence of baseplate extensions, and the rack stiffnesses are chosen to simulate local structural detail.
- h. Pedestals are modeled by gap elements in the vertical direction and as "rigid links" for transferring horizontal stress. Each pedestal support is linked to the pool liner (or bearing pad) by two friction springs. The spring rate for the friction springs includes any lateral elasticity of the stub pedestals. Local pedestal vertical spring stiffness accounts for floor elasticity and for local rack elasticity just above the pedestal.
- i. Rattling of fuel assemblies inside the storage locations causes the gap between fuel assemblies and cell wall to change from a maximum of twice the nominal gap to a theoretical zero gap. Fluid coupling coefficients are based on the nominal gap in order to provide a conservative measure of fluid resistance to gap closure.
- j. The model for the rack is considered supported, at the base level, on four pedestals modeled as non-linear compression only gap spring elements and eight piecewise linear friction spring elements. These elements are properly located with respect to the centerline of the rack beam, and allow for arbitrary rocking and sliding motions.

#### 6.5.1.2 Element Details

Figure 6.5.1 shows a schematic of the dynamic model of a single rack. The schematic depicts many of the characteristics of the model including all of the degrees-of-freedom and some of the spring restraint elements.

Table 6.5.1 provides a complete listing of each of the 22 degrees-of-freedom for a rack model. Six translational and six rotational degrees-of-freedom (three of each type on each end) describe the motion of the rack structure. Rattling fuel mass motions (shown at nodes 1\*, 2\*, 3\*, 4\*, and 5\* in Figure 6.5.1) are described by ten horizontal translational degrees-of-freedom (two at each of the five fuel masses). The vertical fuel mass motion is assumed (and modeled) to be the same as that of the rack baseplate.

Figure 6.5.2 depicts the fuel to rack impact springs (used to develop potential impact loads between the fuel assembly mass and rack cell inner walls) in a schematic isometric. Only one of the five fuel masses is shown in this figure. Four compression only springs, acting in the horizontal direction, are provided at each fuel mass.

Figure 6.5.3 provides a 2-D schematic elevation of the storage rack model, discussed in more detail in Section 6.5.3. This view shows the vertical location of the five storage masses and some of the support pedestal spring members.

Figure 6.5.4 shows the modeling technique and degrees-of-freedom associated with rack elasticity. In each bending plane a shear and bending spring simulate elastic effects [6.5.4]. Linear elastic springs coupling rack vertical and torsional degrees-of-freedom are also included in the model.

Figure 6.5.5 depicts the inter-rack impact springs (used to develop potential impact loads between racks or between rack and wall).

## 6.5.2 Fluid Coupling Effect

In its simplest form, the so-called "fluid coupling effect" [6.5.2, 6.5.3] can be explained by considering the proximate motion of two bodies under water. If one body (mass  $m_1$ ) vibrates adjacent to a second body (mass  $m_2$ ), and both bodies are submerged in frictionless fluid, then Newton's equations of motion for the two bodies are:

$$(m_1 + M_{11}) A_1 + M_{12} A_2 = \text{applied forces on mass } m_1 + O(X_1^2)$$

$$M_{21} A_1 + (m_2 + M_{22}) A_2 = \text{applied forces on mass } m_2 + O(X_2^2)$$

$A_1$  and  $A_2$  denote absolute accelerations of masses  $m_1$  and  $m_2$ , respectively, and the notation  $O(X^2)$  denotes nonlinear terms.

$M_{11}$ ,  $M_{12}$ ,  $M_{21}$ , and  $M_{22}$  are fluid coupling coefficients which depend on body shape, relative disposition, etc. Fritz [6.5.3] gives data for  $M_{ij}$  for various body shapes and arrangements. The fluid adds mass to the body ( $M_{11}$  to mass  $m_1$ ), and an inertial force proportional to acceleration of the adjacent body (mass  $m_2$ ). Thus, acceleration of one body affects the force field on another. This force field is a function of inter-body gap, reaching large values for small gaps. Lateral motion of a fuel assembly inside a storage location encounters this effect. For example, fluid coupling behavior will be experienced between nodes 2 and 2\* in Figure 6.5.1. The rack analysis also contains inertial fluid coupling terms, which model the effect of fluid in the gaps between adjacent racks.

Terms modeling the effects of fluid flowing between adjacent racks in a single rack analysis suffer from the inaccuracies described earlier. These terms are usually computed assuming that all racks adjacent to the rack being analyzed are vibrating in-phase or 180° out of phase. The WPMR analyses do not require any assumptions with regard to phase.

Rack-to-rack gap elements have initial gaps set to 100% of the physical gap between the racks or between outermost racks and the adjacent pool walls.

### 6.5.2.1 Multi-Body Fluid Coupling Phenomena

During the seismic event, all racks in the pool are subject to the input excitation simultaneously. The motion of each free-standing module would be autonomous and independent of others as long as they did not impact each other and no water were present in the pool. While the scenario of inter-rack impact is not a common occurrence and depends on rack spacing, the effect of water (the so-called fluid coupling effect) is a universal factor. As noted in Ref. [6.5.2, 6.5.4], the fluid forces can reach rather large values in closely spaced rack geometries. It is, therefore, essential that the contribution of the fluid forces be included in a comprehensive manner. This is possible only if all racks in the pool are *allowed* to execute 3-D motion in the mathematical model. For this reason, single rack or even multi-rack models involving only a portion of the racks in the pool, are inherently inaccurate. The Whole Pool Multi-Rack model removes this intrinsic limitation of the rack dynamic models by simulating the 3-D motion of all modules simultaneously. The fluid coupling effect, therefore, encompasses interaction between *every* set of racks in the pool, i.e., the motion of one rack produces fluid forces on all other racks and on the pool walls. Stated more formally, both near-field and far-field fluid coupling effects are included in the analysis.

The derivation of the fluid coupling matrix [6.5.5] relies on the classical inviscid fluid mechanics principles, namely the principle of continuity and Kelvin's recirculation theorem. While the derivation of the fluid coupling matrix is based on no artificial construct, it has been nevertheless verified by an extensive set of shake table experiments [6.5.5].

### 6.5.3 Stiffness Element Details

Three element types are used in the rack models. Type 1 are linear elastic elements used to represent the beam-like behavior of the integrated rack cell matrix. Type 2 elements are the piece-wise linear friction springs used to develop the appropriate forces between the rack pedestals and the supporting bearing pads. Type 3 elements are non-linear gap elements, which model gap closures and subsequent impact loadings i.e., between fuel assemblies and the storage cell inner walls, and rack outer periphery spaces.

If the simulation model is restricted to two dimensions (one horizontal motion plus one vertical motion, for example), for the purposes of model clarification only, then Figure 6.5.3 describes the configuration. This simpler model is used to elaborate on the various stiffness modeling elements.

Type 3 gap elements modeling impacts between fuel assemblies and racks have local stiffness  $K_i$  in Figure 6.5.3. Support pedestal spring rates  $K_S$  are modeled by type 3 gap elements. Local compliance of the concrete floor is included in  $K_S$ . The type 2 friction elements are shown in Figure 6.5.3 as  $K_f$ . The spring elements depicted in Figure 6.5.4 represent type 1 elements.

Friction at support/liner interface is modeled by the piecewise linear friction springs with suitably large stiffness  $K_f$  up to the limiting lateral load  $\mu N$ , where  $N$  is the current compression load at the interface between support and liner. At every time-step during transient analysis, the current value of  $N$  (either zero if the pedestal has lifted off the liner, or a compressive finite value) is computed.

The gap element  $K_S$ , modeling the effective compression stiffness of the structure in the vicinity of the support, includes stiffness of the pedestal, local stiffness of the underlying pool slab, and local stiffness of the rack cellular structure above the pedestal.

The previous discussion is limited to a 2-D model solely for simplicity. Actual analyses incorporate 3-D motions.

#### 6.5.4 Coefficients of Friction

To eliminate the last significant element of uncertainty in rack dynamic analyses, multiple simulations are performed to adjust the friction coefficient ascribed to the support pedestal/pool bearing pad interface. These friction coefficients are chosen consistent with the two bounding extremes from Rabinowicz's data [6.5.1]. Simulations are also performed by imposing intermediate value friction coefficients, both 0.5 and those developed by a random number generator with Gaussian normal distribution characteristics. The assigned values are then held constant during the entire simulation in

order to obtain reproducible results.<sup>†</sup> Thus, in this manner, the WPMR analysis results are brought closer to the realistic structural conditions.

The coefficient of friction ( $\mu$ ) between the pedestal supports and the pool floor is indeterminate. According to Rabinowicz [6.5.1], results of 199 tests performed on austenitic stainless steel plates submerged in water show a mean value of  $\mu$  to be 0.503 with standard deviation of 0.125. Upper and lower bounds (based on twice standard deviation) are 0.753 and 0.253, respectively. Analyses are therefore performed for coefficient of friction values of 0.2 (lower limit), 0.5 and 0.8 (upper limit), as well as for random friction values clustered about a mean of 0.5. The bounding values of  $\mu = 0.2$  and 0.8 have been found to envelope the upper limit of module response in previous rerack projects.

#### 6.5.5 Governing Equations of Motion

Using the structural model discussed in the foregoing, equations of motion corresponding to each degree-of-freedom are obtained using Lagrange's Formulation [6.5.4]. The system kinetic energy includes contributions from solid structures and from trapped and surrounding fluid. The final system of equations obtained have the matrix form:

$$[M] \left[ \frac{d^2 q}{dt^2} \right] = [Q] + [G]$$

where:

[M] - total mass matrix (including structural and fluid mass contributions). The size of this matrix will be  $22n \times 22n$  for a WPMR analysis ( $n$  = number of racks in the model).

---

<sup>†</sup> It is noted that DYNARACK has the capability to change the coefficient of friction at any pedestal at each instant of contact based on a random reading of the computer clock cycle. However, exercising this option would yield results that could not be reproduced. Therefore, the random choice of coefficients is made only once per run.

- q - the nodal displacement vector relative to the pool slab displacement (the term with q indicates the second derivative with respect to time, i.e., acceleration)
- [G] - a vector dependent on the given ground acceleration
- [Q] - a vector dependent on the spring forces (linear and nonlinear) and the coupling between degrees-of-freedom

The above column vectors have length 22n. The equations can be rewritten as follows:

$$\left[ \frac{d^2 q}{dt^2} \right] = [M]^{-1} [Q] + [M]^{-1} [G]$$

This equation set is mass uncoupled, displacement coupled at each instant in time. The numerical solution uses a central difference scheme built into the proprietary computer program DYNARACK [6.2.4].

## 6.6 Structural Evaluation of Spent Fuel Rack Design

### 6.6.1 Kinematic and Stress Acceptance Criteria

There are two sets of criteria to be satisfied by the rack modules:

#### a. Kinematic Criteria

An isolated fuel rack situated in the middle of the storage cavity is most vulnerable to overturning because such a rack would be hydrodynamically uncoupled from any adjacent structures. Therefore, to assess the margin against overturning, a single rack module is evaluated. According to Ref [6.1.2 and 6.1.3], the minimum required safety margins under the OBE and SSE events are 1.5 and 1.1, respectively. In order to ensure that these

safety factors are met, the simulations resulting in the highest top of rack displacements were re-performed with earthquake excitation multipliers of 1.5 for OBE and 1.1 for SSE. The maximum rotations of the rack (about the two principal axes) are obtained from a post processing of the rack time history response output. The ratio of the rotation required to produce incipient tipping in either principal plane to the actual maximum rotation in that plane from the time history solution is the margin of safety. Since the factors of safety are conservatively embedded in the earthquake multipliers, meeting the acceptance criteria is established by the ratio described above being greater than 1.0.

b. Stress Limit Criteria

Stress limits must not be exceeded under the postulated load combinations provided herein.

6.6.2 Stress Limit Evaluations

The stress limits presented below apply to the rack structure and are derived from the ASME Code, Section III, Subsection NF [6.6.1]. Parameters and terminology are in accordance with the ASME Code. Material properties are obtained from the ASME Code Appendices [6.6.2], and are listed in Table 6.3.1.

(i) Normal Conditions (Level A)

- a. Allowable stress in tension on a net section is:

$$F_t = 0.6 S_y$$

Where,  $S_y$  = yield stress at temperature, and  $F_t$  is equivalent to primary membrane stress.

- b. Allowable stress in shear on a net section is:

$$F_v = .4 S_y$$

- c. Allowable stress in compression on a net section is:

$$F_a = S_y \left( .47 - \frac{kl}{444 r} \right)$$

where  $kl/r$  for the main rack body is based on the full height and cross section of the honeycomb region and does not exceed 120 for all sections.

$l$  = unsupported length of component

$k$  = length coefficient which gives influence of boundary conditions. The following values are appropriate for the described end conditions:

1 (simple support both ends)

2 (cantilever beam)

$\frac{1}{2}$  (clamped at both ends)

$r$  = radius of gyration of component

- d. Maximum allowable bending stress at the outermost fiber of a net section, due to flexure about one plane of symmetry is:

$$F_b = 0.60 S_y \quad (\text{equivalent to primary bending})$$

- e. Combined bending and compression on a net section satisfies:

$$\frac{f_a}{F_a} + \frac{C_{mx} f_{bx}}{D_x F_{bx}} + \frac{C_{my} f_{by}}{D_y F_{by}} < 1$$

where:

$f_a$  = Direct compressive stress in the section

$f_{bx}$  = Maximum bending stress along x-axis

$f_{by}$  = Maximum bending stress along y-axis

$C_{mx}$  = 0.85

$C_{my}$  = 0.85

$D_x$  =  $1 - (f_a/F'_{ex})$

$D_y$  =  $1 - (f_a/F'_{ey})$

$F'_{ex,ey}$  =  $(\pi^2 E)/(2.15 (kl/r)_{x,y}^2)$

$E$  = Young's Modulus

and subscripts x,y reflect the particular bending plane.

- f. Combined flexure and compression (or tension) on a net section:

$$\frac{f_a}{0.6 S_y} + \frac{f_{bx}}{F_{bx}} + \frac{f_{by}}{F_{by}} < 1.0$$

The above requirements are to be met for both direct tension or compression.

- g. Welds

Allowable maximum shear stress on the net section of a weld is given by:

$$F_w = 0.3 S_u$$

where  $S_u$  is the weld material ultimate strength at temperature. For fillet weld legs in contact with base metal, the shear stress on the gross section is limited to  $0.4S_y$ , where  $S_y$  is the base material yield strength at temperature.

(ii) Level B Service Limits (Upset Conditions, including OBE)

Section NF-3321 (ASME Section III, Subsection NF [6.6.1]) states that, for the Level B condition, the allowable stresses for those given above in (i) may be increased by a factor of 1.33.

(iii) Level D Service Limits (including SSE)

Section F-1334 (ASME Section III, Appendix F [6.6.2]), states that limits for the Level D condition are the smaller of 2 or  $1.167S_u/S_y$  times the corresponding limits for the Level A condition if  $S_u > 1.2S_y$ , or 1.4 if  $S_u$  less than or equal  $1.2S_y$  except for requirements specifically listed below.  $S_u$ ,  $S_y$  are the ultimate strength and yield strength at the specified rack design temperature. Examination of material properties for 304 stainless demonstrates that 1.2 times the yield strength is less than the ultimate strength.

Exceptions to the above general multiplier are the following:

- a) Stresses in shear shall not exceed the lesser of  $0.72S_y$  or  $0.42S_u$ . In the case of the Austenitic Stainless material used here,  $0.72S_y$  governs.
- b) Axial Compression Loads shall be limited to  $2/3$  of the calculated buckling load.
- c) Combined Axial Compression and Bending - The equations for Level A conditions shall apply except that:

$$F_a = 0.667 \times \text{Buckling Load} / \text{Gross Section Area},$$

and the terms  $F'_{ex}$  and  $F'_{ey}$  may be increased by the factor 1.65.

- d) For welds, the Level D allowable maximum weld stress is not specified in Appendix F of the ASME Code. An appropriate limit for weld throat stress is conservatively set here as:

$$F_w = (0.3 S_u) \times \text{factor}$$

where:

$$\text{factor} = (\text{Level D shear stress limit}) / (\text{Level A shear stress limit})$$

### 6.6.3 Dimensionless Stress Factors

For convenience, the stress results are in dimensionless form. Dimensionless stress factors are defined as the ratio of the actual developed stress to the specified limiting stress value. The limiting value of each stress factor is 1.0.. Stress factors are determined as follows:

$R_1$  = Ratio of direct tensile or compressive stress on a net section to its allowable value (note pedestals only resist compression)

$R_2$  = Ratio of gross shear on a net section in the x-direction to its allowable value

$R_3$  = Ratio of maximum x-axis bending stress to its allowable value for the section

$R_4$  = Ratio of maximum y-axis bending stress to its allowable value for the section

$R_5$  = Combined flexure and compressive factor (as defined in the foregoing)

$R_6$  = Combined flexure and tension (or compression) factor (as defined in the foregoing)

$R_7$  = Ratio of gross shear on a net section in the y-direction to its allowable value

#### 6.6.4 Loads and Loading Combinations for Spent Fuel Racks

The applicable loads and their combinations, which must be considered in the seismic analysis of rack modules, are excerpted from the OT Position [6.1.3] and SRP, Section 3.8.4 [6.1.2]. The load combinations considered are identified below:

Loading Combination	Service Level
$D + L$ $D + L + T_o$ $D + L + T_o + E$	Level A
$D + L + T_a + E$ $D + L + T_o + P_f$	Level B
$D + L + T_a + E'$  $D + L + T_o + F_d$	Level D  The functional capability of the fuel racks must be demonstrated. This load case is discussed in Section 7.0.

Where:

- D = Dead weight-induced loads (including fuel assembly weight)
- L = Live Load (not applicable for the fuel rack, since there are no moving objects in the rack load path)
- $P_f$  = Upward force on the racks caused by postulated stuck fuel assembly
- $F_d$  = Impact force from accidental drop of the heaviest load from the maximum possible height.
- E = Operating Basis Earthquake (OBE)
- $E'$  = Safe Shutdown Earthquake (SSE)
- $T_o$  = Differential temperature induced loads (normal operating or shutdown condition based on the most critical transient or steady state condition)
- $T_a$  = Differential temperature induced loads (the highest temperature associated with the postulated abnormal design conditions)

$T_a$  and  $T_o$  produce local thermal stresses. The worst thermal stress field in a fuel rack is obtained when an isolated storage location has a fuel assembly generating heat at maximum postulated rate and surrounding storage locations contain no fuel. Heated water makes unobstructed contact with the inside of the storage walls, thereby producing maximum possible temperature difference between adjacent cells. Secondary stresses produced are limited to the body of the rack; that is, support pedestals do not experience secondary (thermal) stresses.

### 6.7 Parametric Simulations

The multiple rack models employ the fluid coupling effects for all racks in the pool, as discussed above, and these simulations are referred to as WPMR evaluations. In addition, single rack models are also developed for additional study of the effect of various parameters on rack displacement. The models are described as follows:

( I ) Whole Pool Multi Rack Model An array of twelve racks is modeled with proper interface fluid gaps and a coefficient of friction at the support interface locations with the bearing pad generated by a Gaussian distribution random number generator with 0.5 as the mean and 0.15 standard deviation. The response to both SSE and OBE seismic excitation is determined.

( II ) Single Rack Models : Two models are employed for studying the structural behavior of a single rack. A model is developed for the largest rack and another for the rack with the maximum aspect ratio (defined above as the rack exhibiting the maximum ratio of the height to the smaller of the length or width). In both these models, the rack is modeled as fully loaded (to act as a baseline), half loaded (east-west, north-south and diagonally) and nearly empty. The coefficient of friction between male pedestal and baseplate is taken as one of four possibilities: 0.2, 0.5, 0.8 or as selected by a Gaussian random number generator as introduced in the prior section. For these models, either inphase or opposed phase motion is assumed. The inphase case is implemented by assuming that the maximum actual water gaps that exist between the racks and the four walls of the SFP surround the single rack, in the same north-east-south-west orientation. This reflects the behavior that would occur if all the racks moved in unison. For the opposed phase case, one-half the actual gap is attributed to each rack side. All single rack cases in the study are done for both SSE and OBE excitation.

( III ) Single Rack Overturning Check Model This model is developed to study the potential for rack overturning in the Spent Fuel Pool. The SSE case which had the maximum displacement in the study is

run, subjected to 1.1 times the SSE excitation and the OBE case which had the maximum displacement is run, subjected to 1.5 times the OBE excitation.

The displacements calculated from the single rack runs are performed as a more conservative check for kinematic stability. To inquire into the effect that temporary installation of miscellaneous equipment on top of a rack might have, single rack study case 15 was re-run with an additional 2000 lb distributed among the topmost nodes of the 78 cells containing fuel.

The Whole Pool and Single Rack simulations listed on the following tables have been performed to investigate the structural integrity of the rack array.

LIST OF WPMR SIMULATIONS			
<u>Case</u>	<u>Load Case</u>	<u>COF</u>	<u>Event</u>
1	All Racks Fully Loaded	Random	SSE
2	All Racks Fully Loaded	Random	OBE

where Random = Gaussian distribution with a mean coeff. of friction of 0.5.  
 (upper and lower limits of 0.8 and 0.2, respectively) and  
 COF = Coefficient of Friction

LIST OF SINGLE RACK SIMULATIONS				
<u>Case</u>	<u>Motion</u>	<u>Load Case</u>	<u>COF</u>	<u>Event</u>
1	INPHASE	Largest Rack Fully Loaded	Random	SSE
2	INPHASE	Largest Rack Fully Loaded	0.2	SSE
3	INPHASE	Largest Rack Fully Loaded	0.5	SSE
4	INPHASE	Largest Rack Fully Loaded	0.8	SSE
5	INPHASE	Largest Rack Half Loaded (E-W)	Random	SSE
6	INPHASE	Largest Rack Half Loaded (E-W)	0.2	SSE
7	INPHASE	Largest Rack Half Loaded (E-W)	0.5	SSE
8	INPHASE	Largest Rack Half Loaded (E-W)	0.8	SSE
9	INPHASE	Largest Rack Half Loaded (N-S)	Random	SSE
10	INPHASE	Largest Rack Half Loaded (N-S)	0.2	SSE
11	INPHASE	Largest Rack Half Loaded (N-S)	0.5	SSE

12	INPHASE	Largest Rack Half Loaded (N-S)	0.8	SSE
13	INPHASE	Largest Rack Half Loaded (Diag)	Random	SSE
14	INPHASE	Largest Rack Half Loaded (Diag)	0.2	SSE
15	INPHASE	Largest Rack Half Loaded (Diag)	0.5	SSE
16	INPHASE	Largest Rack Half Loaded (Diag)	0.8	SSE
17	INPHASE	Largest Rack Nearly Empty	Random	SSE
18	INPHASE	Largest Rack Nearly Empty	0.2	SSE
19	INPHASE	Largest Rack Nearly Empty	0.5	SSE
20	INPHASE	Largest Rack Nearly Empty	0.8	SSE
21	OPPOSED	Largest Rack Fully Loaded	Random	SSE
22	OPPOSED	Largest Rack Fully Loaded	0.2	SSE
23	OPPOSED	Largest Rack Fully Loaded	0.5	SSE
24	OPPOSED	Largest Rack Fully Loaded	0.8	SSE
25	OPPOSED	Largest Rack Half Loaded (E-W)	Random	SSE
26	OPPOSED	Largest Rack Half Loaded (E-W)	0.2	SSE
27	OPPOSED	Largest Rack Half Loaded (E-W)	0.5	SSE
28	OPPOSED	Largest Rack Half Loaded (E-W)	0.8	SSE
29	OPPOSED	Largest Rack Half Loaded (N-S)	Random	SSE
30	OPPOSED	Largest Rack Half Loaded (N-S)	0.2	SSE
31	OPPOSED	Largest Rack Half Loaded (N-S)	0.5	SSE
32	OPPOSED	Largest Rack Half Loaded (N-S)	0.8	SSE
33	OPPOSED	Largest Rack Half Loaded (Diag)	Random	SSE
34	OPPOSED	Largest Rack Half Loaded (Diag)	0.2	SSE
35	OPPOSED	Largest Rack Half Loaded (Diag)	0.5	SSE
36	OPPOSED	Largest Rack Half Loaded (Diag)	0.8	SSE
37	OPPOSED	Largest Rack Nearly Empty	Random	SSE
38	OPPOSED	Largest Rack Nearly Empty	0.2	SSE
39	OPPOSED	Largest Rack Nearly Empty	0.5	SSE
40	OPPOSED	Largest Rack Nearly Empty	0.8	SSE
41	INPHASE	Largest Rack Fully Loaded	Random	OBE
42	INPHASE	Largest Rack Fully Loaded	0.2	OBE
43	INPHASE	Largest Rack Fully Loaded	0.5	OBE

44	INPHASE	Largest Rack Fully Loaded	0.8	OBE
45	INPHASE	Largest Rack Half Loaded (E-W)	Random	OBE
46	INPHASE	Largest Rack Half Loaded (E-W)	0.2	OBE
47	INPHASE	Largest Rack Half Loaded (E-W)	0.5	OBE
48	INPHASE	Largest Rack Half Loaded (E-W)	0.8	OBE
49	INPHASE	Largest Rack Half Loaded (N-S)	Random	OBE
50	INPHASE	Largest Rack Half Loaded (N-S)	0.2	OBE
51	INPHASE	Largest Rack Half Loaded (N-S)	0.5	OBE
52	INPHASE	Largest Rack Half Loaded (N-S)	0.8	OBE
53	INPHASE	Largest Rack Half Loaded (Diag)	Random	OBE
54	INPHASE	Largest Rack Half Loaded (Diag)	0.2	OBE
55	INPHASE	Largest Rack Half Loaded (Diag)	0.5	OBE
56	INPHASE	Largest Rack Half Loaded (Diag)	0.8	OBE
57	INPHASE	Largest Rack Nearly Empty	Random	OBE
58	INPHASE	Largest Rack Nearly Empty	0.2	OBE
59	INPHASE	Largest Rack Nearly Empty	0.5	OBE
60	INPHASE	Largest Rack Nearly Empty	0.8	OBE
61	OPPOSED	Largest Rack Fully Loaded	Random	OBE
62	OPPOSED	Largest Rack Fully Loaded	0.2	OBE
63	OPPOSED	Largest Rack Fully Loaded	0.5	OBE
64	OPPOSED	Largest Rack Fully Loaded	0.8	OBE
65	OPPOSED	Largest Rack Half Loaded (E-W)	Random	OBE
66	OPPOSED	Largest Rack Half Loaded (E-W)	0.2	OBE
67	OPPOSED	Largest Rack Half Loaded (E-W)	0.5	OBE
68	OPPOSED	Largest Rack Half Loaded (E-W)	0.8	OBE
69	OPPOSED	Largest Rack Half Loaded (N-S)	Random	OBE
70	OPPOSED	Largest Rack Half Loaded (N-S)	0.2	OBE
71	OPPOSED	Largest Rack Half Loaded (N-S)	0.5	OBE
72	OPPOSED	Largest Rack Half Loaded (N-S)	0.8	OBE
73	OPPOSED	Largest Rack Half Loaded (Diag)	Random	OBE
74	OPPOSED	Largest Rack Half Loaded (Diag)	0.2	OBE
75	OPPOSED	Largest Rack Half Loaded (Diag)	0.5	OBE

76	OPPOSED	Largest Rack Half Loaded (Diag)	0.8	OBE
77	OPPOSED	Largest Rack Nearly Empty	Random	OBE
78	OPPOSED	Largest Rack Nearly Empty	0.2	OBE
79	OPPOSED	Largest Rack Nearly Empty	0.5	OBE
80	OPPOSED	Largest Rack Nearly Empty	0.8	OBE
81	INPHASE	Aspect Rack Fully Loaded	Random	SSE
82	INPHASE	Aspect Rack Fully Loaded	0.2	SSE
83	INPHASE	Aspect Rack Fully Loaded	0.5	SSE
84	INPHASE	Aspect Rack Fully Loaded	0.8	SSE
85	INPHASE	Aspect Rack Half Loaded (E-W)	Random	SSE
86	INPHASE	Aspect Rack Half Loaded (E-W)	0.2	SSE
87	INPHASE	Aspect Rack Half Loaded (E-W)	0.5	SSE
88	INPHASE	Aspect Rack Half Loaded (E-W)	0.8	SSE
89	INPHASE	Aspect Rack Half Loaded (N-S)	Random	SSE
90	INPHASE	Aspect Rack Half Loaded (N-S)	0.2	SSE
91	INPHASE	Aspect Rack Half Loaded (N-S)	0.5	SSE
92	INPHASE	Aspect Rack Half Loaded (N-S)	0.8	SSE
93	INPHASE	Aspect Rack Half Loaded (Diag)	Random	SSE
94	INPHASE	Aspect Rack Half Loaded (Diag)	0.2	SSE
95	INPHASE	Aspect Rack Half Loaded (Diag)	0.5	SSE
96	INPHASE	Aspect Rack Half Loaded (Diag)	0.8	SSE
97	INPHASE	Aspect Rack Nearly Empty	Random	SSE
98	INPHASE	Aspect Rack Nearly Empty	0.2	SSE
99	INPHASE	Aspect Rack Nearly Empty	0.5	SSE
100	INPHASE	Aspect Rack Nearly Empty	0.8	SSE
101	OPPOSED	Aspect Rack Fully Loaded	Random	SSE
102	OPPOSED	Aspect Rack Fully Loaded	0.2	SSE
103	OPPOSED	Aspect Rack Fully Loaded	0.5	SSE
104	OPPOSED	Aspect Rack Fully Loaded	0.8	SSE
105	OPPOSED	Aspect Rack Half Loaded (E-W)	Random	SSE
106	OPPOSED	Aspect Rack Half Loaded (E-W)	0.2	SSE
107	OPPOSED	Aspect Rack Half Loaded (E-W)	0.5	SSE

108	OPPOSED	Aspect Rack Half Loaded (E-W)	0.8	SSE
109	OPPOSED	Aspect Rack Half Loaded (N-S)	Random	SSE
110	OPPOSED	Aspect Rack Half Loaded (N-S)	0.2	SSE
111	OPPOSED	Aspect Rack Half Loaded (N-S)	0.5	SSE
112	OPPOSED	Aspect Rack Half Loaded (N-S)	0.8	SSE
113	OPPOSED	Aspect Rack Half Loaded (Diag)	Random	SSE
114	OPPOSED	Aspect Rack Half Loaded (Diag)	0.2	SSE
115	OPPOSED	Aspect Rack Half Loaded (Diag)	0.5	SSE
116	OPPOSED	Aspect Rack Half Loaded (Diag)	0.8	SSE
117	OPPOSED	Aspect Rack Nearly Empty	Random	SSE
118	OPPOSED	Aspect Rack Nearly Empty	0.2	SSE
119	OPPOSED	Aspect Rack Nearly Empty	0.5	SSE
120	OPPOSED	Aspect Rack Nearly Empty	0.8	SSE
121	INPHASE	Aspect Rack Fully Loaded	Random	OBE
122	INPHASE	Aspect Rack Fully Loaded	0.2	OBE
123	INPHASE	Aspect Rack Fully Loaded	0.5	OBE
124	INPHASE	Aspect Rack Fully Loaded	0.8	OBE
125	INPHASE	Aspect Rack Half Loaded (E-W)	Random	OBE
126	INPHASE	Aspect Rack Half Loaded (E-W)	0.2	OBE
127	INPHASE	Aspect Rack Half Loaded (E-W)	0.5	OBE
128	INPHASE	Aspect Rack Half Loaded (E-W)	0.8	OBE
129	INPHASE	Aspect Rack Half Loaded (N-S)	Random	OBE
130	INPHASE	Aspect Rack Half Loaded (N-S)	0.2	OBE
131	INPHASE	Aspect Rack Half Loaded (N-S)	0.5	OBE
132	INPHASE	Aspect Rack Half Loaded (N-S)	0.8	OBE
133	INPHASE	Aspect Rack Half Loaded (Diag)	Random	OBE
134	INPHASE	Aspect Rack Half Loaded (Diag)	0.2	OBE
135	INPHASE	Aspect Rack Half Loaded (Diag)	0.5	OBE
136	INPHASE	Aspect Rack Half Loaded (Diag)	0.8	OBE
137	INPHASE	Aspect Rack Nearly Empty	Random	OBE
138	INPHASE	Aspect Rack Nearly Empty	0.2	OBE
139	INPHASE	Aspect Rack Nearly Empty	0.5	OBE

140	INPHASE	Aspect Rack Nearly Empty	0.8	OBE
141	OPPOSED	Aspect Rack Fully Loaded	Random	OBE
142	OPPOSED	Aspect Rack Fully Loaded	0.2	OBE
143	OPPOSED	Aspect Rack Fully Loaded	0.5	OBE
144	OPPOSED	Aspect Rack Fully Loaded	0.8	OBE
145	OPPOSED	Aspect Rack Half Loaded (E-W)	Random	OBE
146	OPPOSED	Aspect Rack Half Loaded (E-W)	0.2	OBE
147	OPPOSED	Aspect Rack Half Loaded (E-W)	0.5	OBE
148	OPPOSED	Aspect Rack Half Loaded (E-W)	0.8	OBE
149	OPPOSED	Aspect Rack Half Loaded (N-S)	Random	OBE
150	OPPOSED	Aspect Rack Half Loaded (N-S)	0.2	OBE
151	OPPOSED	Aspect Rack Half Loaded (N-S)	0.5	OBE
152	OPPOSED	Aspect Rack Half Loaded (N-S)	0.8	OBE
153	OPPOSED	Aspect Rack Half Loaded (Diag)	Random	OBE
154	OPPOSED	Aspect Rack Half Loaded (Diag)	0.2	OBE
155	OPPOSED	Aspect Rack Half Loaded (Diag)	0.5	OBE
156	OPPOSED	Aspect Rack Half Loaded (Diag)	0.8	OBE
157	OPPOSED	Aspect Rack Nearly Empty	Random	OBE
158	OPPOSED	Aspect Rack Nearly Empty	0.2	OBE
159	OPPOSED	Aspect Rack Nearly Empty	0.5	OBE
160	OPPOSED	Aspect Rack Nearly Empty	0.8	OBE
161	INPHASE	Largest Rack Half Loaded (Diag)	0.5	1.1xSSE
162	INPHASE	Largest Rack Fully Loaded	0.2	1.5xOBE
163	INPHASE	Largest Rack Half Loaded Diagonally (2000 lb added at top)	0.5	SSE

## 6.8 Time History Simulation Results

The results from the DYNARACK runs may be seen in the raw data output files. However, due to the huge quantity of output data, a post-processor is used to scan for worst case conditions and develop the stress factors discussed in subsection 6.6.3. Further reduction in this bulk of information is provided in this section by extracting the worst case values from the parameters of interest; namely displacements,

support pedestal forces, impact loads, and stress factors. This section also summarizes additional analyses performed to develop and evaluate structural member stresses which are not determined by the post processor.

### 6.8.1 Rack Displacements

The maximum rack displacements are obtained from the time histories of the motion of the upper and lower four corners of each rack in each of the simulations. The maximum absolute value of displacement in the two horizontal directions, relative to the pool slab, is determined by the post-processor for each rack, at the top and bottom corners. The maximum displacements in either direction reported from the WPMR analyses is 0.810" at the top of module B2 during the SSE events and 0.892" at the top of module C1 during the OBE events. The maximum displacement in either direction reported from the single rack analyses is 1.154" from simulation 15, which was performed for module A4. The maximum displacement for simulation 163, occurring at the top of the rack in the study, was 1.094". Therefore, displacements are more sensitive to fuel mass offsets from rack centroid than from the fictitious mass on top of the racks.

To assess the kinematic stability safety margin, the maximum displacement single rack cases were run again, using 1.1 times the SSE excitation and 1.5 times the OBE excitation, respectively. These are single rack cases 161 and 162. The maximum displacements from these runs were 1.194" and 1.520", respectively, as opposed to 1.154" and 0.772" without excitation increase. The result from run 162 is used to compute the safety factor against overturning. It was shown to be more than 51, which far exceeds the acceptance criteria of 1.0.

### 6.8.2 Pedestal Vertical Forces

The maximum vertical pedestal force obtained in the WPMR simulations was 319,000 lbf for module A5, one of the 12 x 13 racks in the SSE simulation. The maximum vertical pedestal force obtained in the OBE simulation was 301,000 lbf for module A4, another 12 x 13 rack.

### 6.8.3 Pedestal Friction Forces

The maximum interface shear force value in any direction bounding all pedestals in the WPMR simulations is 170,000 lbf for module B2 in the SSE case.

### 6.8.4 Rack Impact Loads

A freestanding rack, by definition, is a structure subject to potential impacts during a seismic event. Impacts arise from rattling of the fuel assemblies in the storage rack locations and, in some instances, from localized impacts between the racks, or between a peripheral rack and the pool wall. The following sections discuss the bounding values of these impact loads.

#### 6.8.4.1 Rack to Rack Impacts

Gap elements track the potential for impacts between any rack and the pool walls. The results for each simulation have been scanned for non-zero values. The simulation results show that no gap element between any two rack tops closes. The tabular results do show some contact forces develop between rack-to-rack at the baseplate elevation during the simulations. Baseplate gaps are initially set to zero, so impact loads (contact forces) are expected in those locations. The maximum contact forces occurring at localized rack baseplate locations in the WPMR runs is 16,460 lbf in the SSE run and 16,750 lbf in the OBE run.

#### 6.8.4.2 Rack to Wall Impacts

The storage racks do not impact the pool walls under any simulation.

#### 6.8.4.3 Fuel to Cell Wall Impact Loads

A review of all simulations performed allows determination of the maximum instantaneous impact load between fuel assembly and fuel cell wall at any modeled impact site. The maximum fuel/cell wall impact loads are 743 lbf in module B2 in the SSE case of the WPMR analyses and 529 lbf for the OBE case in module A6. The cell wall integrity under this instantaneous impact load has been evaluated and shown to remain intact with no permanent damage.

## 6.9 Rack Structural Evaluation

### 6.9.1 Rack Stress Factors

The time history results from the DYNARACK solver provide the pedestal normal and lateral interface forces, which may be converted to the limiting bending moment and shear force at the bottom baseplate-pedestal interface. In particular, maximum values for the previously defined stress factors are determined for every pedestal in the array of racks. With this information available, the structural integrity of the pedestal can be assessed and reported. The net section maximum (in time) bending moments and shear forces can also be determined at the bottom baseplate-rack cellular structure interface for each spent fuel rack in the pool. Using these forces and moments, the maximum stress in the limiting rack cell (box) can be evaluated.

The stress factor results for male and female pedestals, and for the entire spent fuel rack cellular cross section just above the bottom casting has been determined. These factors are reported for every rack in each simulation, and for each pedestal in every rack. These locations are the most heavily loaded net

sections in the structure so that satisfaction of the stress factor criteria at these locations ensures that the overall structural criteria set forth in Section 6.6 are met.

An evaluation of the stress factors for all of the WPMR simulations performed leads to the conclusion that all stress factors, as defined in Section 6.6.3, are less than the mandated limit of 1.0 for the load cases examined. The bounding stress factors were found to be 0.728 (R5) and 0.708 (R6) for the OBE simulation, occurring in the pedestals of module A4. The maximum calculated SSE stress factor were 0.447 (R5) and 0.448 (R6) for module B2. Relevant stress factors are for cell wall stresses above the baseplate, since these control over the pedestal stress factors. The values for all other defined stress factors are archived and show that the requirements of Section 6.6 are indeed satisfied for the load levels considered for every limiting location in every rack in the array.

#### 6.9.2 Pedestal Thread Shear Stress

The maximum thread engagement stresses under faulted conditions for every pedestal for every rack in the pool from the WPMR simulations run was 12,497 psi for the SSE run and 11,792 psi for the OBE run. By ASME code section NF-3321, the Level A allowable stress is  $0.4 \cdot F_y = 0.4(25,000) = 10,000$  psi. Referring to section 6.6.4, for Level B (OBE), the allowable is increased by the factor 1.33 from table NF-3523(b), resulting in an allowable stress of 13,300 psi, which exceeds both calculated stresses.

#### 6.9.3 Local Stresses Due to Impacts

Impact loads at the pedestal base (discussed in subsection 6.8.4.1) produce stresses in the pedestal for which explicit stress limits are prescribed in the Code. However, impact loads on the cellular region of the racks, as discussed in subsection 6.8.4.3 above, produce stresses which attenuate rapidly away from the loaded region. This behavior is characteristic of secondary stresses.

Even though limits on secondary stresses are not prescribed in the Code for class 3 NF structures, evaluations are made to ensure that the localized impacts do not lead to plastic deformations in the storage cells which affect the sub-criticality of the stored fuel array.

a. Impact Loading Between Fuel Assembly and Cell Wall

Local cell wall integrity is conservatively estimated from peak impact loads. Plastic analysis is used to obtain the limiting impact load which would lead to gross permanent deformation. As shown in Table 6.9.1, the limiting impact load (of 3,031 lbf, including a safety factor of 2.0) is much greater than the highest calculated impact load value (of 743 lbf, see subsection 6.8.4.3) obtained from any of the rack analyses. Therefore, fuel impacts do not represent a significant concern with respect to fuel rack cell deformation.

b. Impacts Between Adjacent Racks

As may be seen from subsection 6.8.4.1, the bottom of the storage racks will impact each other at a few locations during seismic events. Since the loading is presented edge-on to the 3/4" baseplate membrane, the distributed stresses after local deformation will be negligible. The impact loading will be distributed over a large area (a significant portion of the entire minimum baseplate length of about 107 inches by its 3/4 inch thickness). The resulting compressive stress from the highest impact load of 16,750 lbs distributed over 80 sq. inches is only 210 psi, which is negligible. This is a conservative computation, since the simulation assumes a local impact site. Therefore, any deformation will not affect the configuration of the stored fuel.

#### 6.9.4 Weld Stresses

Weld locations subjected to significant seismic loading are at the bottom of the rack at the baseplate-to-cell connection, at the top of the pedestal support at the baseplate connection, and at cell-to-cell connections. Bounding values of resultant loads are used to qualify the connections.

a. Baseplate-to-Rack Cell Welds

For Level A or B conditions, Ref. [6.6.1] permits an allowable weld stress of  $\tau = .3 S_u = 21300$  psi (multiplied by 1.33 for Level B). As stated in subsection 6.6.2, the allowable may be increased for Level D by an amplification factor which is equal to 1.8 ( $= .72S_y/.4S_y$ ). The allowable stress increase factor of 1.8 greatly exceeds the ratio of maximum SSE to OBE stresses. Therefore, Level B becomes the governing condition.

Weld dimensionless stress factors are produced through the use of a simple conversion (ratio) factor applied to the corresponding stress factor in the adjacent rack material. The ratio 2.18 is developed from the differences in material thickness and length versus weld throat dimension and length:

$$RATIO = ( \text{[REDACTED]} )$$

The highest predicted weld stress for OBE is calculated from the highest cell wall (above the baseplate) R6 value, 0.668, (corresponding to the same simulation as the highest pedestal R6 value of 0.708 as reported in subsection 6.9.1) as follows:

$$R6 * [(0.6) F_y] * RATIO = 0.668 * [0.6 * 25000] * 2.18 = 21,846 \text{ psi}$$

This value is less than the Level B allowable weld stress value, which is  $1.33 \times 21,300 = 28329$  psi. Therefore, all weld stresses between the baseplate and cell wall base are acceptable.

b. Baseplate-to-Pedestal Welds

The weld between baseplate and support pedestal is checked using finite element analysis to determine that the maximum stress is 32,051 psi under a Level D event. This calculated stress value is well below the SSE allowable of  $1.8 \times 21,300 = 38,340$  psi. A similar approach is used

for a Level B event to find a maximum stress of 23,000 psi. This also compares favorably with the OBE allowable of  $1.33 \times 21,300 = 28329$  psi.

c. Cell-to-Cell Welds

Cell-to-cell connections are by a series of connecting welds along the cell height. Stresses in storage cell to cell welds develop due to fuel assembly impacts with the cell wall. These weld stresses are conservatively calculated by assuming that fuel assemblies in adjacent cells are moving out of phase with one another so that impact loads in two adjacent cells are in opposite directions; this tends to separate the two cells from each other at the weld.

Table 6.9.1 gives the computed results for the maximum allowable load that can be transferred by these welds based on the available weld area. The upper bound on the applied load transferred is also given in Table 6.9.1. This upper bound value is very conservatively obtained by applying the bounding rack-to-fuel impact load from any simulation in two orthogonal directions simultaneously, and multiplying the result by 2 to account for the simultaneous impact of two assemblies in adjacent cells moving in opposing directions. An equilibrium analysis at the connection then yields the upper bound load to be transferred. As shown in Table 6.9.1, the calculated stress of 8325 psi is below the allowable stress of 8520 psi.

6.9.5 Bearing Pad Analysis

To protect the pool slab from highly localized dynamic loadings, bearing pads are placed between the pedestal base and the slab. Fuel rack pedestals impact on these bearing pads during a seismic event and pedestal loading is transferred to the liner. Bearing pad dimensions are set to ensure that the average pressure on the slab surface due to a static load plus a dynamic impact load does not exceed the American Concrete Institute, ACI-349 [6.9.1] limit on bearing pressures. Section 10.17 of [6.9.2] gives the design bearing strength as

$$f_b = \phi (.85 f_c') \leq$$

where  $\phi = .7$  and  $f_c'$  is the specified concrete strength for the spent fuel pool.  $\epsilon = 1$  except when the supporting surface is wider on all sides than the loaded area. In that case,  $\epsilon = (A_2/A_1)^{.5}$ , but not more than 2.  $A_1$  is the actual loaded area, and  $A_2$  is an area greater than  $A_1$  and is defined in [6.9.2]. Using a value of  $\epsilon > 1$  includes credit for the confining effect of the surrounding concrete. It is noted that this criterion is in conformance with the ultimate strength primary design methodology of the American Concrete Institute in use since 1971. For the VCSNS,  $f_c' = 3,000$  psi and the allowable static bearing pressure is  $f_b = 3,570$  psi, assuming full concrete confinement. This allowable bearing pressure is utilized because concrete confinement is not actually compromised in the leak chase region. This is because the leak chase passageways are formed from 1½"x 3" channels that are stronger than the concrete in which they are embedded. The primary objective of the bearing pad analysis is to show that this primarily compressive component remains in the elastic range.

The analyses are performed with ANSYS using finite element models, which place a bearing pad and rack pedestal directly above a leak chase location, and in areas of existing liner hold down plates. The liner hold down plates are approximately 1.75" in height above the liner. These configurations are selected with the intent of bounding all other possible bearing pad/pool floor interfaces. The analysis applies the maximum total vertical pedestal load from results for all bearing pads, scanned from the time-history solution from the SSE simulation. The maximum vertical pedestal load over a leakchase (which is modeled to remove a 3" wide strip of concrete from under the bearing pad) is found to be 299.2 kips on an effectively 14" x 13" bearing pad.

The bearing pads in the SFP will be 1.5" thick. All bearing pads will be made from austenitic stainless steel plate stock. In areas without liner hold down plates, which have existing 1.625" adapter pads, shims will be used to bring their height to 1.75". Bearing pad models were prepared to evaluate all possible configurations. Figure 6.9.1 provides an isometric of the controlling ANSYS finite element model (leak chase condition). The model permits the bearing pad to deform and lose contact with the liner, if the conditions of elastostatics so dictate. Figure 6.9.1 shows the bearing pad and underlying leak chase located within the supporting concrete. The slab is modeled as an elastic foundation. Figure 6.9.2 shows the stress profile in the underlying concrete computed by the ANSYS analysis.

The average pressure at the pad to liner interface is computed and compared against the above-mentioned limit. Calculations show that the average pressure at the slab / liner interface is 2,195 psi, which is well below the allowable value of 3,570 psi, providing a factor of safety of 1.63. The stress distribution in the bearing pad is also evaluated, with the results shown in Figure 6.9.3 (top and bottom views). The peak stress in the bearing pad during a Level D event is 40,098 psi. The material yield strength of 25,000 psi at 200°F provides an allowable stress of  $2 \times 0.9 \times S_y$  (i.e., 45,000 psi) producing a factor of safety against yield of about 1.12. Therefore, the bearing pad design devised for the VCSNS SFP is deemed appropriate for the prescribed loadings.

#### 6.10 Level A Evaluation

The Level A condition is not a governing condition for spent fuel racks since the general level of loading is far less than Level B or D loading. The stress allowable for Level B loading is only approximately 1/3 greater than the corresponding Level A stress allowable. The increase between Level A and B loading far exceeds this 1/3 value. Therefore Level A is acceptable by comparison.

#### 6.11 Hydrodynamic Loads on Pool Walls

The hydrodynamic pressures that develop between adjacent racks and the pool walls can be developed from the archived results produced by the WPMR analysis. Of the racks next to the SFP walls, the one that resulted in the maximum displacement generates the maximum hydrodynamic load on its adjacent wall. Time dependent hydrodynamic pressures are determined for subsequent analysis as discussed in Section 8.0. The pressure plots on the four walls of the SFP at the time of maximum (in absolute value) instantaneous hydrodynamic pressure for the SSE event are shown in Figure 6.11.1.

#### 6.12 Local Stress Considerations

This section presents the results of evaluations for the possibility of cell wall buckling and the secondary stresses produced by temperature effects.

### 6.12.1 Cell Wall Buckling

The allowable local buckling stresses in the fuel cell walls are obtained by using classical plate buckling analysis. The evaluation for cell wall buckling is based on the applied stress being uniform along the entire length of the cell wall. In the actual fuel rack, the compressive stress comes from consideration of overall bending of the rack structures during a seismic event, and as such is negligible at the rack top, and maximum at the rack bottom.

The critical buckling stress is determined to be 13,588 psi. The computed compressive stress in the cell wall, based on the R5 stress factor, is 10,198 psi. Therefore, there is a 24.9% margin of safety against local cell wall buckling.

### 6.12.2 Analysis of Welded Joints in the Racks

Cell-to-cell welded joints are examined under the loading conditions arising from thermal effects due to an isolated hot cell in this subsection. This secondary stress condition is evaluated alone and not combined with primary stresses from other load conditions.

A thermal gradient between cells will develop when an isolated storage location contains a fuel assembly emitting maximum postulated heat, while surrounding locations are empty. We obtain a conservative estimate of weld stresses along the length of an isolated hot cell by considering a beam strip uniformly heated by 75°F, and restrained from growth along one long edge. This temperature rise is based on thermal-hydraulic evaluations discussed in Section 5.0, which show that a conservative upper bound for the difference between local cell maximum temperatures and the bulk temperature in the pool is less than 45°F. The analyzed configuration is shown in Figure 6.12.1.

Using shear beam theory, as discussed in Holtec generic calculation HI-89330 [6.9.3], and subjecting the strip to a uniform temperature rise  $\Delta T = 75^\circ\text{F}$ , we can calculate an estimate of the maximum value of the average shear stress in the strip. The strip is subjected to the following boundary conditions.

- a. Displacement  $U_x(x,y) = 0$  at  $x = 0$ , at  $y = H$ , all  $x$ .
- b. Average force  $M_x$ , acting on the cross section  $Ht = 0$  at  $x = l$ , all  $y$ .

The final result for wall shear stress, maximum at  $x = 1$ , is found to be given as

$$\tau_{\max} = \frac{E\alpha\Delta T}{0.931}$$

where  $E = 27.6 \times 10^6$  psi,  $\alpha = 9.5 \times 10^{-6}$  in/in °F and  $\Delta T = 75^\circ\text{F}$ .

Therefore, we obtain an estimate of maximum weld shear stress in an isolated hot cell, due to thermal gradient, as

$$\tau_{\max} = 21,122 \text{ psi}$$

Since this is a secondary thermal stress, we use the allowable shear stress criteria for faulted conditions ( $0.42 \cdot S_u = 27,804$  psi) as a guide to indicate that this maximum shear is acceptable. Therefore, there is a margin of safety of 24% against cell wall shear failure due to secondary thermal stresses from cell wall growth under the worst case hot cell conditions.

## 6.13 References

- [6.1.1] USNRC NUREG-0800, Standard Review Plan, June 1987.
- [6.1.2] (USNRC Office of Technology) "OT Position for Review and Acceptance of Spent Fuel Storage and Handling Applications", dated April 14, 1978, and January 18, 1979 amendment thereto.
- [6.2.1] Soler, A.I. and Singh, K.P., "Seismic Responses of Free Standing Fuel Rack Constructions to 3-D Motions", Nuclear Engineering and Design, Vol. 80, pp. 315-329 (1984).
- [6.2.2] Soler, A.I. and Singh, K.P., "Some Results from Simultaneous Seismic Simulations of All Racks in a Fuel Pool", INNEM Spent Fuel Management Seminar X, January, 1993.
- [6.2.3] Singh, K.P. and Soler, A.I., "Seismic Qualification of Free Standing Nuclear Fuel Storage Racks - the Chin Shan Experience, Nuclear Engineering International, UK (March 1991).
- [6.2.4] Holtec Proprietary Report HI-961465 - WPMR Analysis User Manual for Pre&Post Processors & Solver, August, 1997.
- [6.4.1] Holtec Proprietary Report HI-89364 - Verification and User's Manual for Computer Code GENEQ, January, 1990.
- [6.5.1] Rabinowicz, E., "Friction Coefficients of Water Lubricated Stainless Steels for a Spent Fuel Rack Facility," MIT, a report for Boston Edison Company, 1976.
- [6.5.2] Singh, K.P. and Soler, A.I., "Dynamic Coupling in a Closely Spaced Two-Body System Vibrating in Liquid Medium: The Case of Fuel Racks," 3rd International Conference on Nuclear Power Safety, Keswick, England, May 1982.

- [6.5.3] Fritz, R.J., "The Effects of Liquids on the Dynamic Motions of Immersed Solids," Journal of Engineering for Industry, Trans. of the ASME, February 1972, pp 167-172.
- [6.5.4] Levy, S. and Wilkinson, J.P.D., "The Component Element Method in Dynamics with Application to Earthquake and Vehicle Engineering," McGraw Hill, 1976.
- [6.5.5] Paul, B., "Fluid Coupling in Fuel Racks: Correlation of Theory and Experiment", (Proprietary), NUSCO/Holtec Report HI-88243.
- [6.6.1] ASME Boiler & Pressure Vessel Code, Section III, Subsection NF, 1989 Edition.
- [6.6.2] ASME Boiler & Pressure Vessel Code, Section III, Appendices, 1989 Edition.
- [6.8.1] Chun, R., Witte, M. and Schwartz, M., "Dynamic Impact Effects on Spent Fuel Assemblies," UCID-21246, Lawrence Livermore National Laboratory, October 1987.
- [6.9.1] ACI 349-85, Code Requirements for Nuclear Safety Related Concrete Structures, American Concrete Institute, Detroit, Michigan, 1985.
- [6.9.2] ACI 318-95, Building Code requirements for Structural Concrete," American Concrete Institute, Detroit, Michigan, 1995.
- [6.9.3] Holtec report HI-89330, Rev. 1, "A Seismic Analysis of High Density Fuel Racks; Part III: Structural Design Calculations - Theory."

Table 6.2.1

## PARTIAL LISTING OF FUEL RACK APPLICATIONS USING DYNARACK

PLANT	DOCKET NUMBER(s)	YEAR
Enrico Fermi Unit 2	USNRC 50-341	1980
Quad Cities 1 & 2	USNRC 50-254, 50-265	1981
Rancho Seco	USNRC 50-312	1982
Grand Gulf Unit 1	USNRC 50-416	1984
Oyster Creek	USNRC 50-219	1984
Pilgrim	USNRC 50-293	1985
V.C. Summer	USNRC 50-395	1984
Diablo Canyon Units 1 & 2	USNRC 50-275, 50-323	1986
Byron Units 1 & 2	USNRC 50-454, 50-455	1987
Braidwood Units 1 & 2	USNRC 50-456, 50-457	1987
Vogtle Unit 2	USNRC 50-425	1988
St. Lucie Unit 1	USNRC 50-335	1987
Millstone Point Unit 1	USNRC 50-245	1989
Chinshan	Taiwan Power	1988
D.C. Cook Units 1 & 2	USNRC 50-315, 50-316	1992
Indian Point Unit 2	USNRC 50-247	1990
Three Mile Island Unit 1	USNRC 50-289	1991
James A. FitzPatrick	USNRC 50-333	1990
Shearon Harris Unit 2	USNRC 50-401	1991
Hope Creek	USNRC 50-354	1990
Kuosheng Units 1 & 2	Taiwan Power Company	1990

Table 6.2.1

## PARTIAL LISTING OF FUEL RACK APPLICATIONS USING DYNARACK

PLANT	DOCKET NUMBER(s)	YEAR
Ulchin Unit 2	Korea Electric Power Co.	1990
Laguna Verde Units 1 & 2	Comision Federal de Electricidad	1991
Zion Station Units 1 & 2	USNRC 50-295, 50-304	1992
Sequoyah	USNRC 50-327, 50-328	1992
LaSalle Unit 1	USNRC 50-373	1992
Duane Arnold Energy Center	USNRC 50-331	1992
Fort Calhoun	USNRC 50-285	1992
Nine Mile Point Unit 1	USNRC 50-220	1993
Beaver Valley Unit 1	USNRC 50-334	1992
Salem Units 1 & 2	USNRC 50-272, 50-311	1993
Limerick	USNRC 50-352, 50-353	1994
Ulchin Unit 1	KINS	1995
Yonggwang Units 1 & 2	KINS	1996
Kori-4	KINS	1996
Connecticut Yankee	USNRC 50-213	1996
Angra Unit 1	Brazil	1996
Sizewell B	United Kingdom	1996
Waterford 3	USNRC 50-382	1997
J.A. Fitzpatrick	USNRC 50-333	1998
Callaway	USNRC 50-483	1998
Nine Mile Unit 1	USNRC 50-220	1998

Table 6.2.1

## PARTIAL LISTING OF FUEL RACK APPLICATIONS USING DYNARACK

PLANT	DOCKET NUMBER(s)	YEAR
Chin Shan	Taiwan Power Company	1998
Vermont Yankee	USNRC 50-271	1998
Millstone 3	USNRC 50-423	1998
Byron/Braidwood	USNRC 50-454, 50-455, 50-567, 50-457	1999
Wolf Creek	USNRC 50-482	1999
Plant Hatch Units 1 & 2	USNRC 50-321, 50-366	1999
Harris Pools C and D	USNRC 50-401	1999
Davis-Besse	USNRC 50-346	1999
Enrico Fermi Unit 2	USNRC 50-341	2000
Kewaunee	USNRC 50-305	2001

Table 6.3.1 RACK MATERIAL DATA (200°F) (ASME - Section II, Part D)			
Stainless Steel Material	Young's Modulus E (psi)	Yield Strength S <sub>y</sub> (psi)	Ultimate Strength S <sub>u</sub> (psi)
SA240, Type 304L (cell boxes)	27.6 x 10 <sup>6</sup>	21,300	66,200
SUPPORT MATERIAL DATA (200°F)			
SA240, Type 304L (upper part of support feet)	27.6 x 10 <sup>6</sup>	21,300	66,200
SA-564-630 (lower part of support feet; age hardened at 1100°F)	28.5 x 10 <sup>6</sup>	106,300	140,000
SA240, Type 304 (Bearing Pads)	27.6 x 10 <sup>6</sup>	25,000	71,000

Table 6.4.1 TIME-HISTORY STATISTICAL CORRELATION RESULTS	
OBE	
Data1 to Data2	0.067
Data1 to Data3	0.044
Data2 to Data3	0.068
SSE	
Data1 to Data2	0.037
Data1 to Data3	0.026
Data2 to Data3	0.065

Data1 corresponds to the time-history acceleration values along the X axis (South)

Data2 corresponds to the time-history acceleration values along the Y axis (East)

Data3 corresponds to the time-history acceleration values along the Z axis (Vertical)

Table 6.5.1

Degrees-of-freedom

LOCATION (Node)	DISPLACEMENT			ROTATION		
	$U_x$	$U_y$	$U_z$	$\theta_x$	$\theta_y$	$\theta_z$
1	$p_1$	$p_2$	$p_3$	$q_4$	$q_5$	$q_6$
2	$p_{17}$	$p_{18}$	$p_{19}$	$q_{20}$	$q_{21}$	$q_{22}$
<p>Node 1 is assumed to be attached to the rack at the bottom most point.                      Node 2 is assumed to be attached to the rack at the top most point.                      Refer to Figure 6.5.1 for node identification.</p>						
2*	$p_7$	$p_8$				
3*	$p_9$	$p_{10}$				
4*	$p_{11}$	$p_{12}$				
5*	$p_{13}$	$p_{14}$				
1*	$p_{15}$	$p_{16}$				
<p>where the relative displacement variables <math>q_i</math> are defined as:</p> $p_i = q_i(t) + U_x(t) \quad i = 1,7,9,11,13,15,17$ $= q_i(t) + U_y(t) \quad i = 2,8,10,12,14,16,18$ $= q_i(t) + U_z(t) \quad i = 3,19$ $= q_i(t) \quad i = 4,5,6,20,21,22$ <p><math>p_i</math> denotes absolute displacement with respect to inertial space  <math>q_i</math> denotes relative rotation with respect to the floor slab</p> <p>* denotes fuel mass nodes  <math>U(t)</math> are the three known earthquake displacements</p>						

Table 6.9.1 COMPARISON OF BOUNDING CALCULATED LOADS/STRESSES VS. CODE ALLOWABLES AT IMPACT LOCATIONS AND AT WELDS		
Item/Location	SSE or OBE <sup>†</sup>	
	Calculated	Allowable
Fuel assembly/cell wall impact, lbf.	743 *	2,866 <sup>††</sup> *
Rack/baseplate weld, psi	18,474	19,860
Female pedestal/baseplate weld, psi	32,051*	35,748*
Cell/cell welds, psi <sup>†††</sup>	8,325 *	8,520

<sup>†</sup> Loads and Allowables given are for the more limiting of OBE or SSE (When applicable to SSE case, it is denoted by an asterisk, \*).

<sup>††</sup> Based on the limit load for a cell wall. The allowable load on the fuel assembly itself may be less than this value (see discussion in Section 6.8.4.3), but is greater than 743 lbs.

<sup>†††</sup> Calculated value is based on the cell wall base metal stresses resulting from fuel impacts conservatively added to cell wall stresses resulting from the maximum shear flow developed between two adjacent cells, both under SSE conditions. The allowable value is conservatively based on the Level A condition cell wall material shear stress allowable of  $0.4 \cdot F_y$ .

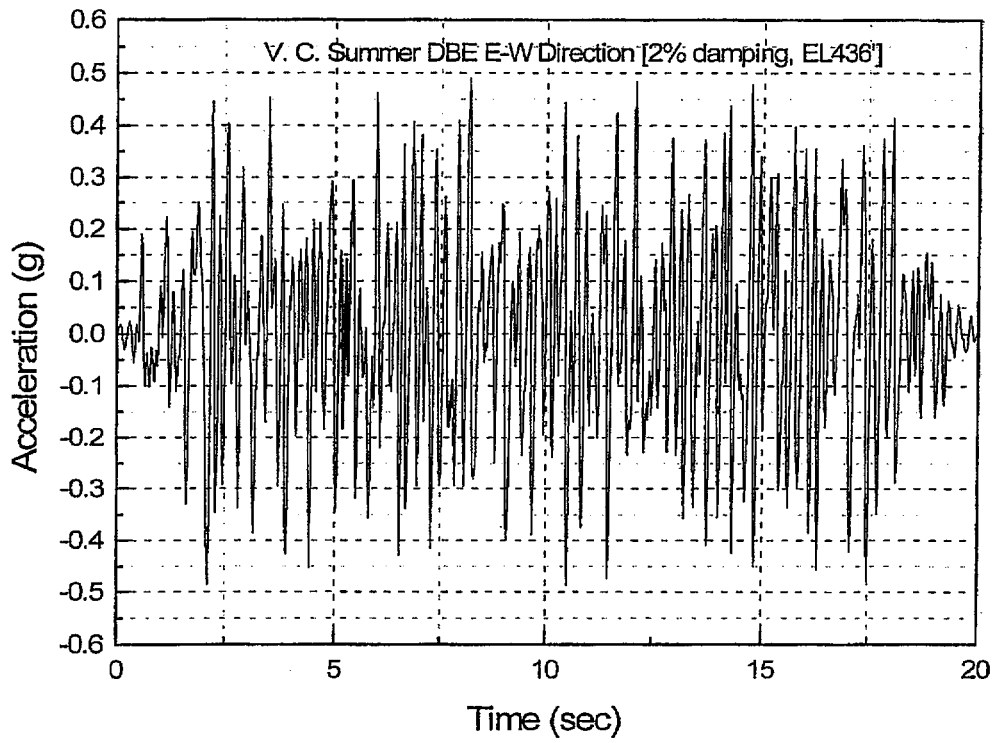


Figure 6.4.1 East-West Accelerogram (SSE)

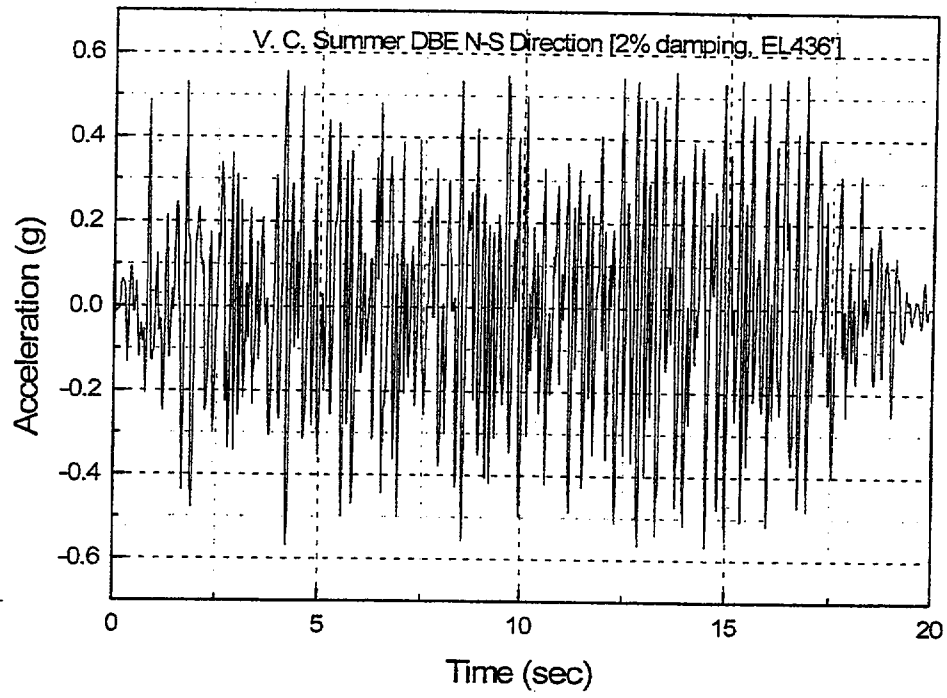


Figure 6.4.2 North-South Accelerogram (SSE)

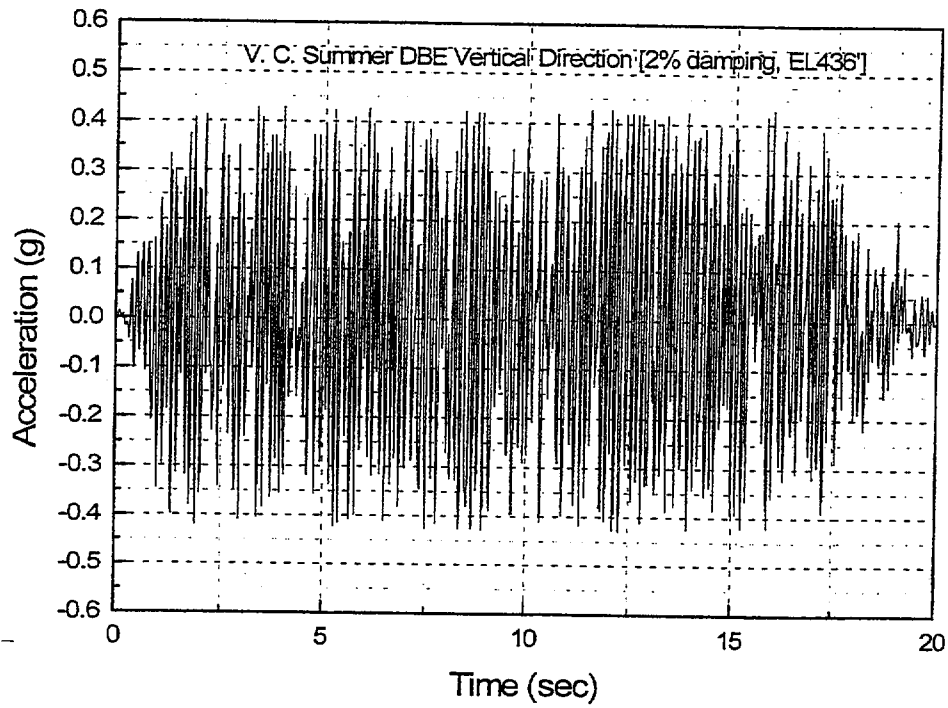


Figure 6.4.3 Vertical Accelerogram (SSE)

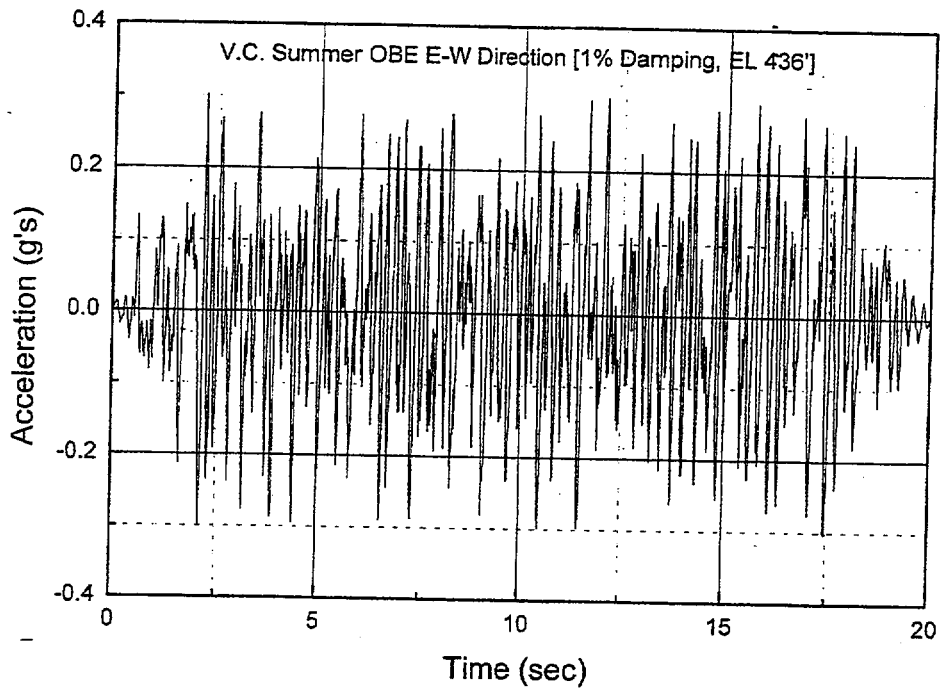


Figure 6.4.4 East-West Accelerogram (OBE)

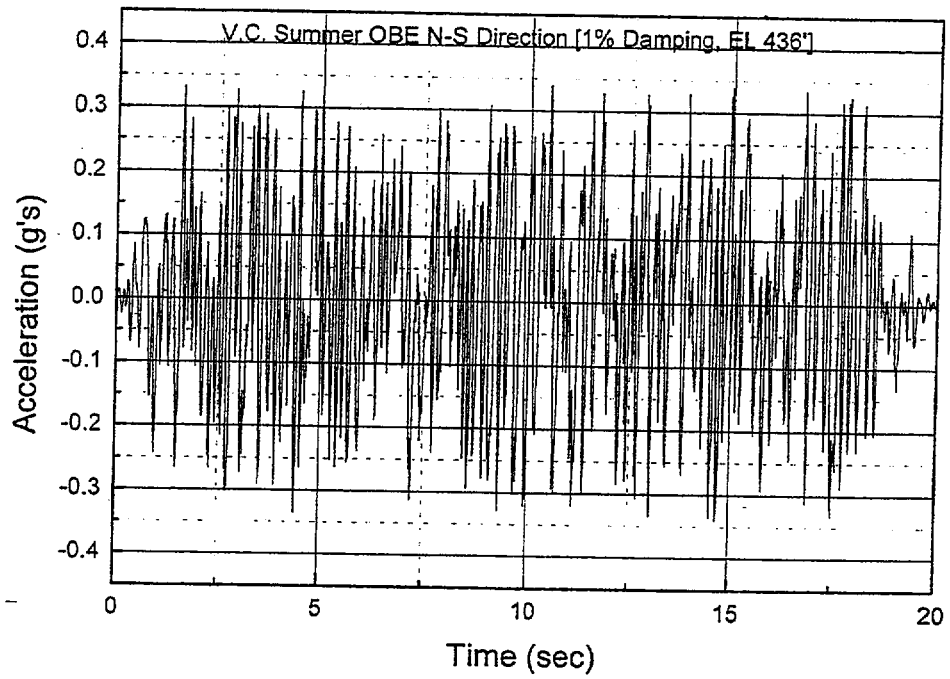


Figure 6.4.5 North-South Accelerogram (OBE)

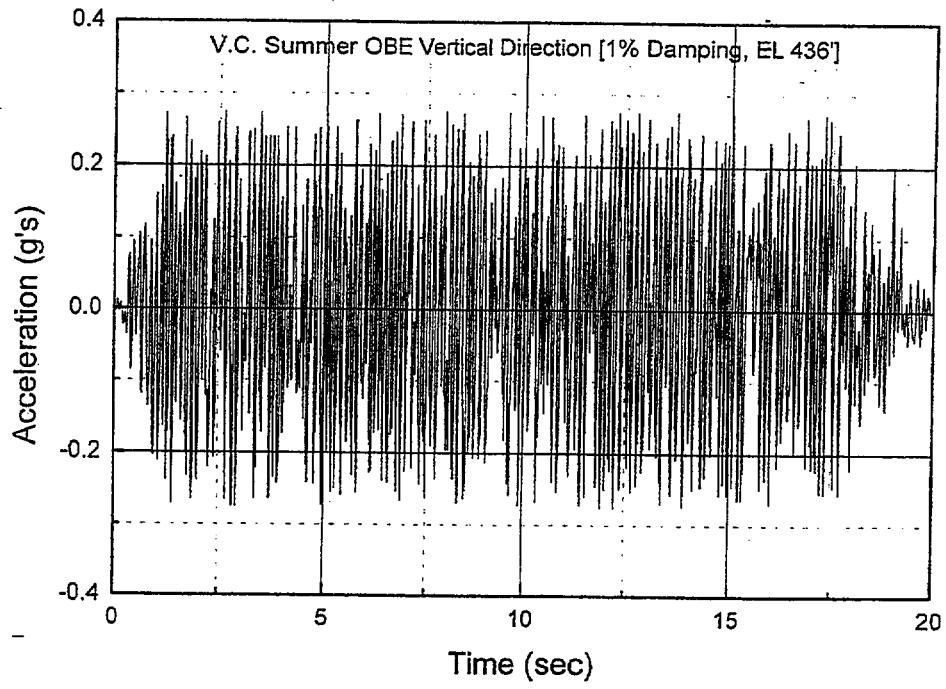


Figure 6.4.6 Vertical Accelerogram (OBE)

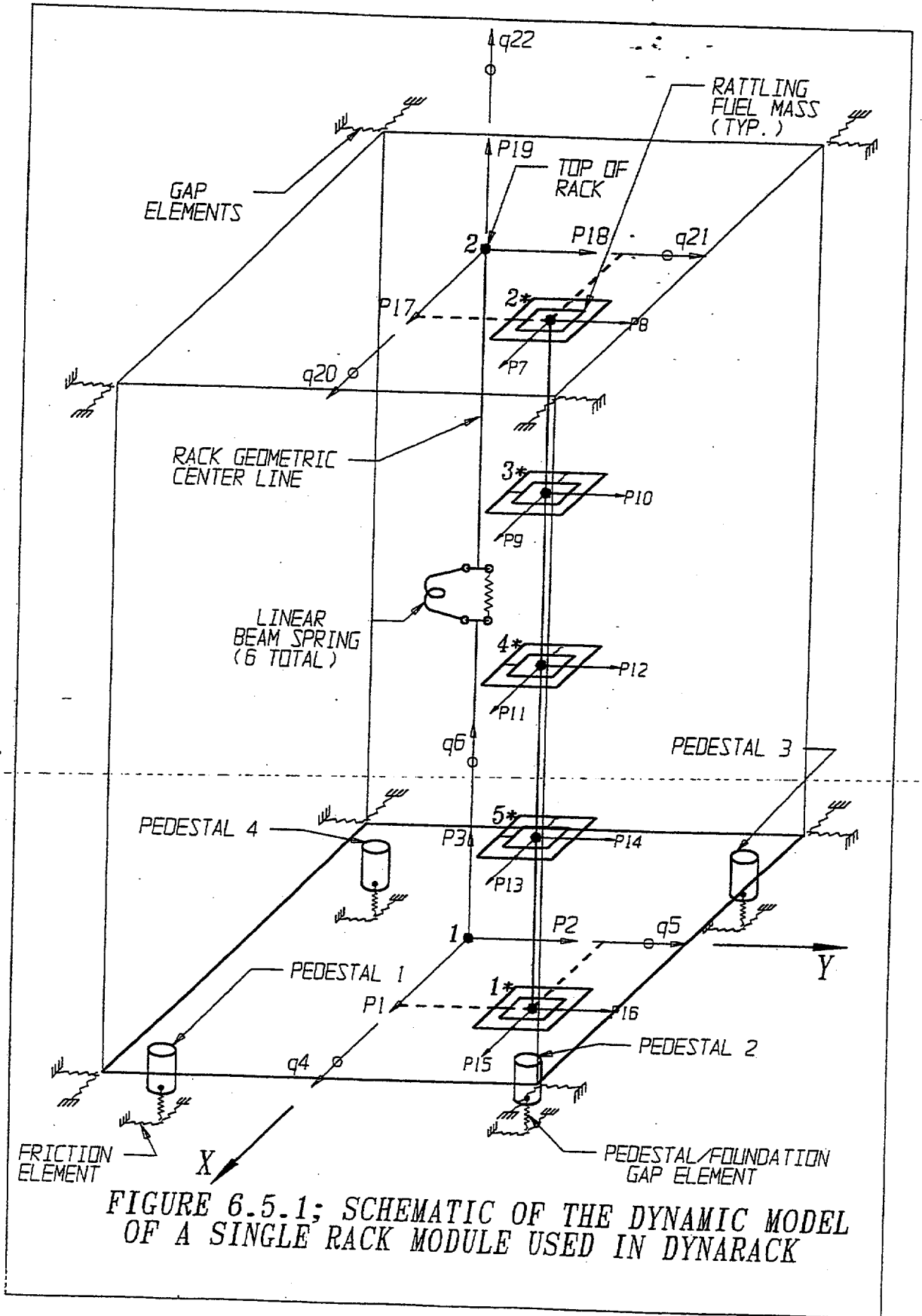


FIGURE 6.5.1; SCHEMATIC OF THE DYNAMIC MODEL OF A SINGLE RACK MODULE USED IN DYNARACK

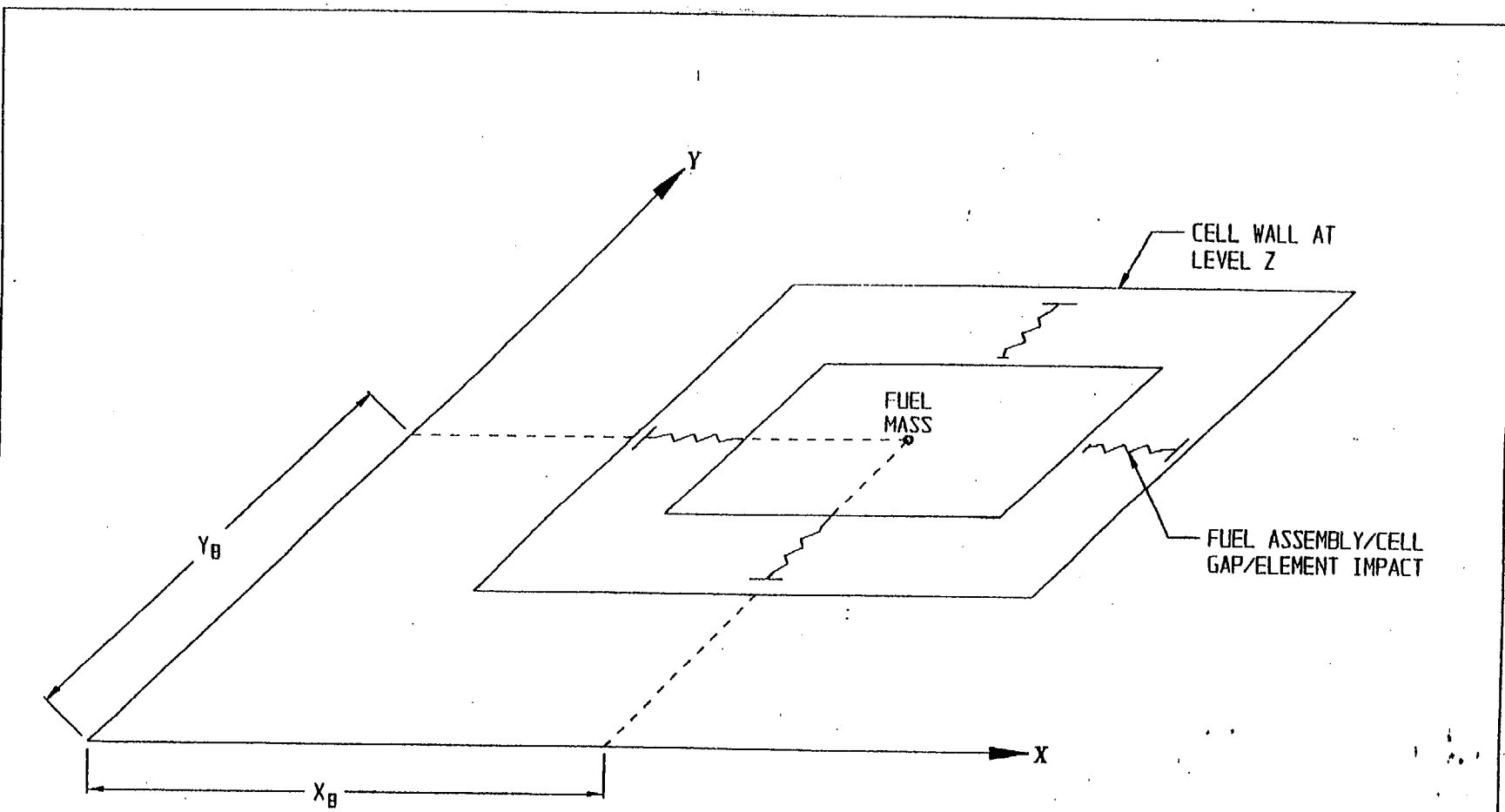


FIGURE 6.5.2 FUEL-TO-RACK GAP/IMPACT ELEMENTS AT LEVEL OF RATTLING MASS

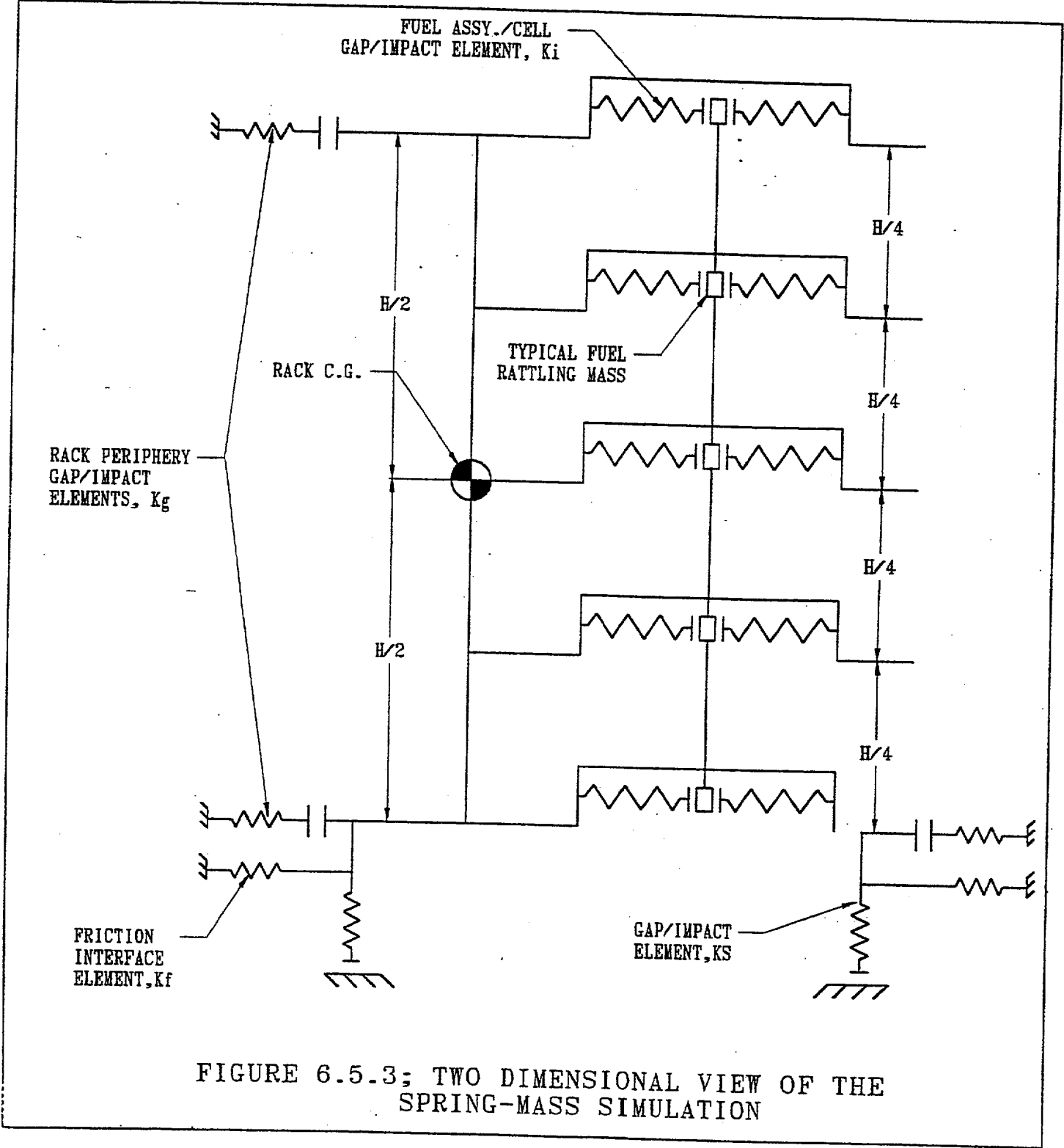
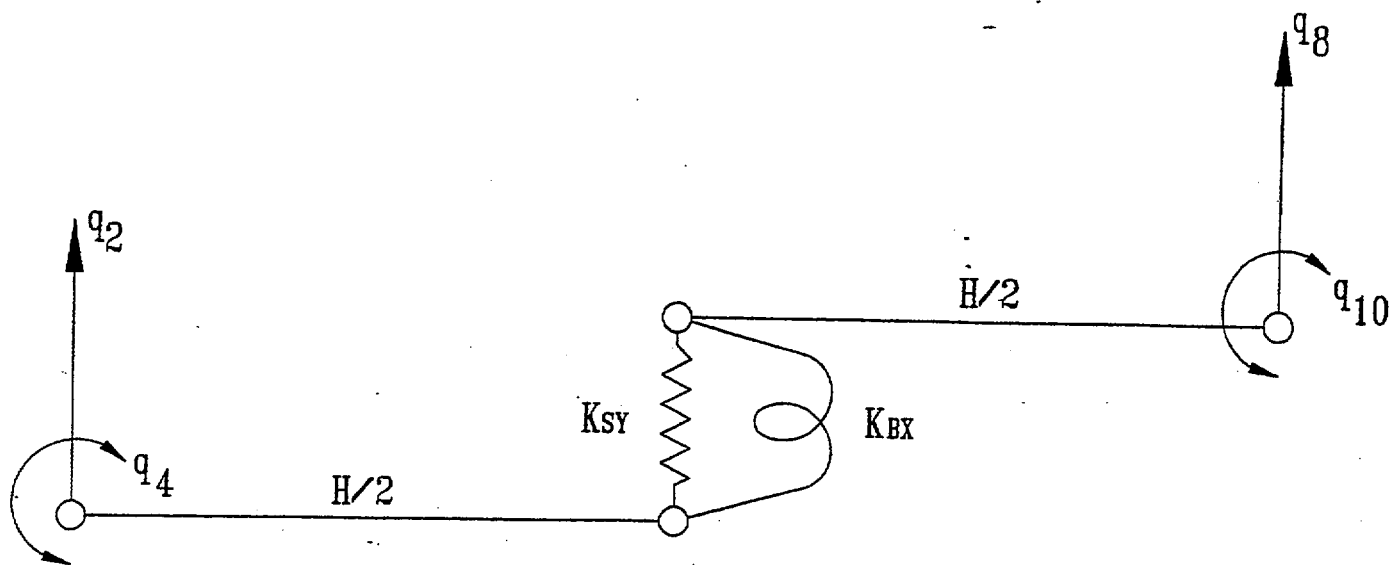
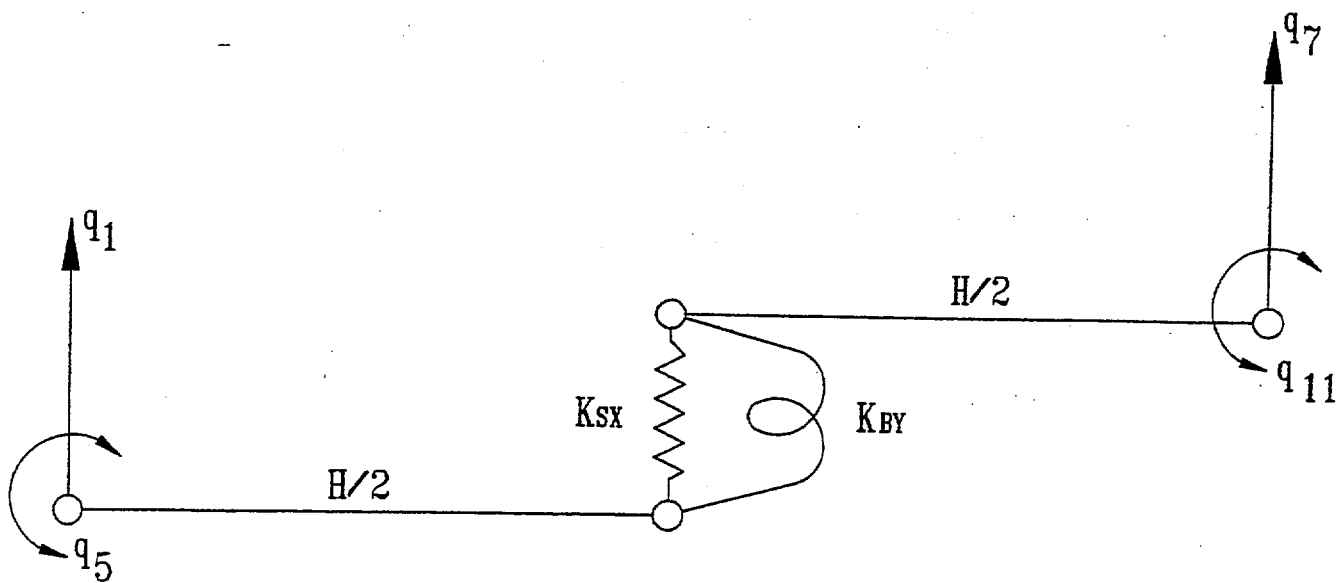


FIGURE 6.5.3; TWO DIMENSIONAL VIEW OF THE SPRING-MASS SIMULATION



FOR Y-Z PLANE BENDING



FOR X-Z PLANE BENDING

FIGURE 6.5.4; RACK DEGREES-OF-FREEDOM WITH SHEAR AND BENDING SPRINGS

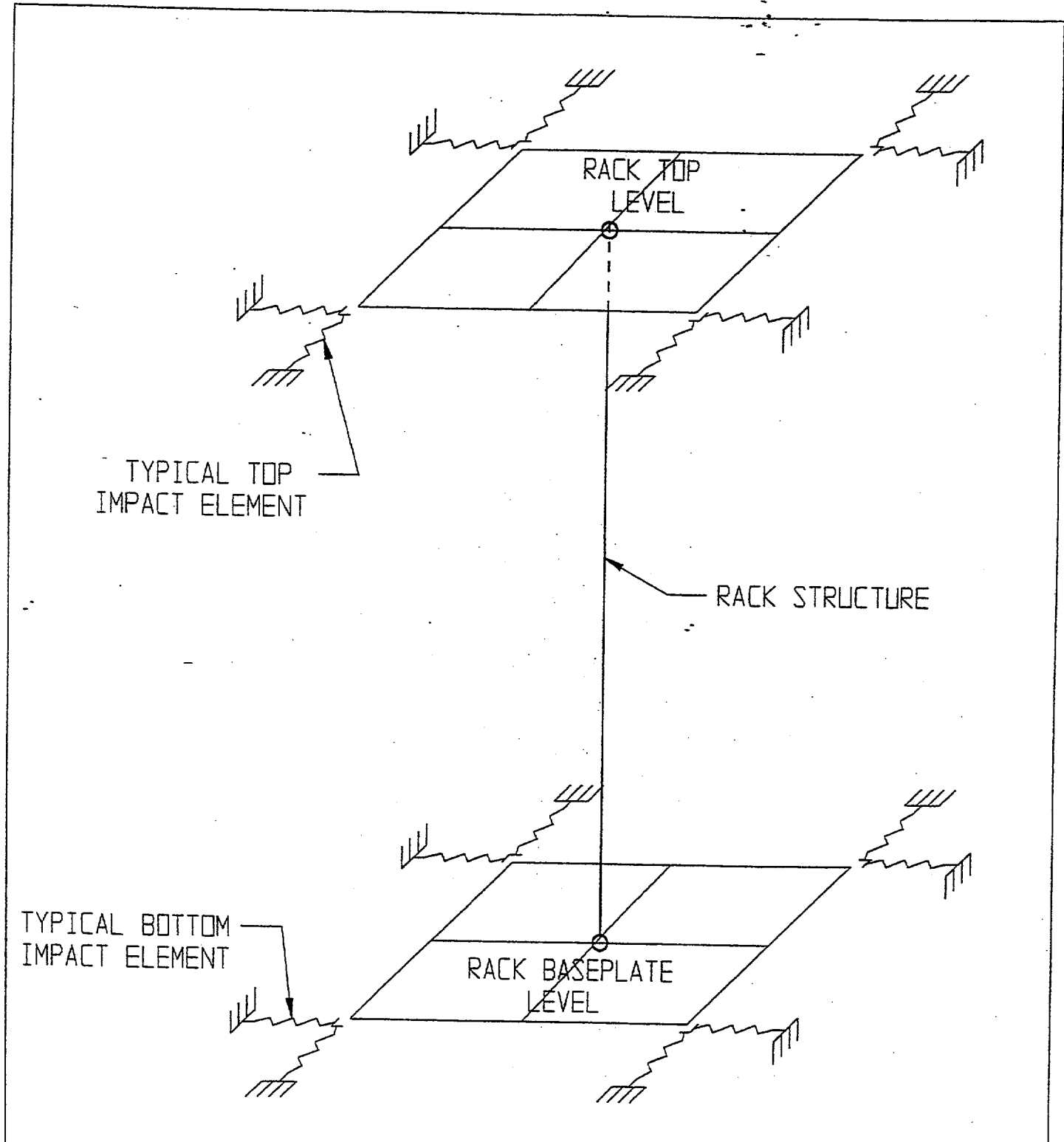


FIGURE 6.5.5; RACK PERIPHERY GAP/IMPACT ELEMENTS

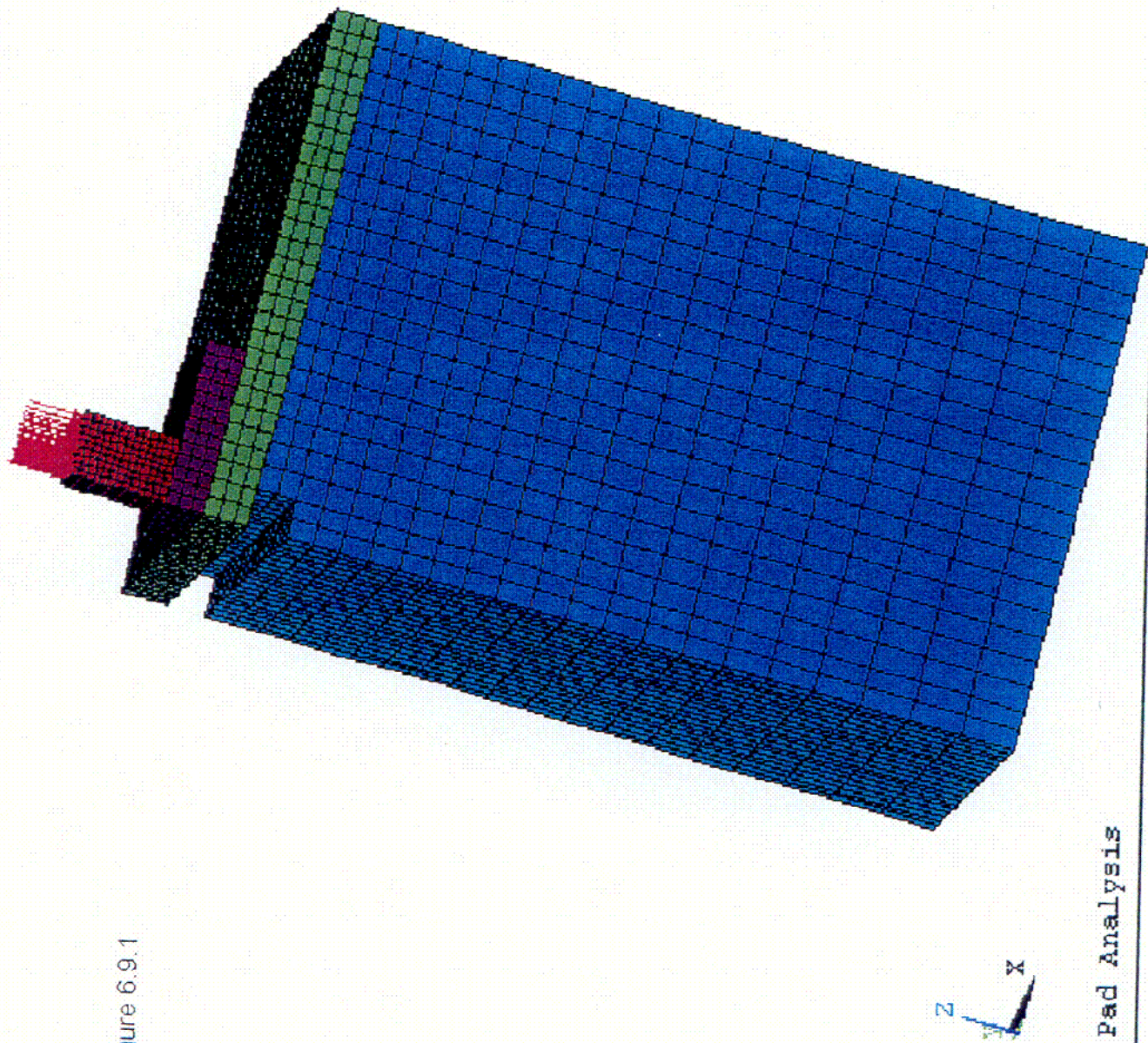


Figure 6.9.1

Bearing Pad Analysis

60

```

ANSYS 5.6
APR  4 2001
09:53:41
MODAL SOLUTION
STEP=1
SUB =1
TIME=1
SZ      (AVG)
RSYS=0
PowerGraphics
EFACET=1
AVRES=Mat
DMX =.012368
SMM =-9238
SMX =33.437

```

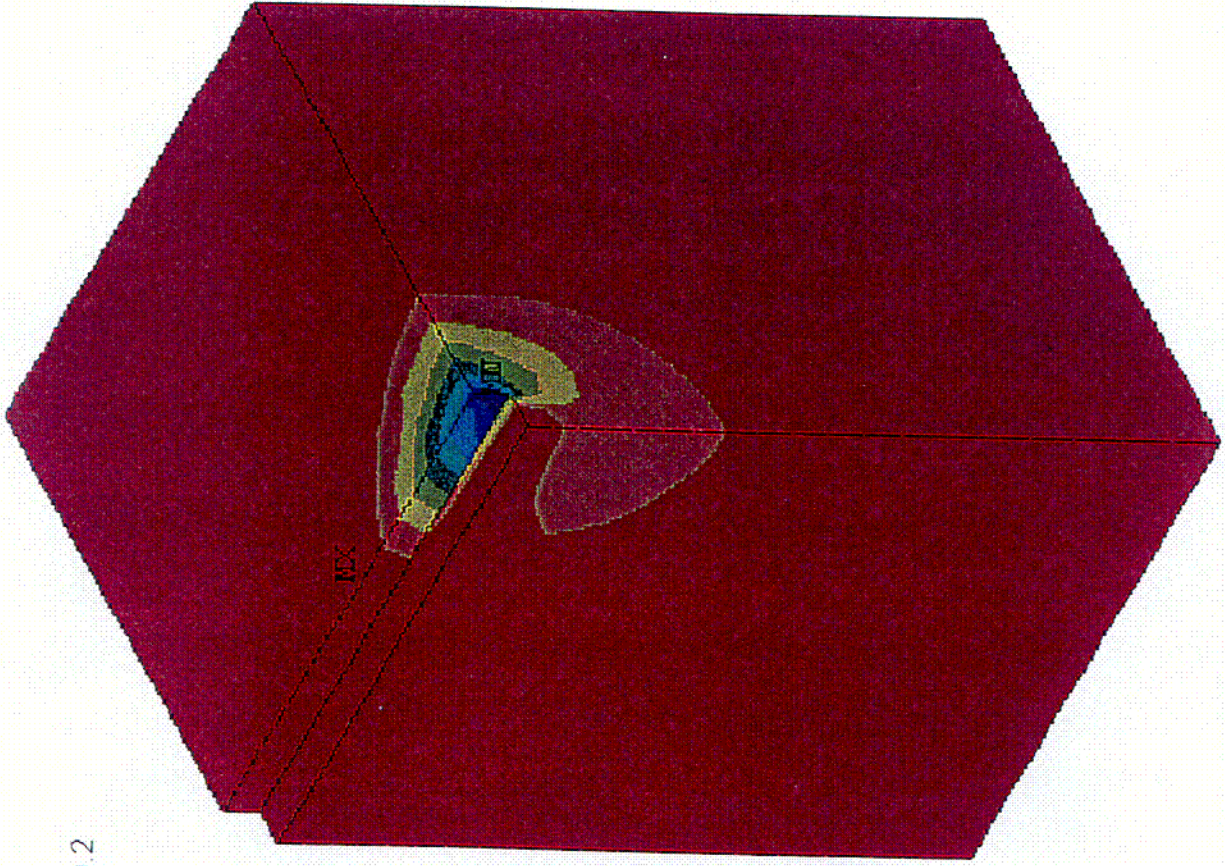
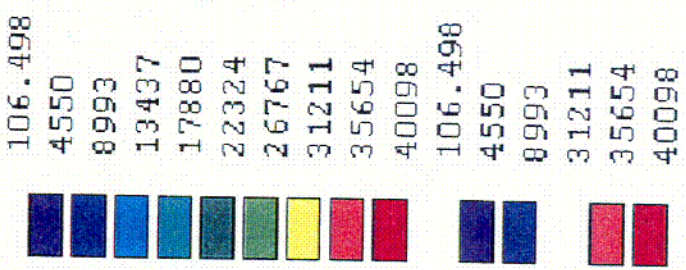


Figure 6.9.2

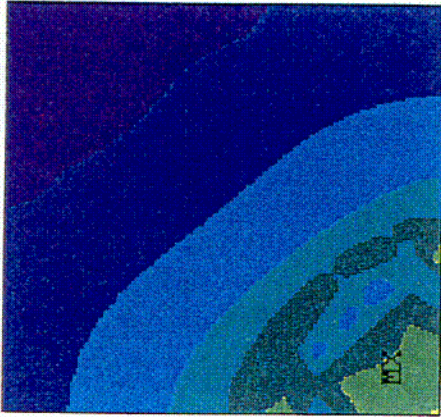
Bearing Pad Analysis

02

ANSYS 5.6  
 APR 4 2001  
 10:47:08  
 NODAL SOLUTION  
 STEP=1  
 SUB =1  
 TIME=1  
 SINT (AVG)  
 PowerGraphics  
 EFACET=1  
 AVRES=Mat  
 DMX =.01785  
 SMN =106.498  
 SMX =40098



MM

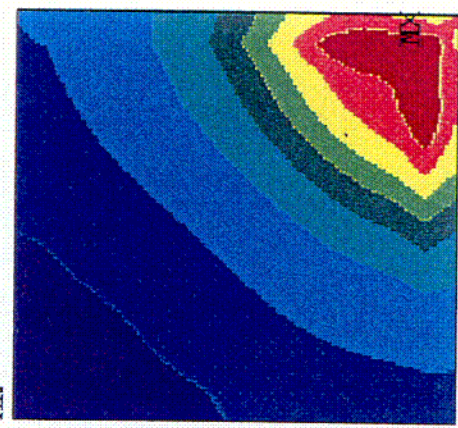


Top



Figure 6.9.3

MM



Bottom



C03

Bearing Pad Analysis

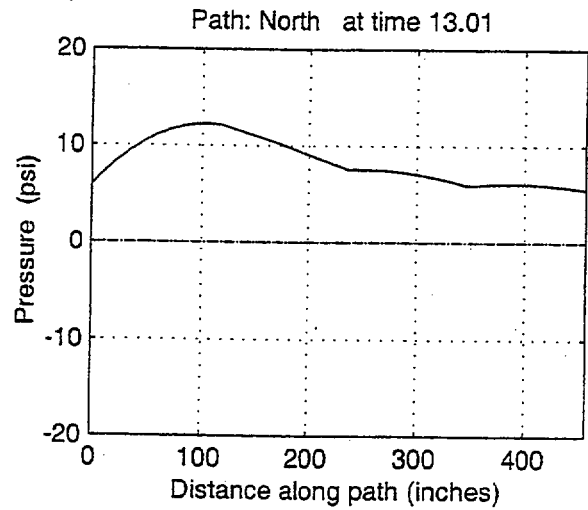
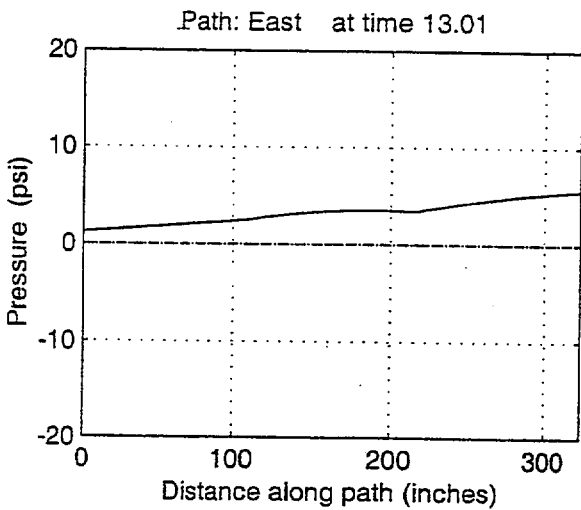
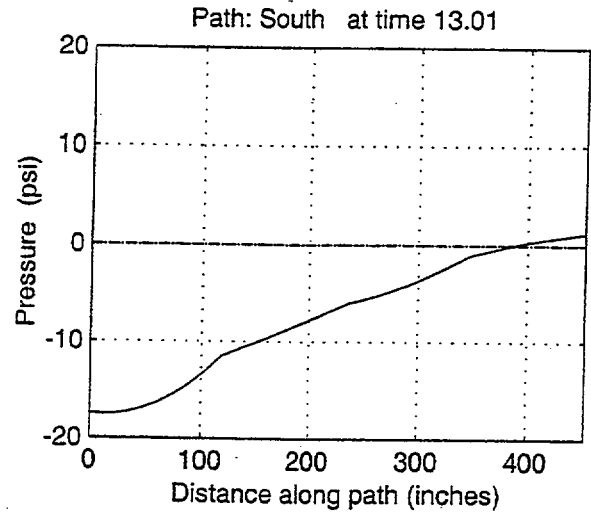
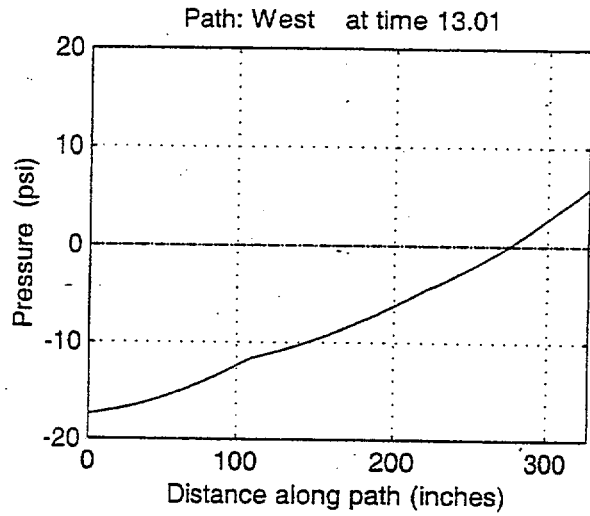


**Figure 6.11.1**  
**Hydrodynamic Pressure Plots**  
**at Time of Maximum Absolute Value for SSE**

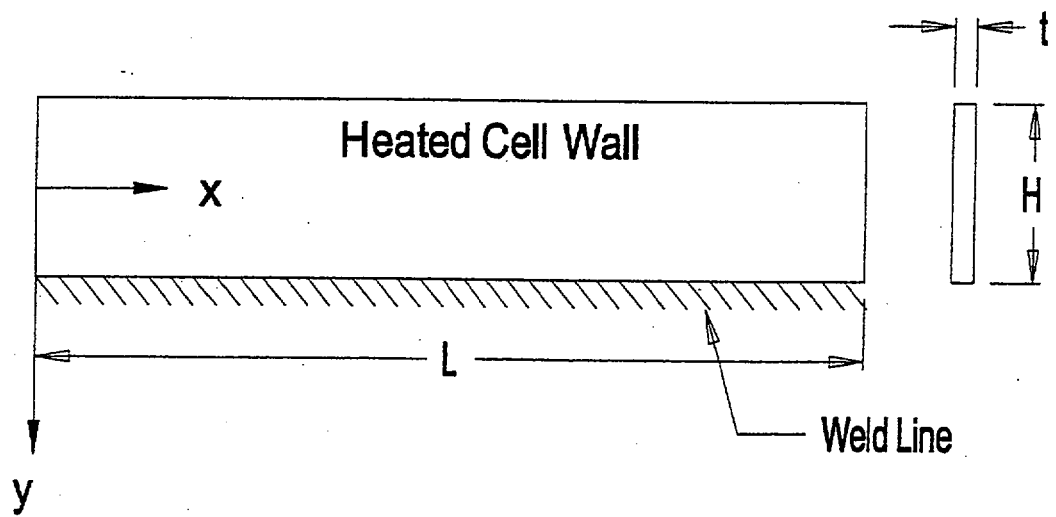


FIGURE 6.12.1; WELDED JOINT IN RACK

## 7.0 MECHANICAL ACCIDENTS

### 7.1 Introduction

The USNRC OT position paper [7.1.1] specifies that the design of the rack must ensure the functional integrity of the spent fuel racks under all credible fuel assembly drop events.

This chapter contains synopses of the analyses carried out to demonstrate the regulatory compliance of the proposed racks under postulated accidental drop events germane to the fuel pools; namely, that of a fuel assembly and a fuel rack.

The proposed change does not impact assumptions in the current licensing basis on the potential fuel damage due to mechanical accidents.

### 7.2 Description of Mechanical Accidents

Several categories of accidental drop events are considered. Analyses are performed to evaluate the racks subsequent to a fuel assembly impact under various fuel assembly drop scenarios. The spent fuel pool floor is evaluated for fuel and rack drop accidents.

In the so-called “shallow” drop event, a fuel assembly, along with the portion of handling tool, which is severable in the case of a single element failure, is assumed to drop vertically and hit the top of the rack. Inasmuch as the new racks are of honeycomb construction, the deformation produced by the impact is expected to be confined to the region of collision. However, the “depth” of damage to the affected cell walls must be demonstrated to remain limited to the portion of the cell above the top of the “active fuel region”, which is essentially the elevation of the top of the Boron neutron absorber. Stated in qualitative terms, this criterion implies that the plastic deformation of the rack cell walls should not extend more than 19 inches (downwards) from the top. In order to utilize an upper bound of kinetic energy at impact, the impactor is assumed to weigh 2,000 lbs and the free-fall height is conservatively assumed to be 24 inches [7.1.2], which is greater than the maximum possible free-fall height.

It is readily apparent from the description of the rack modules in Section 3 that the impact resistance of a rack at its periphery is considerably less than its interior. Accordingly, the limiting shallow drop scenario, which would produce maximum cell wall deformation, consists of the case where the fuel assembly impacts the peripheral cell wall, as shown in Figure 7.2.1.

The second class of fuel drop event postulates that the impactor falls through an empty storage cell impacting the fuel assembly support surface (i.e., rack baseplate). This so-called “deep” drop event threatens the structural integrity of the baseplate. If the baseplate is pierced, and fuel assembly impacts the pool liner, then an abnormal condition of the enriched zone of fuel assembly outside the “poisoned” space of the fuel rack may develop. To preclude damage to the pool liner and to avoid the potential of an abnormal fuel storage configuration in the aftermath of a deep drop event, it is required that the baseplate remain unpierced and that the maximum lowering of the baseplate is shown to be acceptable by the criticality evaluations.

The deep drop event can be classified into two scenarios, namely, drop in an interior cell away from the support pedestal, as shown in Figure 7.2.2, and drop through cell located above a support leg, as shown in Figure 7.2.3. In deep drop scenario 1, the fuel assembly impacts the baseplate away from the support pedestal, where it is more flexible. Severing or large deflection of the baseplate leading to a secondary impact with the pool liner are unacceptable results. In deep drop scenario 2, the baseplate is buttressed by the support pedestal and presents a hardened impact surface, resulting in a high load. The principal design objective is to ensure that the support pedestal does not tear the liner that overlays the reinforced concrete pool slab.

In the third type of drop event, a rack is assumed to drop 45 feet and hits the liner plate, as shown in Figure 7.2.4. The total weight of the heaviest rack in the pool (36,300 lbs, 11×11 cells) and the rack handling tools (with a bounding weight of 2,400 lbs) is used for the rack drop analysis. The structural integrity of the concrete floor must be demonstrated to be maintained in the rack drop event and the effect on the liner plate is also evaluated. The acceptance criterion is that catastrophic pool structure damage, such that there is uncontrollable loss of pool water inventory, is not allowed.

### 7.3 Incident Impact Velocity

#### 7.4 Mathematical Model

In the first step of the solution process, the velocity of the dropped object (impactor) is computed for the condition of underwater free fall in the manner of the formulation presented in the above section. Table 7.4.1 contains the computed velocities for the various drop events.

## 7.5 Results

### 7.5.1 Shallow Drop Event

For the shallow drop event, the dynamic analysis shows that the top of the impacted region undergoes localized plastic deformation. Figure 7.5.1 shows an isometric view of the post-impact geometry of the rack. The maximum depth of plastic deformation is limited to 10 inches, which is below the design limit of 19 inches.

### 7.5.2 Deep Drop Events

The deep drop through an interior cell does produce some deformation of the baseplate with no severing of the baseplate/cell wall welds. Figure 7.5.2 shows the deformed baseplate configuration. The fuel assembly support surface is lowered by a maximum of 2.55 inches, which is much less than the distance of 5.5 inches from the baseplate to the liner. Therefore, the pool liner will not be contacted by the deformed baseplate. The deformation of the baseplate has been determined to be acceptable with respect to lowering the fuel seating position and the resulting criticality consequences, as discussed in Chapter 4.0.

The deep drop event wherein the impact region is located above the support pedestal is found to produce a maximum stress of 20,753 psi in the liner, which is less than the failure limit stress of 71 ksi for the liner material, as shown in Figure 7.5.3. However, the maximum compressive stress of 6,735.1 psi in the concrete slab is larger than the concrete compressive strength of 3,000 psi, as shown in Figure 7.5.4. The concrete is locally crushed, but substantial damage to the pool slab is not indicated. Therefore, there will be no abrupt or uncontrollable loss of water from the fuel pool.

### 7.5.3 Rack Drop Event

The liner plate is locally damaged in the heaviest rack drop accident as shown in Figure 7.5.5, indicating that there may be consequent water leakage across the liner that will be controlled by the concrete pool structure. The maximum compressive stress in the concrete slab is shown to be 22,044 psi in Figure 7.5.6, which is much higher than the concrete compressive strength of 3,000 psi. However, the stress contour plot shows that the rack drop accident would crush the concrete only locally. Analyses on the integrity of the pool slab indicate that a primary failure in the spent fuel pool structure will not occur.

### 7.6 Conclusion

The drop events postulated for the V.C. Summer spent fuel pool were analyzed and found to produce localized damage well within the design limits for the racks. The shallow drop event is found to produce some localized plastic deformation in the top of the storage cell, but the region of permanent strain is limited to the portion of the rack structure situated above the top of the active fuel region. The analysis of the deep drop event at cell locations selected to maximize baseplate deformation indicates that the downward displacement of the baseplate is limited to 2.55 inches, which ensures that a secondary impact of the fuel assembly with the pool liner would not occur. The deep drop case analyzed for the scenario to produce maximum pedestal force indicates that the pedestal axial load is sufficiently small to preclude liner damage. Rack drop analysis (in a construction accident scenario) shows that, although the liner is locally damaged, the concrete slab can maintain its structural integrity under the postulated impact of the heaviest rack in the pool. Only local concrete crushing is observed. Therefore, there will be no uncontrollable loss of pool water inventory. In conclusion, the new Holtec high-density spent fuel racks for the V.C. Summer pool possess acceptable margins of safety under the postulated mechanical accidents.

7.7 References for Chapter 7.0

[7.1.1] "OT Position for Review and Acceptance of Spent Fuel Storage and Handling Applications," dated April 14, 1978, and addendum dated 1979.

[7.1.2] "Furnish and Install Spent Fuel Storage Racks," V.C. Summer Technical Specification, SP-837, Rev. 0, May 18, 2000.

[7.4.1] NUREG/CR-6608, "Summary and Evaluation of Low-Velocity Impact Tests of Solid Steel Billet Onto Concrete Pads", dated February 1998.

Table 7.4.1

## IMPACT EVENT DATA

Case	Impactor Weight (lb)	Impactor Type	Drop Height (in)	Impact Velocity (in/sec)
1. Shallow drop event	2,000	Fuel assembly & handling tools	24	123.6
2. Deep drop event scenario 1 (away from pedestal)	2,000	Fuel assembly & handling tools	191	270.5
3. Deep drop event scenario 2 (above pedestal)	2,000	Fuel assembly & handling tools	191	112.0
4. Rack drop event	38,700	Heaviest rack & handling tools	540	276.1

Table 7.4.2

## MATERIAL DEFINITION

Material Name	Material Type	Density (pcf)	Elastic Modulus (psi)	Stress		Strain	
				First Yield (psi)	Failure (psi)	Elastic	Failure
Stainless Steel Rack Walls and Female Pedestal	SA240-304L	490	2.760e+07	2.130e+04	6.620e+04	7.717e-04	3.800e-01
Stainless Steel Liner	SA240-304	490	2.760e+07	2.500e+04	7.100e+04	7.717e-04	3.800e-01
Zircaloy Fuel Cladding	--	404	1.040e+07	8.05e+04	8.05e+04	1.000e-02	1.500e-02
Stainless Steel Male Pedestal	SA564-630	490	2.760e+07	1.063e+05	1.400e+05	3.851e-02	3.800e-01
Concrete †	f <sub>c</sub> =3,000 psi	150	3.122e+06	--	3.000e+03	--	--

† The concrete is modeled as recommended in NUREG /CR-6608 [7.4.1].

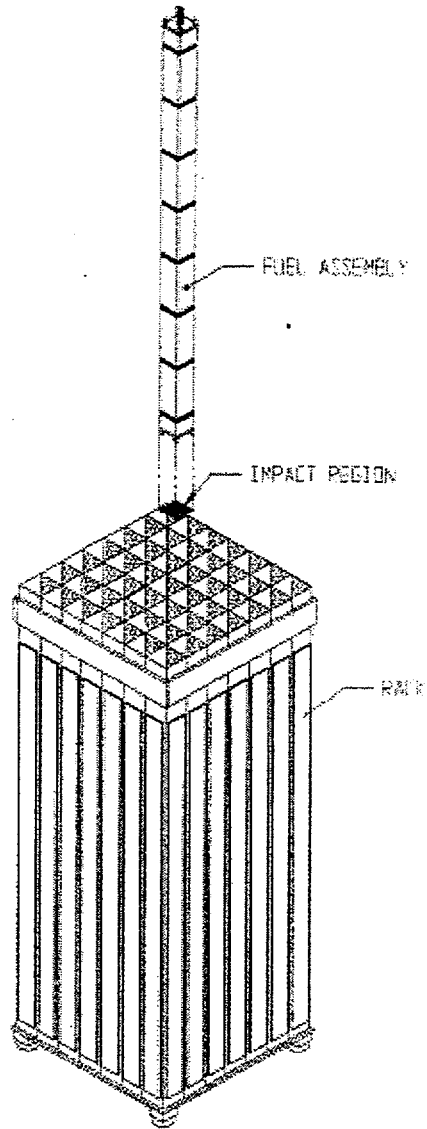


Fig. 7.2.1 Schematics of the "shallow" drop event

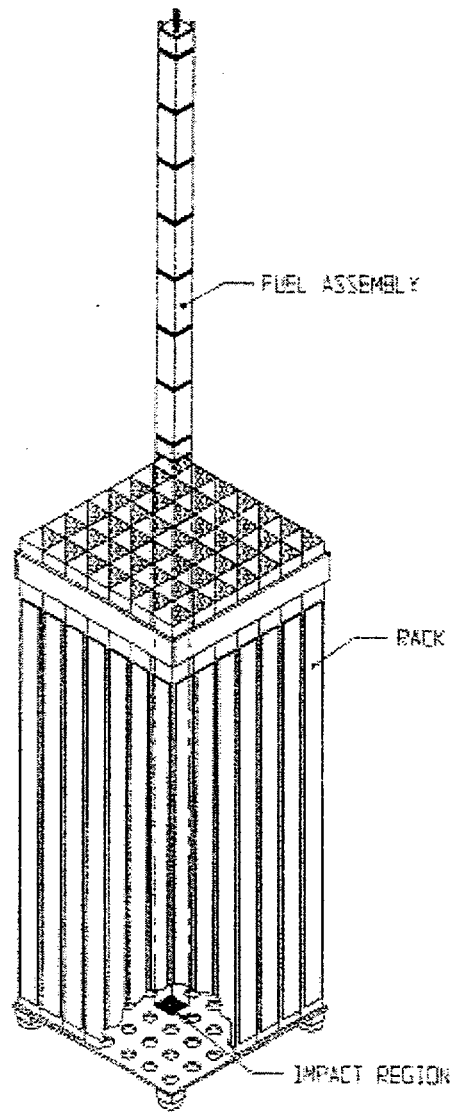


Fig. 7.2.2 Schematics of the “deep” drop scenario 1

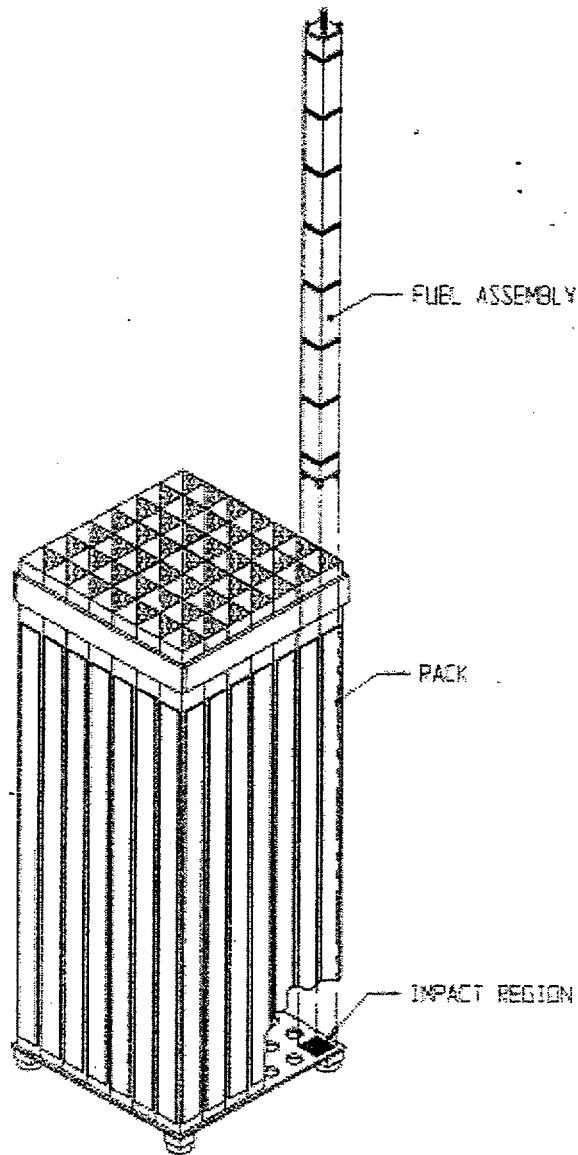


Fig. 7.2.3 Schematics of the “deep” drop scenario 2

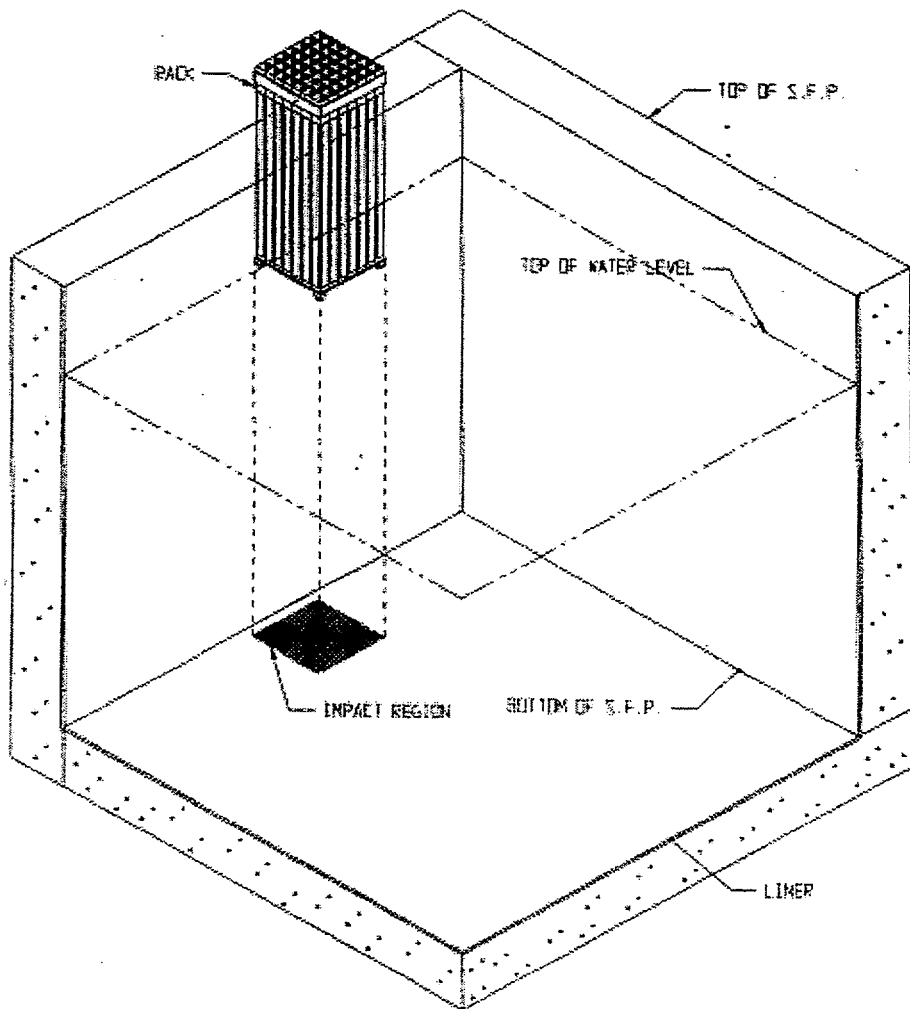


Fig. 7.2.4 Schematics of the rack drop event

"SHALLOW DROP" OF FUEL ASSEMBLY  
STEP 38 TIME = 1.3000064E-001  
PSTN(MID)

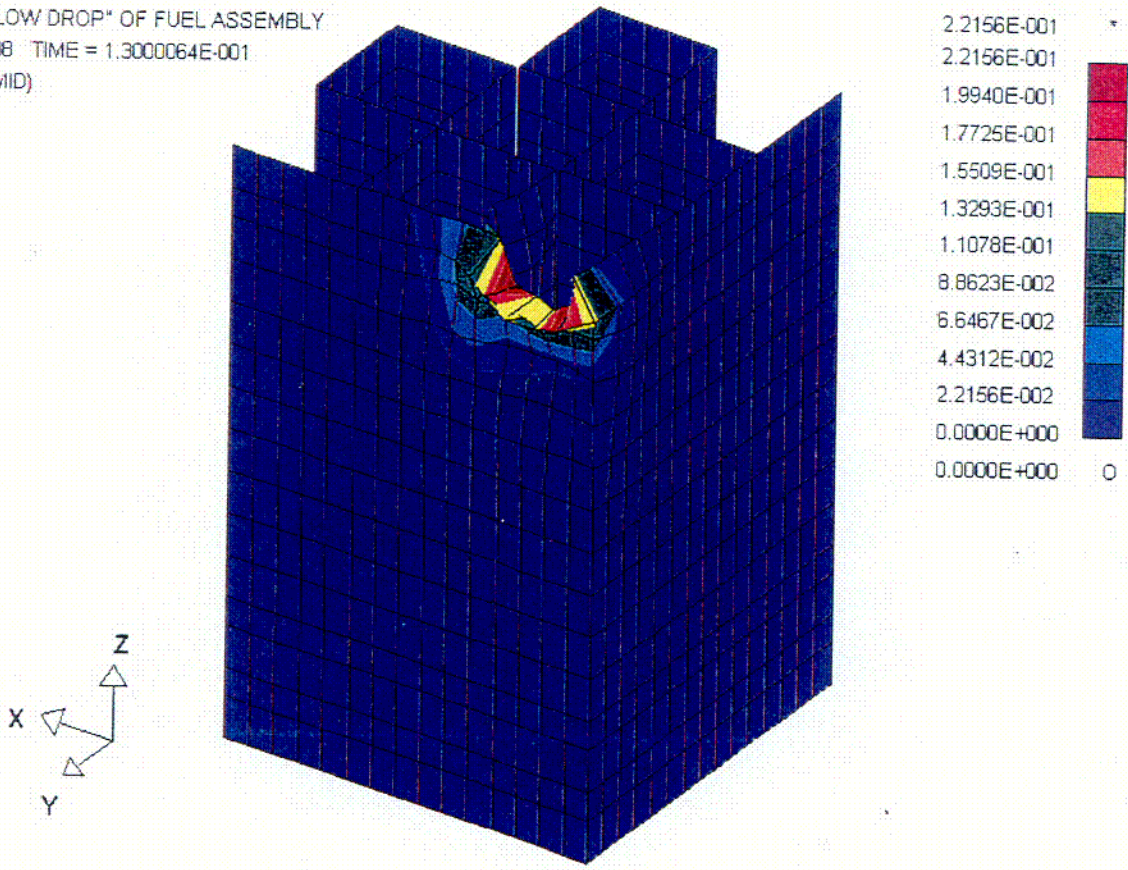


Fig. 7.5.1 "Shallow" Drop: Maximum Plastic Strain

STEP 32 TIME = 1.5999906E-002  
Z COORDINATE DISPLACEMENT

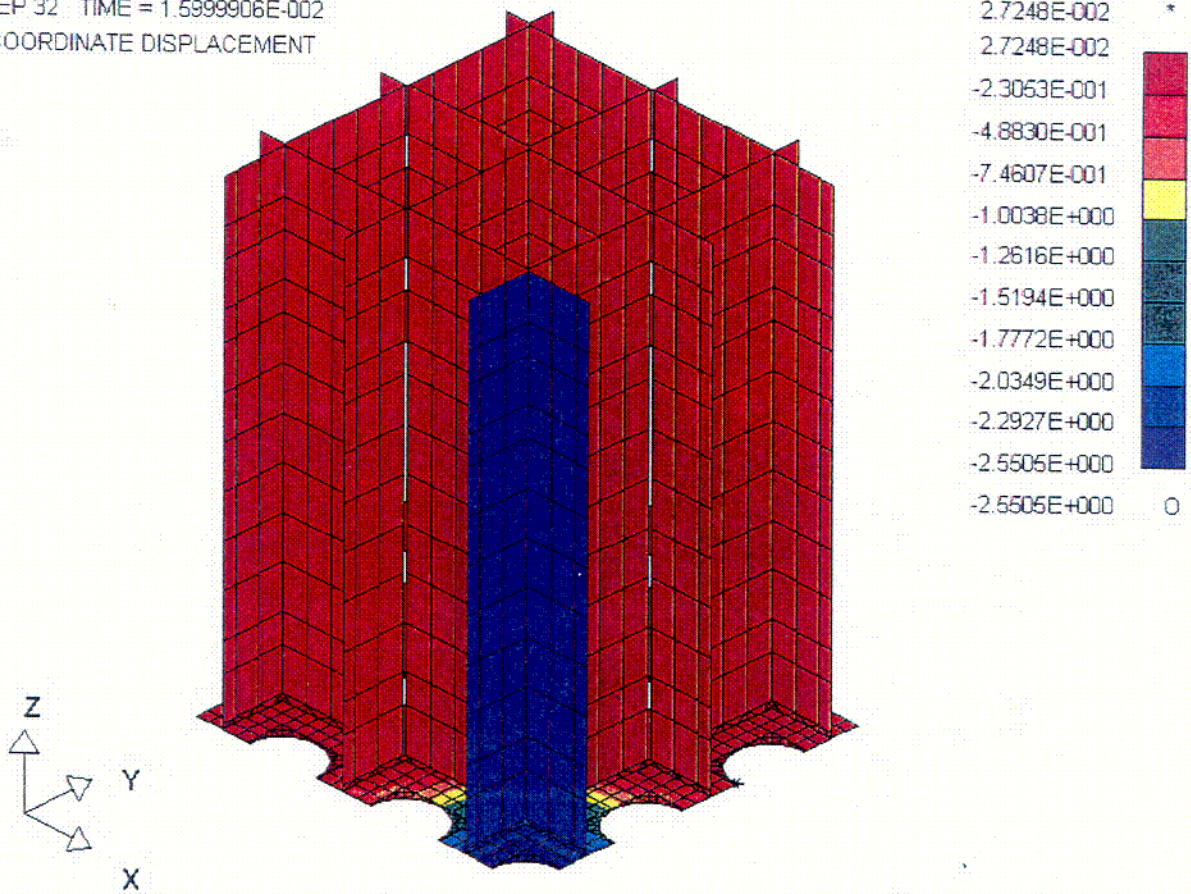


Fig. 7.5.2 "Deep" Drop Scenario 1: Maximum Vertical Displacement

FUEL ASSEMBLY "DEEP DROP" SCENARIO 2  
STEP 16 TIME = 2.5597359E-003  
MAX\_VONMISES

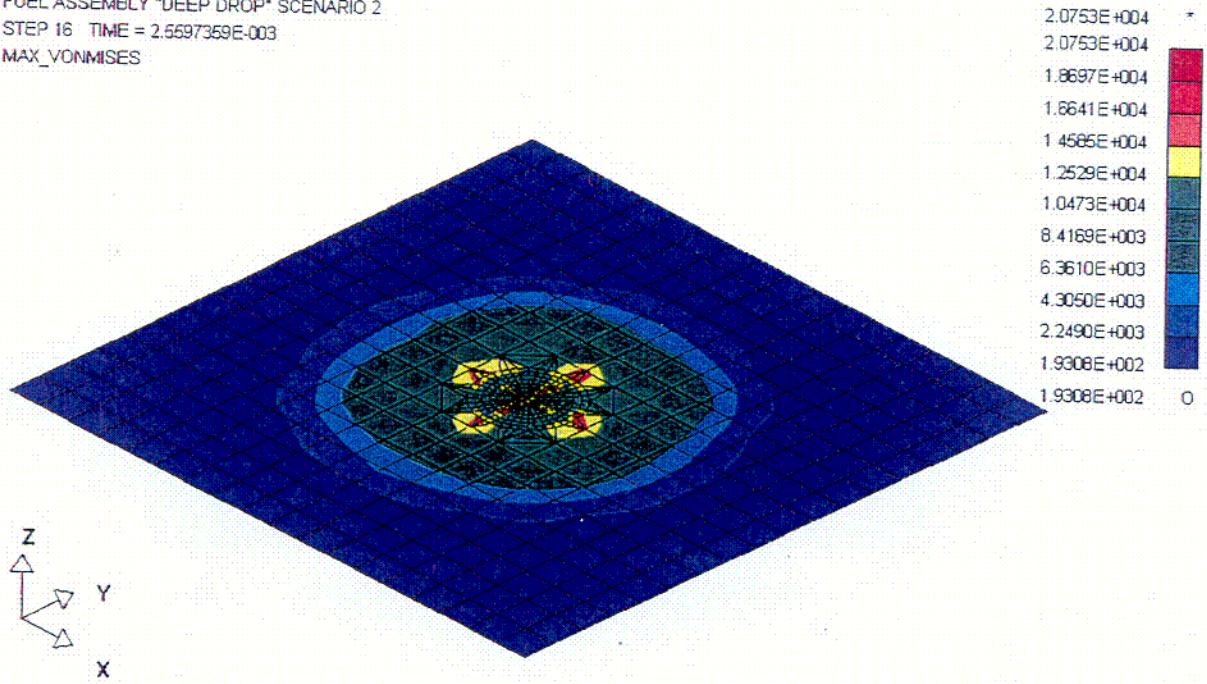


Fig. 7.5.3 "Deep" Drop Scenario 2: Maximum Von Mises Stress – Liner

FUEL ASSEMBLY "DEEP DROP" SCENARIO 2  
STEP 16 TIME = 2.5597359E-003  
SIGZZ(MID)

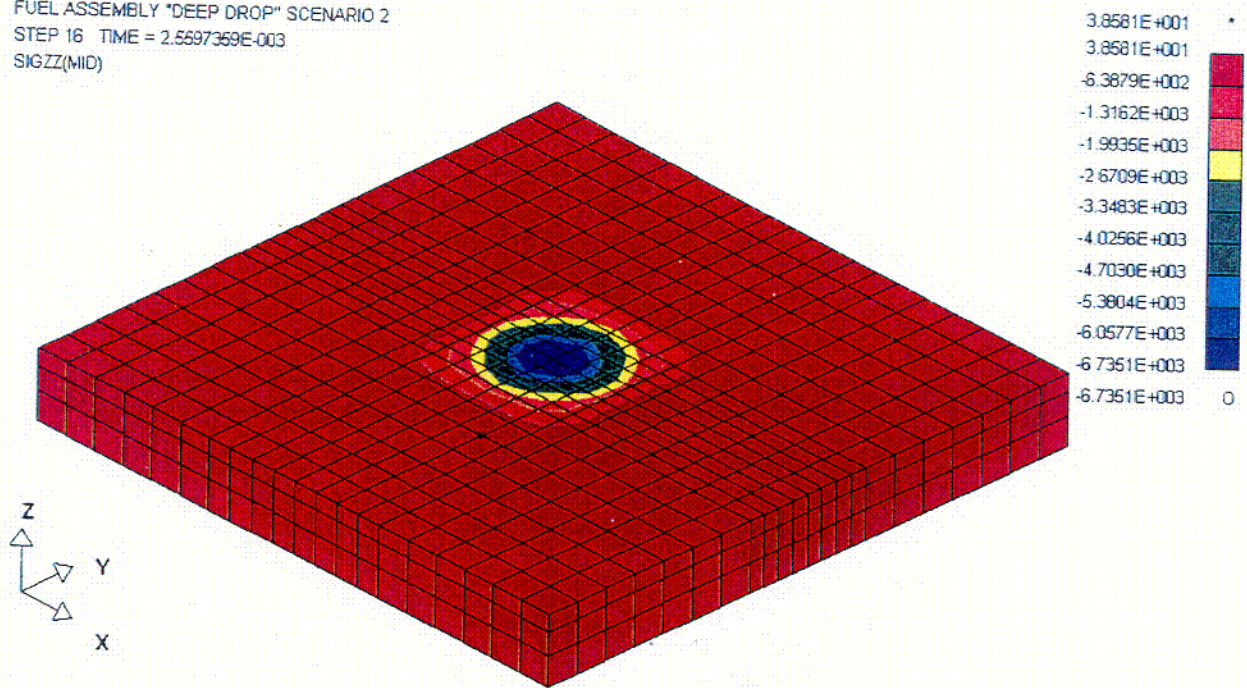


Fig. 7.5.4 "Deep" Drop Scenario 2: Maximum Compressive Stress – Concrete

RACK DROP ONTO SFP FLOOR  
STEP 41 TIME = 1.000163E-002  
MAX\_VONMISES

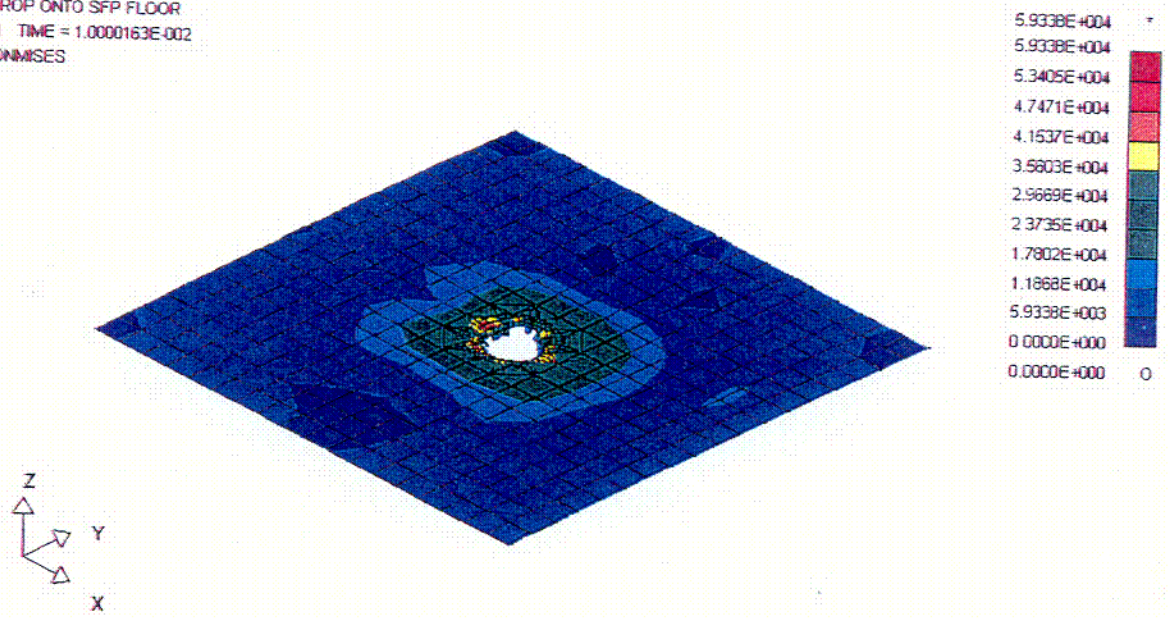


Fig. 7.5.5 Rack Drop: Maximum Von Mises Stress – Liner

RACK DROP ONTO SFP FLOOR  
STEP 27 TIME = 6.7499764E-003  
SIGZZ(MID)

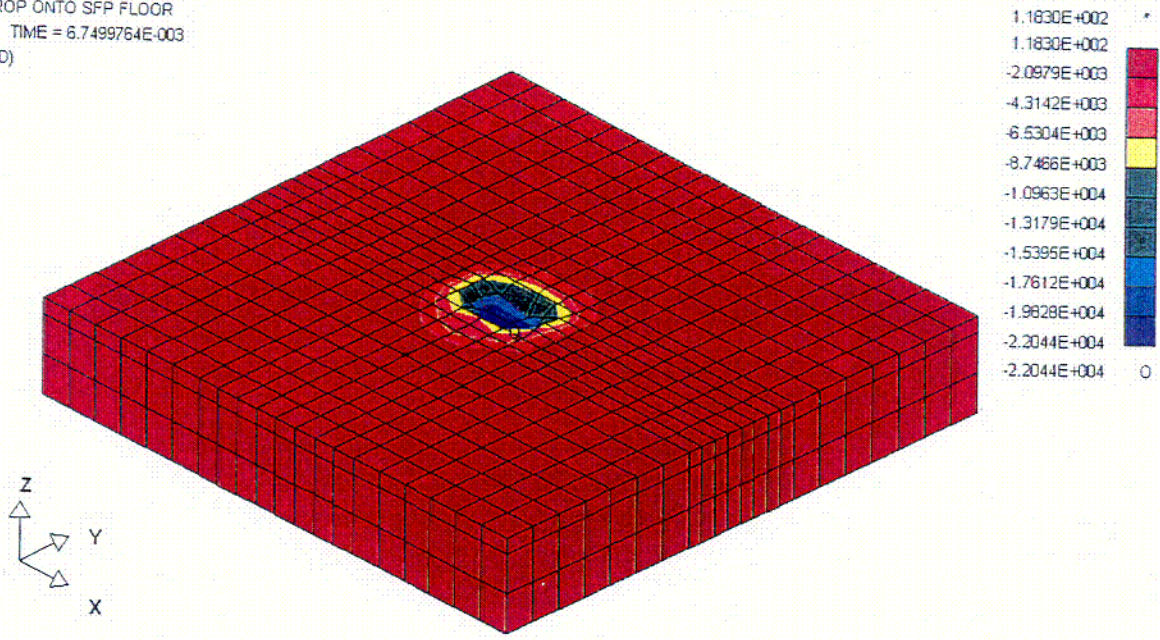


Fig. 7.5.6 Rack Drop: Maximum Compressive Stress – Concrete

C09

## 8.0 SPENT FUEL POOL STRUCTURAL INTEGRITY CONSIDERATIONS

### 8.1 Introduction

The proposed installation of new high-density racks will increase the mechanical and thermal loads on the Spent Fuel Pool (SFP) structure. The loads on the pool slab increase due to the increased combined weight of the racks and the spent fuel. However, the pool was previously evaluated for loading due to storage of consolidated fuel, which exceeds the loading represented by the new rack configuration. The closer gap between the new racks and the pool walls increases the seismic hydrodynamic pressures on the walls due to coupling effects. The higher normal operating conditions pool water temperature increases the thermal bending stresses in the pool slab and walls. This chapter summarizes the analyses performed to demonstrate the structural adequacy of the V.C. Summer Spent Fuel Pool that is classified as a safety-related, Seismic Category I, reinforced concrete structure.

### 8.2 Description of Pool Structure

The Spent Fuel Pool is located at the south-west corner of the of the Fuel Handling Building (FHB) basement. The pool west wall is part of the FHB basement outer wall. The pool key structural members include four reinforced concrete walls and a base slab that are lined with a stainless steel liner. The pool south and west walls are supported by reinforced concrete columns and a mass foundation that rest on the fill mats of the Auxiliary Building and the Reactor Building. The remaining part of the Spent Fuel Pool is supported by a system of caissons that extend below the pool slab, through the supporting soil, and into the underlying bedrock. Floor slabs at the ground elevation and pool walls top elevation provide horizontal bracing to the pool north and south walls. Figure 8.2.1 presents a plan view of the Fuel Handling Building at the pool operating deck level. Figures 8.2.2 and 8.2.3 show sectional views looking west and north of the Fuel Handling Building structure. Table 8.2.1 summarizes the key geometric parameters relevant for the analysis of the SFP structure.

The pool walls and slab are reinforced on each face with # 11 bars. The re-bar spacing is 12" on the inside face adjacent to the spent fuel pool and 6" on the outside face away from the pool.

### 8.3 Definition of Loads

Pool structural loading involves the following discrete components (capital letters in parentheses represent load type identifiers used later to define the relevant load combinations) defined in accordance with the applicable governing document:

#### 8.3.1 Dead Loads (D)

- Weight of concrete structure and steel liner - A unit weight density of 150 lb./ft<sup>3</sup> accounts for the weight of the reinforced concrete and the pool liner.
- Maximum weight of rack modules and fuel assemblies stored in the modules - A load from the combined buoyant weight of the racks and the contained fuel is uniformly distributed on the slab by dividing it by the total plan area of the spent fuel pool.
- Hydrostatic pressure - A gradient horizontal pressure is applied on the surfaces of the pool walls and uniform pressure on pool slab. The applied pressure is zero at the top of the pool walls and rises to a maximum value at the pool floor slab elevation.

#### 8.3.2 Live Loads (L)

- Live load from floor slab – Consistent with the previous pool wall evaluation, the 119.1 kip live load considered for the rail cars on the floor slab at elevation 436'-0" is transferred as a downward reaction and bending moment on the pool north wall.

#### 8.3.3 Seismic Induced Loads (OBE = E; SSE = E')

A quasi-static analysis evaluates the pool structural response under two levels of design seismic excitations: an Operating Basis Earthquake (OBE) (E) and a Safe Shutdown Earthquake (SSE) (E'). The following earthquake induced loads are considered:

- Self-inertia loads - Quasi-static accelerations are applied to the mass of the pool structure model with g-values equal to the magnitudes of the maximum floor accelerations at the pool floor slab elevation.
- Rack pedestal seismic loads - Vertical loads are transmitted by the rack support pedestals to the slab during the OBE (E) and SSE (E') seismic events. Quasi-static "pressure adders", applied uniformly on the total area of the slab, account for the additional loads generated by the dynamic motion of the racks. Whole Pool Multi-Rack (WPMR) analyses (discussed in Section 6.0) provide the total load from all pedestals, less the dead weight, as function of time (Figure 8.3.1). Instantaneous peak loads are identified and distributed uniformly on the area of pool slab to obtain the corresponding OBE and SSE "pressure adders".
- Hydrodynamic inertia and sloshing loads – Hydrodynamic pressures arise on the pool walls and slab during the seismic events (E or E') from the inertia and the sloshing of the contained pool water. Equivalent uniform quasi-static pressures are applied on the walls wet areas to account for the action of impulsive and convective water pressures generated by the horizontal components of the OBE and SSE excitations. The vertical components of the seismic excitations and the water inertia generate hydrodynamic pressures on the walls and the slab of the pool with magnitudes equal to the hydrostatic pressures times the corresponding vertical OBE and SSE acceleration values in the units of g.
- Hydrodynamic coupling pressures – The rack motion in the pool during the seismic events (E and E') generates hydrodynamic pressures between racks and pool walls. Uniform lateral pressures, applied on the pool walls below the top of the spent fuel racks, simulate the effects of water pressure increase and suction on the walls. Figures 8.3.2 to 8.3.5 present the time histories of the OBE and SSE hydrodynamic pressures on each of the pool walls that are obtained from the results from the WPMR analyses as an average of the pressures acting throughout the width of the area that the new racks project on the wall. The maximum values of these pressure time histories are selected to represent the magnitudes of the equivalent quasi-static pressures

resulting from water coupling effects. Table 8.3.1 lists the magnitudes of the static and quasi-static loads applied on the slab and the walls of the spent fuel pool.

#### 8.3.4 Thermal Loading ( $T_0$ and $T_a$ )

The design thermal loads include normal operating temperatures  $T_0$  and abnormal (accidental) temperatures  $T_a$ . The difference in temperature inside and outside the spent fuel pool results in thermal gradients across the thickness of the reinforced concrete members. The change of the mean temperature in the pool walls and slab from the temperature when the concrete was cast to  $T_0$  and  $T_a$  values generates thermal thrust loads. Table 8.3.2 lists the input temperatures for the thermal stress analysis of the pool structure. The analysis of the bulk pool temperature provides the input temperature for the spent fuel pool water under normal operating conditions. The accidental thermal loads include boiling temperature of the pool water.

#### 8.4 Analysis Procedures

The structural compliance of the pool walls and the slab to the governing ACI 318 standard [8.4.1] is evaluated by comparing the ultimate capacities of the reinforced members with the internal force and bending moment resultants under the action of the specified design loads that are combined in factored load combinations. Interaction diagrams define the resistance of the reinforced concrete structural members against combined action of bending moments and in-plane axial forces. The effect of the in plane axial forces on the concrete ultimate capacity for shear is also considered.

The structural integrity of the column and caisson foundation members supporting the Spent Fuel Pool has been verified for the loads associated with the installation of new high density racks. Table 8.3.1 lists 2.402 ksf for the uniformly distributed load due to the buoyant weight of the new racks plus fuel. For the current rack configuration, the uniformly distributed weight of racks plus fuel analyzed was 1.973 ksf. The columns and caissons have also been analyzed and found to be acceptable for an assumed load case with a uniformly distributed load due to racks plus fuel of 3.002 ksf. This controlling loading was associated with a hypothetical case assuming rod consolidation. Because the loading due to new racks

plus fuel is reduced from the more severe load case assuming rod consolidation that was previously analyzed, the structural integrity of the columns and caissons is maintained for the loads associated with the installation of the new racks.

#### 8.4.1 Load Combinations

The evaluation of pool structural integrity considers the following critical load combinations:

100	$1.4 D + 1.7 L + 1.9 E$
200	$1.05 D + 1.275 (L + T_0) + 1.425 E$
300	$D + L + T_0 + E'$
400	$D + L + 1.25 E + T_a$
500	$1.05 D + 1.275 (L + T_0)$
600	$D + L + T_a$
700	$D + L + T_a + E'$

where:

- D - Dead Loads
- L - Live Loads
- E - OBE Seismic Loads
- E' - SSE Seismic Loads
- $T_0$  - normal operating thermal loads
- $T_a$  - accident thermal loads

The above load combinations specified by the NUREG 0800 SRP 3.8.4 [8.4.2] are similar in intent and are bounding to the load combinations specified by the ACI-318 code [8.4.1].

#### 8.4.2 Finite Element Analyses

Finite Element (FE) static, quasi-static and thermal stress analyses provide the bending moments, axial forces, and shear forces in the pool walls and slab for each specified load combination. The static and quasi-static analyses uses uncracked concrete properties neglecting the effect of the reinforcement on the Young's Modulus of the reinforced concrete cross sections. The thermal stress analysis utilizes cracked section properties to define the appropriate value of Young's Modulus as function of the contained reinforcement.

A finite element (FE) model, as shown in Figure 8.4.1, evaluates the internal forces in the horizontal and vertical cross sections of the west SFP wall, which controls, since it is the only wall that has no additional horizontal bracing from the adjacent floor slabs. The results from the evaluation of the west wall are bounding for all of the pool walls also because it is a building exterior wall that experiences the highest thermal gradient loads arising from the difference between the outside air temperature and the pool water temperature.

Two 2-D frame models (figures 8.4.2 and 8.4.3) provide conservative estimates of the internal forces in the E-W and N-S cross sections of the pool slab. In order to ensure an accurate distribution of the internal forces throughout the pool structure, the N-S frame model includes the north and south walls and their horizontal bracing from the floor slabs. The E-W frame model considers the loads transferred to the slab from the pool wall by applying reaction moments and forces at the east and west walls centerline locations. The magnitudes of these reaction loads are obtained from the results of the west wall FE analysis. The horizontal and vertical stiffness of the supporting caisson and columns are included in the 2-D frame models.

The analysis employs the following conservative/simplifying assumptions in addition to those assumptions pertaining to the methodologies specified by the governing ACI code [8.6.1]:

- The support that the surrounding soil provides to the pool slab and walls is conservatively neglected.

- All of the new high-density racks in the pool are fully loaded with fuel.
- Horizontal and vertical quasi-static loads are imposed simultaneously in directions that maximize the stresses in different structural elements.
- The peak hydrodynamic coupling pressures, resulting from the rack motion in the pool water, are conservatively assumed to act simultaneously with the hydrodynamic inertia pressures.
- The analysis conservatively neglects the stiffness of the pool steel liner and accounts for its mass by increasing the specified unit weight of the concrete.

## 8.5 Conclusions

The comparison of the factored internal moments/forces with the ultimate capacities of the reinforced concrete cross sections yields safety factors for bending moments and shear forces for the pool walls and slab. Table 8.5.1 presents the calculated minimum safety factors together with the loading combination that is the most critical for the particular reinforced concrete member.

The listed safety factors all have values greater than one, which demonstrates that adequate safety margins exist in the spent fuel pool structure.

The loadings in the supporting columns and caissons are reduced from the conservative loading previously evaluated. Therefore, the structural integrity of the supporting caissons and columns is maintained for the loads associated with the installation of new high density racks in the V.C. Summer Spent Fuel Pool.

8.6 References

[8.4.1] ACI 318-71, Building Code Requirements for Reinforced Concrete Structures, American Concrete Institute, Detroit Michigan, 1971.

[8.4.2] NUREG-0800, SRP-3.8.4, Rev. 1., July 1981.

Table 8.2.1  
KEY GEOMETRIC DATA FOR THE SPENT FUEL POOL

ITEM	VALUE
Pool Depth	40'-4"
Pool N-S Length	28'-0"
Pool E-W Length	39'-0"
Pool Water Elevation	El. 461'-4"
Pool Slab Top Elevation	El. 422'-7 <sup>3</sup> / <sub>4</sub> "
Pool Walls Thickness	6'-0"
Pool Slab Thickness	5'-11 <sup>3</sup> / <sub>4</sub> "
Operating Floor Top Elevation (Pool Top)	463'-0"
Operating Floor Slab Thickness	2'-0"
Mid Floor Slab Elevation	436'-0"
Mid Floor Slab Thickness	3'-0"
Ground Level Elevation	435'-0"
Transfer Canal Slab Elevation	437'-9 <sup>1</sup> / <sub>4</sub> "
Diameter of Caissons under Pool Walls	4'-0"
Diameter of Caissons under Pool Slab	3'-0"
Base Columns Width	4'-10"

Table 8.3.1  
**STATIC AND QUASI STATIC LOADS ON POOL STRUCTURE**

ITEM	DESCRIPTION OF APPLIED LOAD	MAGNITUDE
Structure self weight	Vertical gravity on structure with 150 pcf unit weight	1g
Buoyant weight of racks plus fuel	Uniform slab pressure	2.402 ksf
Hydrostatic Pressure on walls and slab	Gradient on walls from zero to maximum value on slab	2.423 ksf (max)
Live load from floor slab	Vertical Force and Bending Moment on North Wall at El. 436'-0" (per 1 ft' of wall width)	16.06 kips 94.93 kips ft.
OBE Self Inertia Load	Vertical acceleration	0.230 g
	Horizontal E-W acceleration on structure	0.304 g
	Horizontal N-S acceleration on structure	0.328 g
Rack pedestal OBE seismic loads	Uniform slab pressure	1.911 ksf
OBE inertia and sloshing hydrodynamic loads	Uniform pressure on East and West Walls	0.737 ksf
	Uniform pressure on North and South Walls	0.561 ksf
	0.230 times the hydrostatic load on walls and slab	0.557 ksf (max.)
OBE hydrodynamic loads from rack horizontal motion (below the top of the racks)	Uniform pressure on East and West Walls	0.592 ksf
	Uniform pressure on North and South Walls	0.507 ksf
SSE Self Inertia Load (*)	Vertical acceleration	0.373 g
	Horizontal E-W acceleration on structure	0.492 g
	Horizontal N-S acceleration on structure	0.531 g
Rack pedestal SSE seismic loads	Uniform slab pressure	3.546 ksf
SSE inertia and sloshing hydrodynamic loads (*)	Uniform pressure on North and South Walls	1.195 ksf
	Uniform pressure on East and West Walls	0.909 ksf
	0.373 times the hydrostatic load on walls and slab	0.904 ksf (max.)
SSE hydrodynamic loads from rack horizontal motion (below the top of the racks)	Uniform pressure on North and South Walls	1.182 ksf
	Uniform pressure on East and West Walls	0.938 ksf

(\*) The magnitudes of these SSE loads is 1.62 times the OBE loads magnitudes

Table 8.3.2  
TEMPERATURE LOADS ON POOL STRUCTURE

ITEM	TEMPERATURE
Concrete stress free temperature	70 <sup>o</sup> F
Pool water normal operating temperature	170 <sup>o</sup> F
Pool water boiling (accident) temperature	212 <sup>o</sup> F
Outside building ambient temperature	20 <sup>o</sup> F
Inside building ambient temperature	70 <sup>o</sup> F
Soil ambient temperature	55 <sup>o</sup> F

Table 8.5.1

SAFETY FACTORS FOR POOL STRUCTURAL MEMBERS

MEMBER	DIRECTION	EVALUATION	SAFETY FACTOR	CRITICAL LOAD COMBINATION (*)
Slab	E-W	Bending	1.24	LC 100
		Shear	1.05	LC 200
	N-S	Bending	1.26	LC 100
		Shear	2.35	LC 100
West Wall	Vertical	Bending	2.19	LC 200
		Shear	6.12	LC 100
	Horizontal	Bending	1.80	LC 200
		Shear	2.90	LC 200
North & South Walls	Vertical	Bending	1.14	LC 100
		Shear	5.77	LC 200

(\*) See Section 8.4.1 for the Load Combinations designations

PLANT  
NORTH

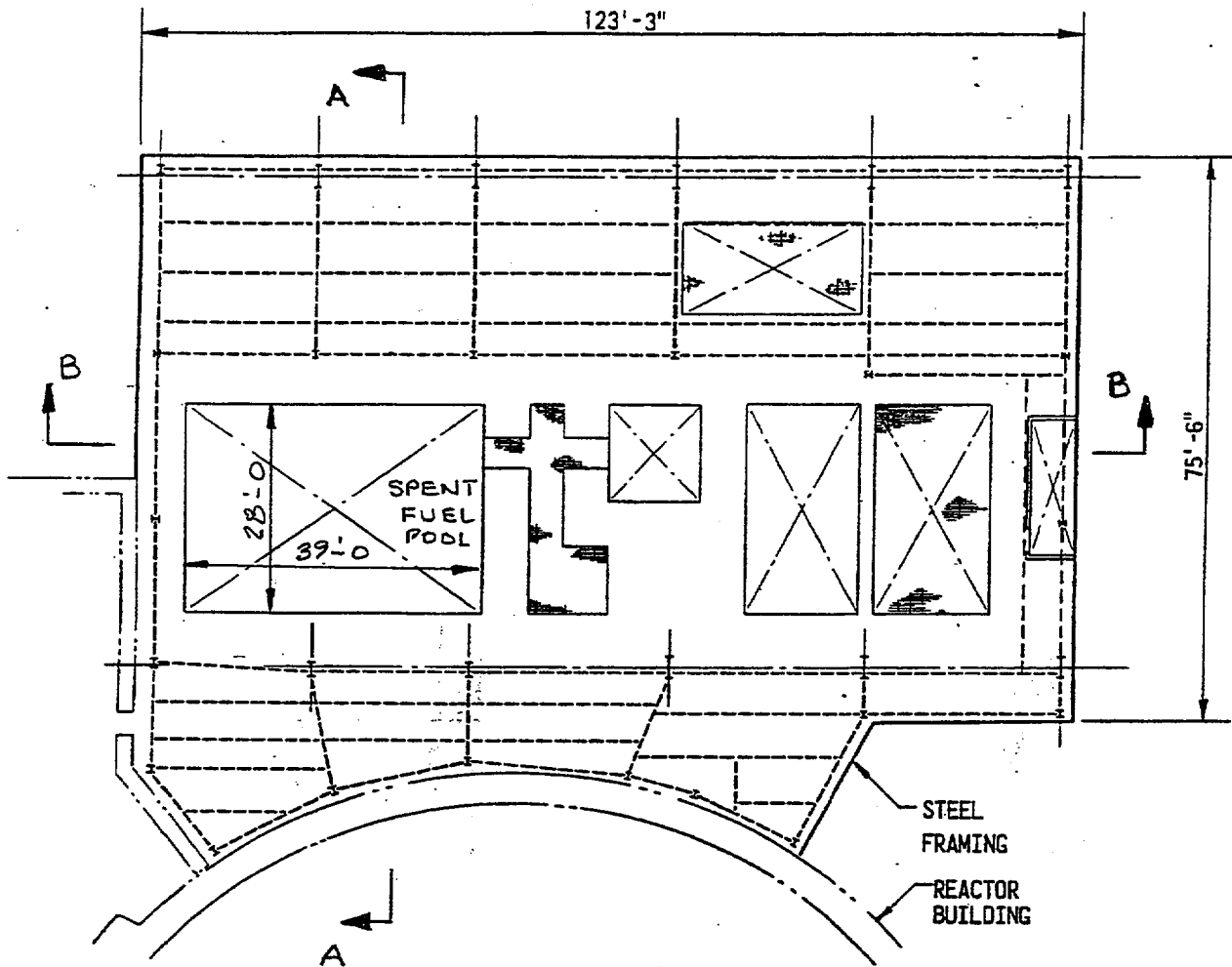


Figure 8.21; Plan View of Operating Floor

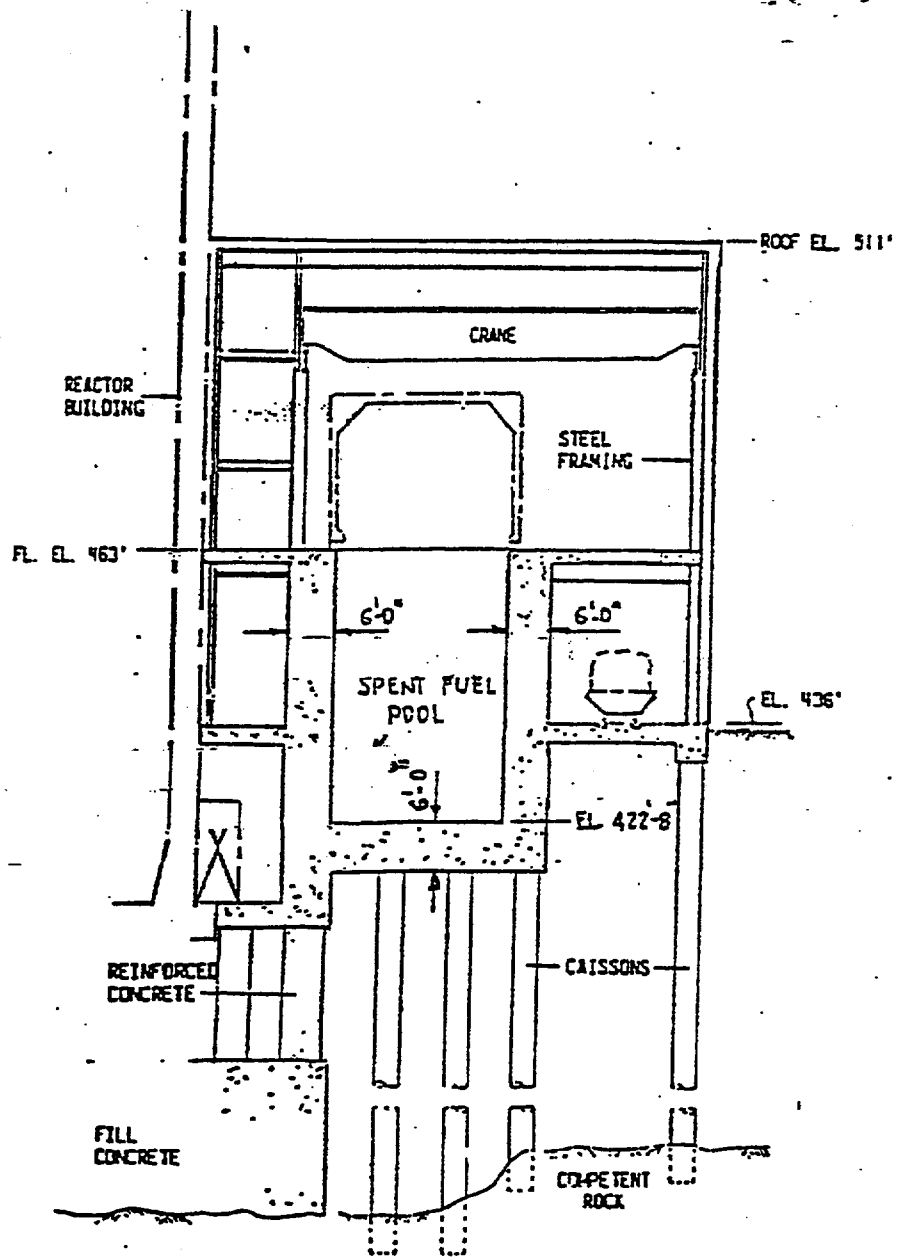


Figure 8.2.2; Fuel Handling Building Section A-A

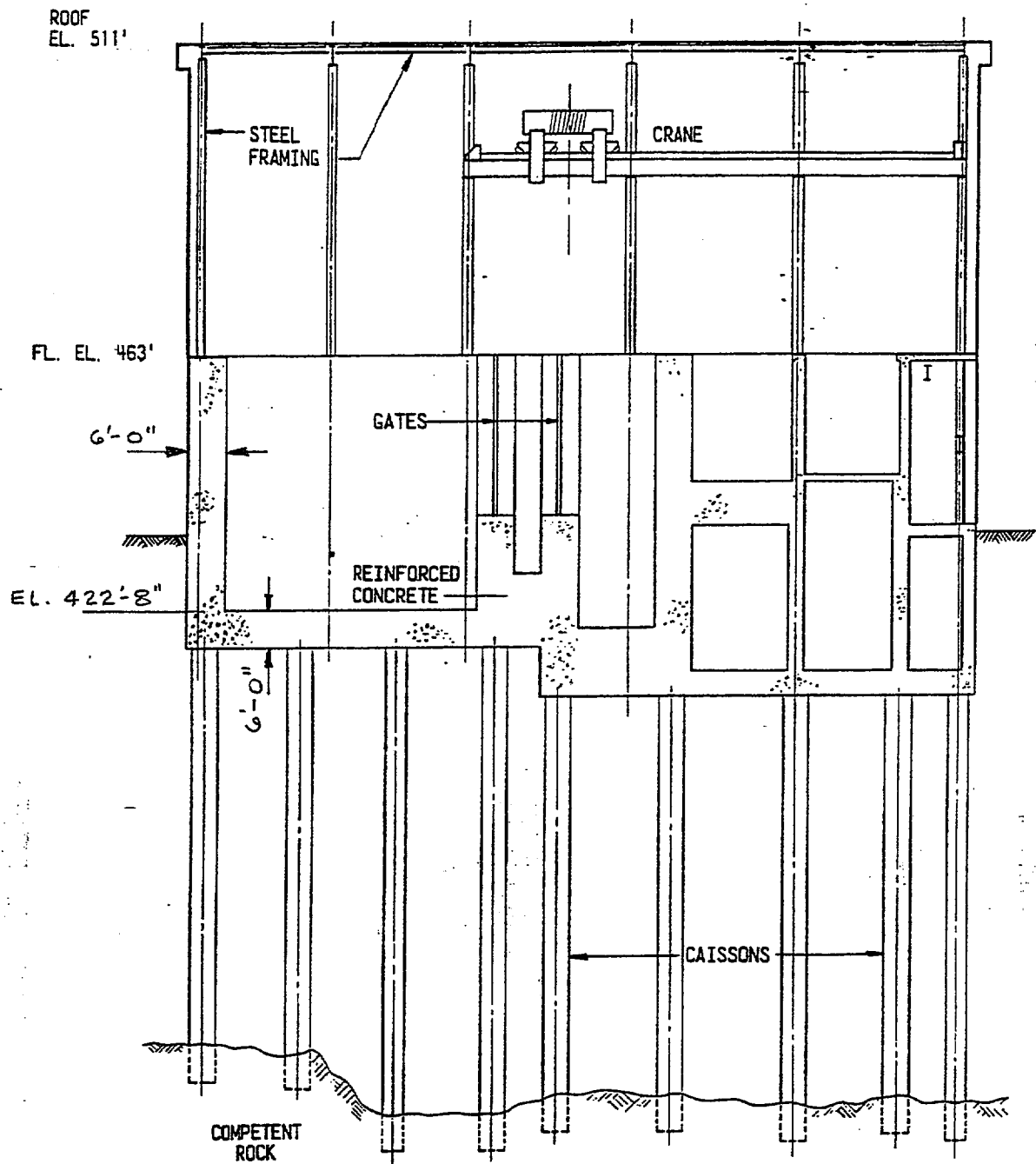
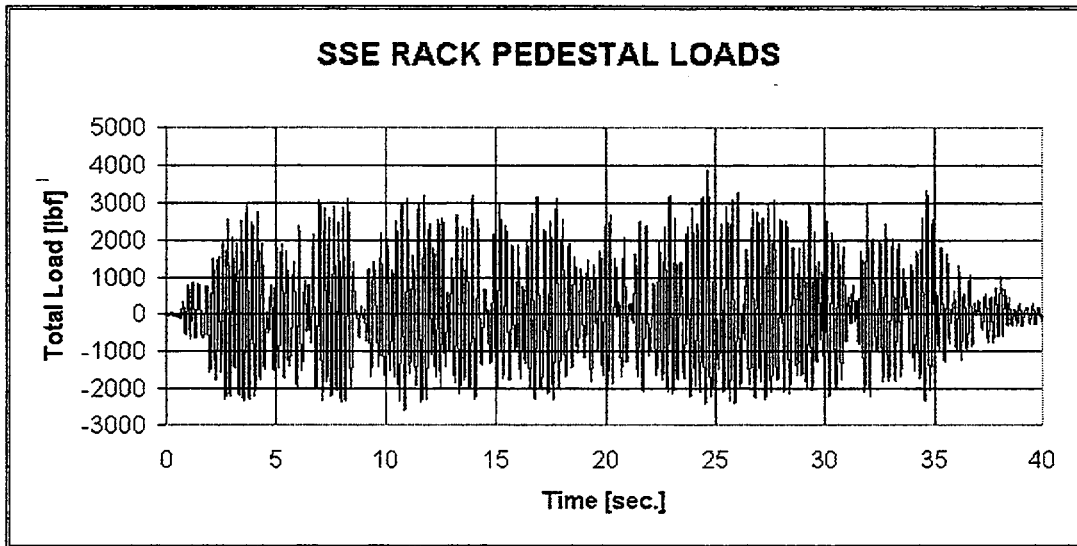
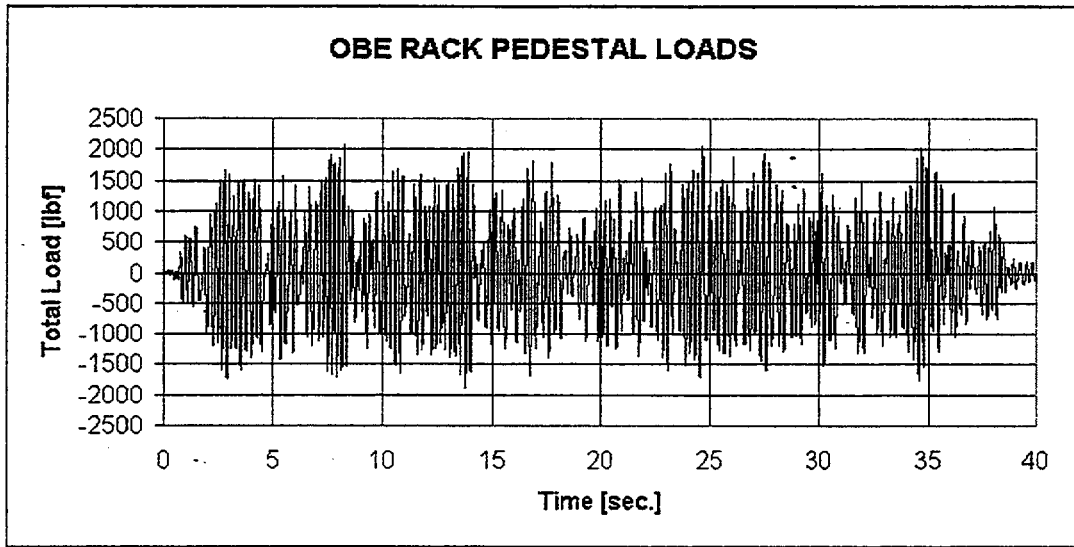
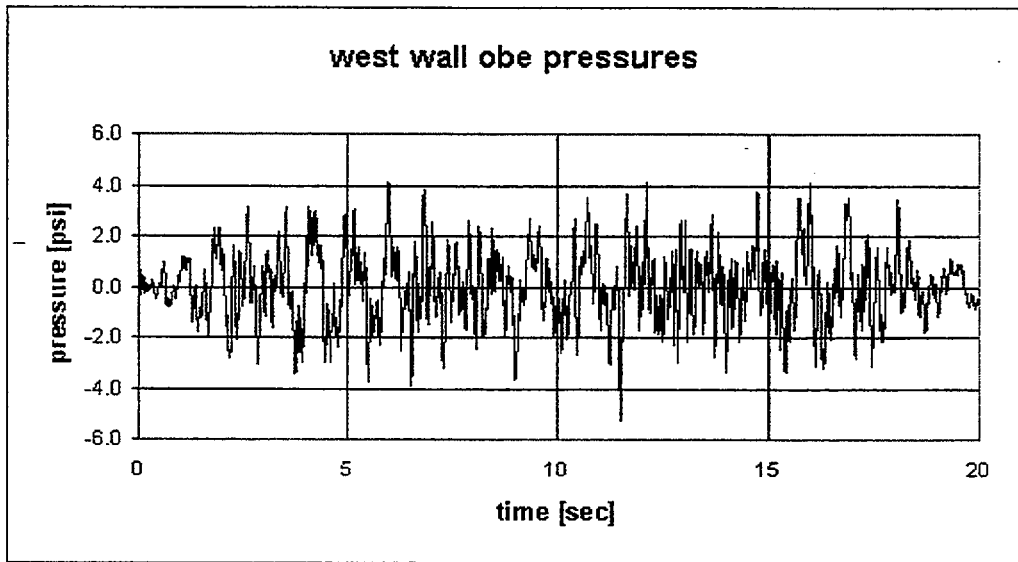
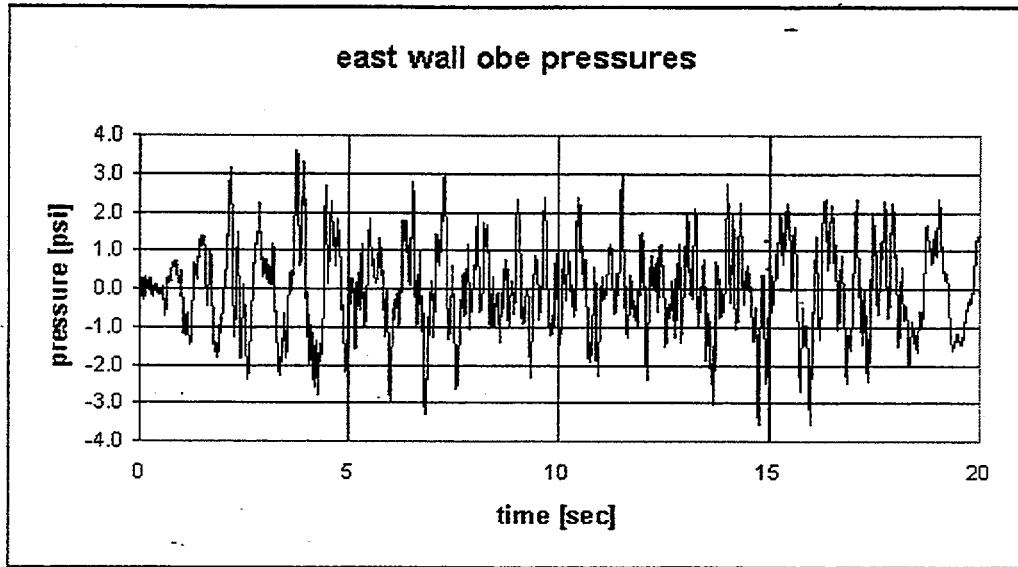


Figure 8.2.3; Fuel Handling Building Section B-B



**FIGURE 8.3.1; Rack Pedestal Seismic Adder Loads**



**FIGURE 8.3.2; Hydrodynamic OBE Rack Pressures on East and West Wall**

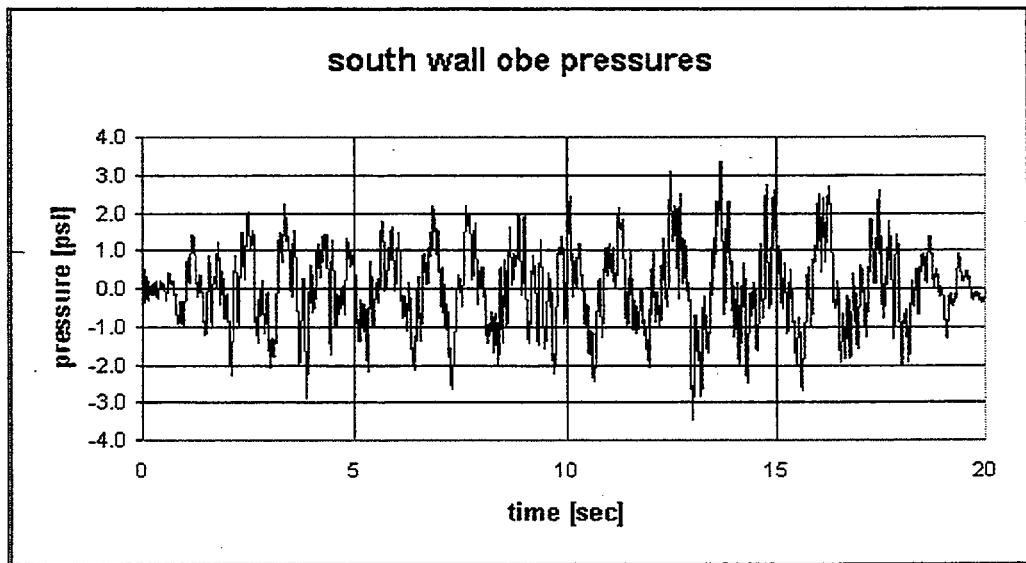
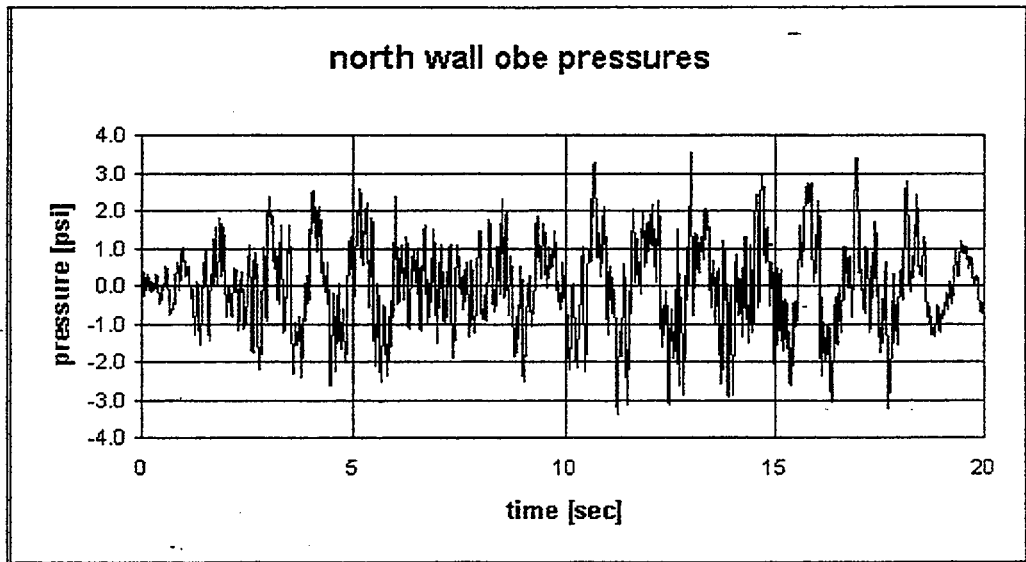


**FIGURE 8.3.3; Hydrodynamic OBE Rack Pressures on North and South Wall**

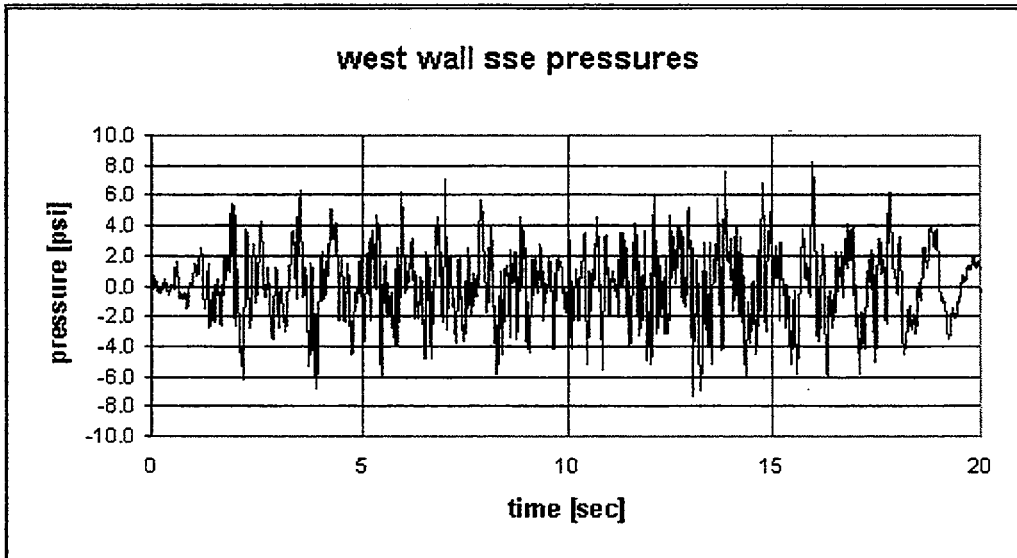
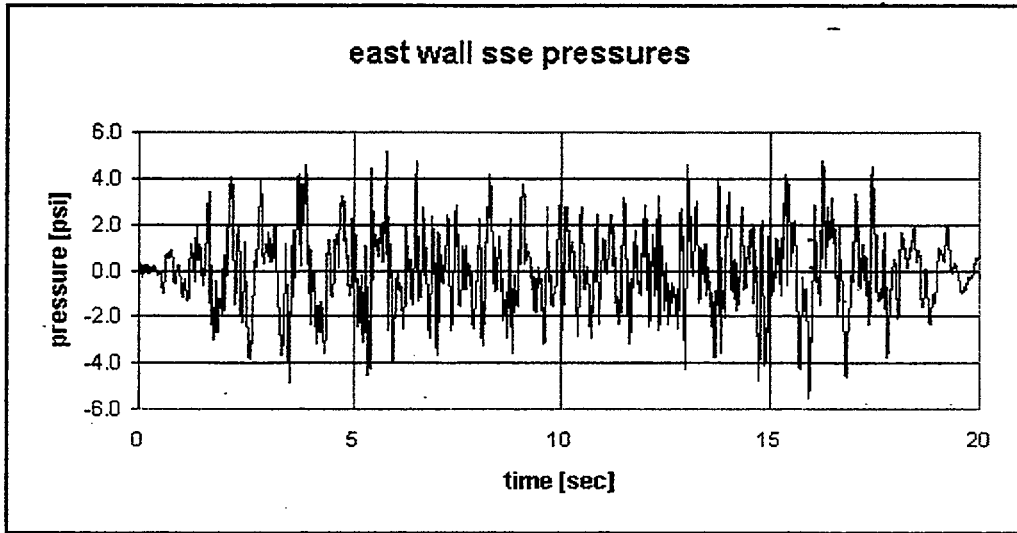


**FIGURE 8.3.4; Hydrodynamic SSE Rack Pressures on East and West Wall**

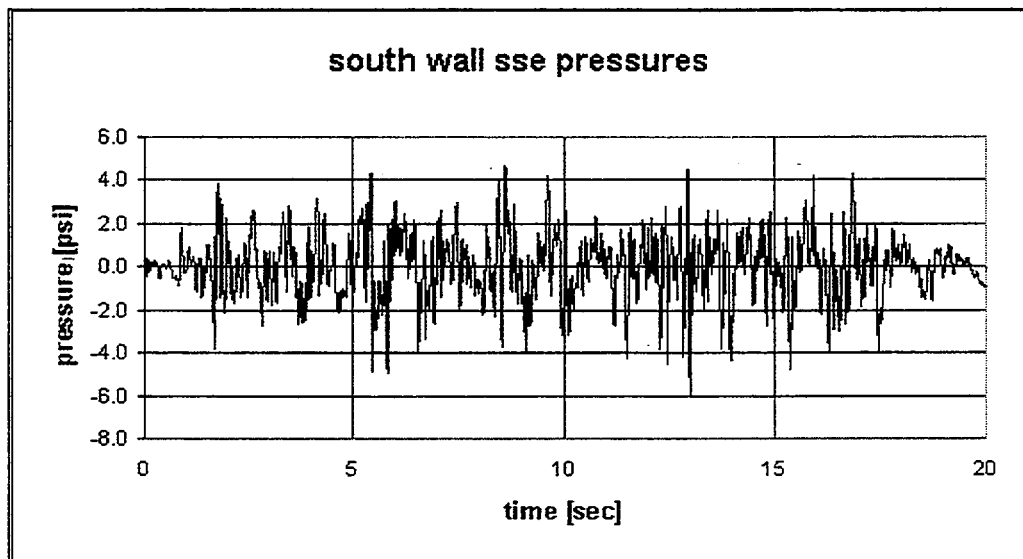
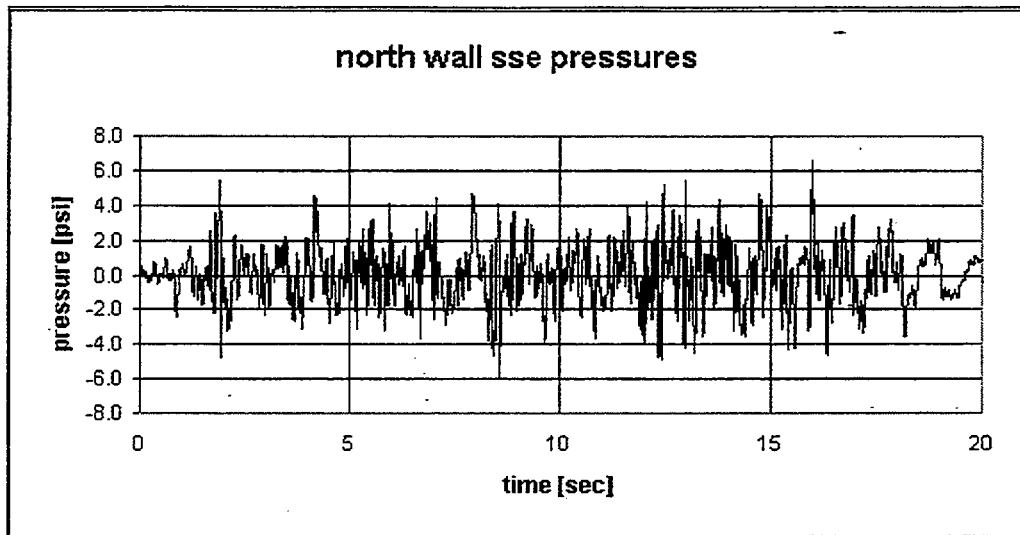


**FIGURE 8.3.5; Hydrodynamic SSE Rack Pressures on North and South Wall**

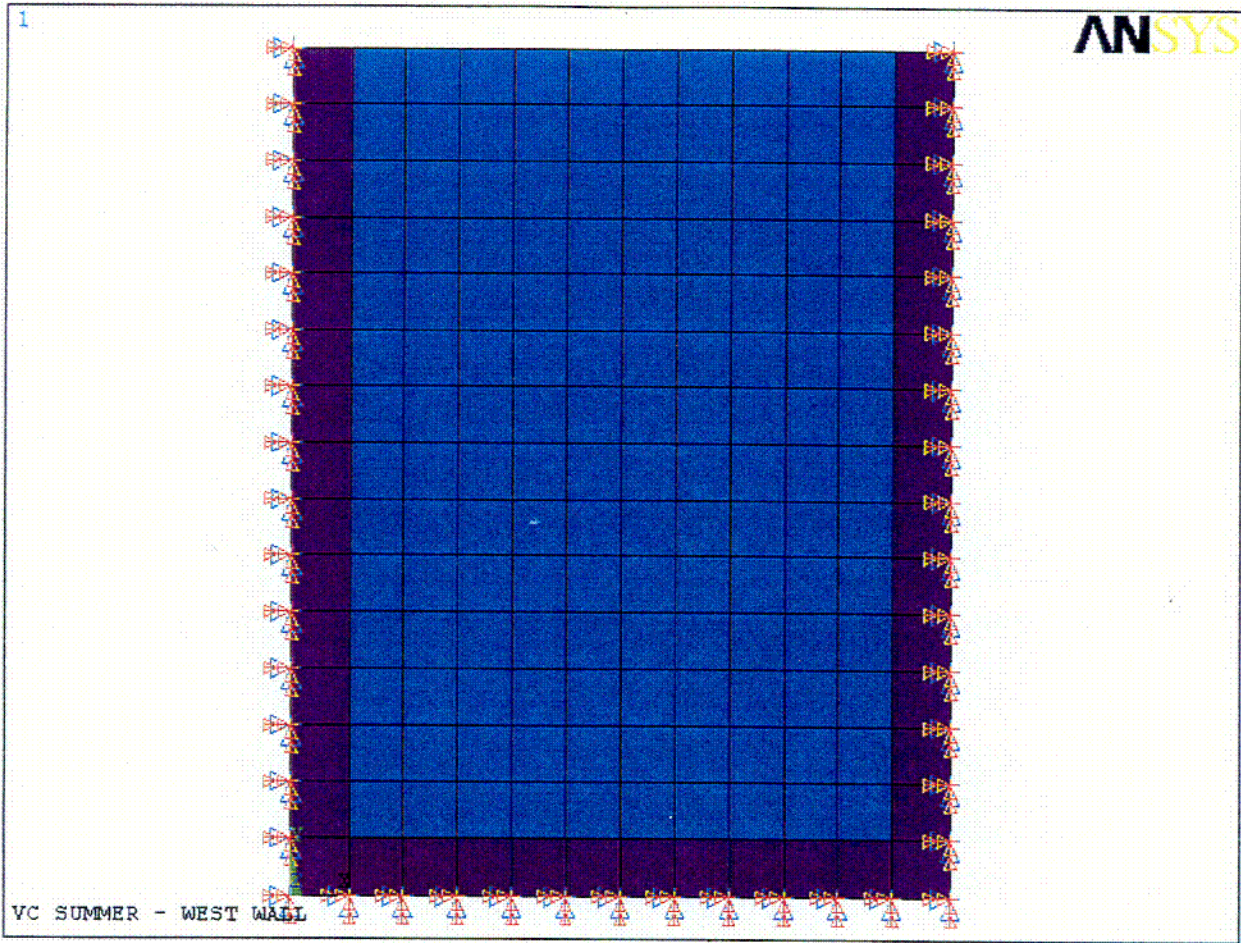


FIGURE 8.4.1; FE Model of West Wall



**FIGURE 8.4.2; FE Model of E-W Frame**

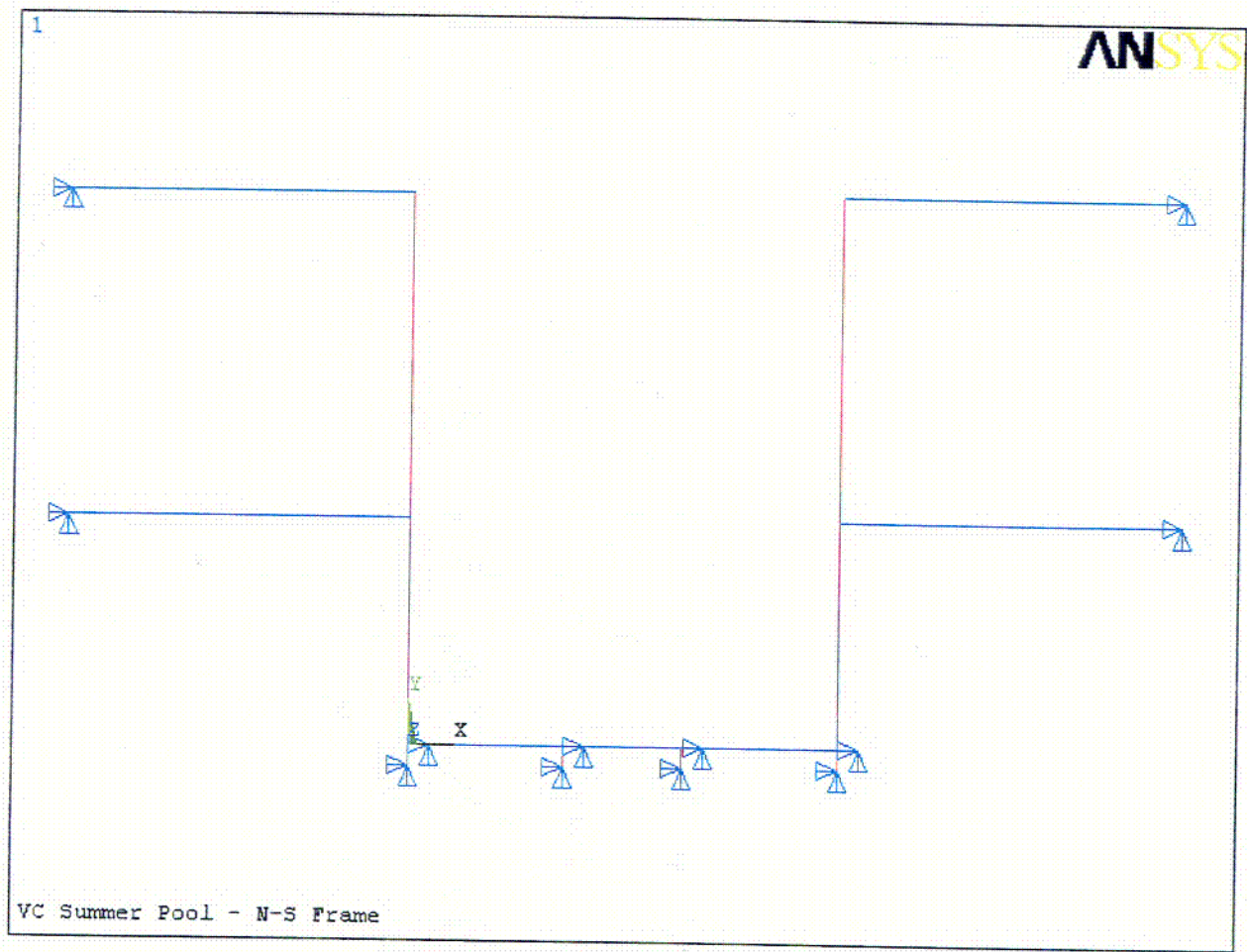


FIGURE 8.4.3; FE Model of N-S Frame

## 9.0 RADIOLOGICAL EVALUATION

### 9.1 Fuel Handling Accident

The potential radiological consequences of a postulated fuel handling accident in the Fuel Handling Building or the Reactor Building of the Virgil C. Summer Nuclear Station have been determined at the station's exclusion area boundary (EAB).

#### 9.1.1 Assumptions and Source Term Calculations

Evaluations of the accident were based conservatively on fuel of 5.0 wt% initial enrichment and five fuel exposures ranging from 35,000 Mwd/MTU to 70,000 Mwd/MTU. For dose calculations, the highest specific inventory of each contributing radionuclide was used, regardless of burnup. The reactor was assumed to have been operating at 2958 Mw thermal power prior to shutdown, with a specific power of 45.00 kw/kgU. The fuel handling accident was assumed to result in the release of the gaseous fission products contained in the fuel/cladding gaps of all 264 fuel rods in a peak-power fuel assembly plus 50 rods in an impacted assembly, for a total of 314 rods. Gap inventories of fission products available for release were estimated using the release fractions identified in Regulatory Guide 1.25<sup>1</sup> except for Iodine-131, for which the release fraction is increased 20% in accordance with NUREG/CR-5009<sup>2</sup>. Cooling time for the failed fuel prior to the accident was 72 hours.

The gaseous fission products that have significant impacts on the off-site doses following short fuel cooling periods are the short-lived nuclides of iodine and xenon, which reach saturation inventories during in-core operation. These inventories depend primarily on the fuel specific power over the few months immediately

---

<sup>1</sup> Regulatory Guide 1.25 (AEC Safety Guide 25), "Assumptions Used For Evaluating The Potential Radiological Consequences Of A Fuel Handling Accident In The Fuel Handling And Storage Facility For Boiling And Pressurized Water Reactors", March 23, 1972.

<sup>2</sup> C. E. Beyer, et al., "Assessment of the Use of Extended Burnup Fuel in Light Water Power Reactors", NUREG/CR-5009, Pacific Northwest Laboratory, February, 1988.

preceding reactor shutdown. In the highest power assemblies, the specific power and hence the inventory of iodine and xenon will be proportional to the peaking factor (assumed to be 1.7 for these evaluations).

At the cooling time of 72 hours used in the V. C. Summer calculations, most of the thyroid dose comes from Iodine-131, while most of the whole-body dose comes from Xenon-133. Though the single iodine and xenon isotopes are the major contributors to off-site doses, the contributions from other radionuclides are calculated and included in the overall dose values.

The present evaluation uses values for atmospheric diffusion factor ( $\chi/Q = 4.08 \times 10^{-4} \text{ sec/m}^3$ ) and for filter efficiencies (95%) which are consistent with the current analyses of record given in Section 15.4.5 of the FSAR. Core specific inventories (Curies per metric ton of uranium) of fission products were estimated with the SAS2H-ORIGEN-S/ARP code<sup>3</sup>, based upon parameters stated earlier (specific power of 45.00 kw/kgU, initial enrichment of 5.0 wt% U, burnup from 35,000 Mwd/MTU to 70,000 Mwd/MTU, and a cooling time of 72 hours). The results of the calculations for isotopes that could contribute to the thyroid and whole-body doses are given in Table 9.1, while Table 9.2 lists pertinent data for the isotopes of interest. These tables include all significant isotopes cited in Regulatory Guide 1.25 and several isotopes whose contribution to dose turns out to be negligible. Data and assumptions used in the dose calculations are given in Table 9.3.

The following equation, from Regulatory Guide 1.25, was used to calculate the thyroid dose (D, in rem) from the inhalation of radioiodine. Values for many of the terms in the equation are given in Table 9.2 and Table 9.3.

$$\text{Dose} = \sum_i \frac{F_g I_i F P B R_i (\chi/Q)}{DF_p DF_r}$$

<sup>3</sup> SAS2H-ORIGEN-S/ARP, in "Scale 4.3 – Modular Code System for Performing Standardized Computer Analyses for Licensing Evaluation", NUREG-CR-0200, Rev.5, Radiation Shielding Information Center, September 1995.

where,

$F_g$ =	fraction of fuel rod iodine inventory in gap space	$R_i$ =	dose conversion factor (rem per curie)
$I_i$ =	core iodine radionuclide inventory at time of the accident (curies)	$\chi/Q$ =	atmospheric diffusion factor (sec per cubic meter)
$F$ =	fraction of core damaged so as to release iodine in the rod gap	$DF_p$ =	effective iodine decon. factor for pool water
$P$ =	core peaking factor	$DF_f$ =	effective iodine decon. factor for filters
$B$ =	breathing rate (cubic meters per second)		

The equations given below were used to calculate the external whole-body dose from beta and gamma radiation in the cloud of radionuclides released in the fuel-handling accident. The equations contain several of the terms defined above.

$$Dose_{\beta} = \sum_i 0.23 (\chi/Q) F P G_i E_{\beta,i}$$

$$Dose_{\gamma} = \sum_i 0.25 (\chi/Q) F P G_i E_{\gamma,i}$$

In these expressions,  $G_i$  is the gap inventory of the gaseous radionuclides of xenon and krypton, while the  $E_{\text{subscript}}$  term is the average energy per disintegration of each radionuclide (in Mev per disintegration, as given in Table 9.2). These functions assume the noble gas decontamination factors in water and the charcoal filters are 1.0. The gap inventories of radioiodine make negligible contributions to the whole body doses,  $D_{\beta}$  and  $D_{\gamma}$ , because of the large decontamination factors appropriate to the iodines.

## 9.1.2 Results

The doses are similar to, but generally somewhat higher than, those given in the FSAR. This is because the fuel cooling time specified for the analyses reported here is 72 hours, whereas the FSAR analyses use a cooling time of 100 hours.

### 9.1.2.1 Accident in the Fuel Handling Building

The doses at the V. C. Summer EAB from the fuel handling accident in the fuel handling building are tabulated below. The doses are based on the release of all gaseous fission product activity in the gaps of 314 fuel rods in highest-power assemblies.

Thyroid dose, rem	=	12.97
Whole-body dose, rem	=	0.678
Skin dose, rem	=	3.02

These potential thyroid and whole-body doses are less than the acceptance criteria of Section 15.7.4 of the Standard Review Plan.

### 9.1.2.2 Accident in the Reactor Building

For the fuel handling accident in the reactor building, the release path of radionuclides would not normally pass through charcoal filters. With no action to limit the consequences of the fuel handling accident in the reactor building, the EAB thyroid dose would be 259 rem. (the whole-body and skin doses would be the same as the doses for the accident in the fuel handling building, for those doses are caused by radionuclides that, in the fuel-handling-building-accident, were not affected by the charcoal filters in the building purge exhaust.) This hypothetical thyroid dose is higher than the criterion of the Standard Review Plan. However, as described in Section 15.4.5.1.4 of the FSAR, instrumentation is available to detect the release of radioactivity, and to close the Reactor Building Purge Exhaust System. This action essentially precludes any radioactive release to the environment for this accident.

If abnormal radiation levels occur as a result of a fuel handling accident in the reactor building, seismically qualified, safety-grade instrumentation sends an isolation signal to the Reactor Building Purge System. With the purge system no longer venting to the atmosphere, the thyroid dose at the EAB from the fuel handling accident in the reactor building would be approximately the same as that from the fuel handling accident in the fuel handling building. This is because the charcoal filters in the fuel handling building exhaust path, which provide iodine decontamination factors of 20, act on the iodine released in the reactor building.

## 9.2 Solid Radwaste

The necessity for resin replacement is determined primarily by the requirement for water clarity, and the resin is normally changed about once a year. No significant increase in the volume of solid radioactive wastes is expected with the expanded storage capacity. During re-racking operations, a small amount of additional resins may be generated by the pool cleanup system on a one-time basis, and the old racks themselves will be a form of solid radwaste.

## 9.3 Gaseous Releases

Gaseous releases from the fuel storage area are combined with other plant exhausts. Normally, the contribution from the fuel storage area is negligible compared to the other releases and no significant increases are expected as a result of the expanded storage capacity.

## 9.4 Personnel Exposures

At V. C. Summer, the regions in the vicinity of the fuel storage pool are designated Radiation Zone II, which specifies that dose rates be less than 2.5 mrem/hr. For gamma dose rate calculations, the range of fuel exposures stated for the EAB doses (35,000 Mwd/MTU to 70,000 Mwd/MTU) was also utilized. At a given gamma energy, the highest specific inventory (photons/sec/MTU) from any burnup was used in establishing the 18-group gamma source term.

The dose rate from stored fuel, at any location above or around the pool, with the pool filled with fuel cooled only 72 hours, would be extremely low – far less than 0.01 mrem/hr. The dose rate to a person on the crane working platform from a 72-hour-cooled fuel assembly in transit at its maximum elevation (as set by the maximum height of the bridge crane hook), will be 2.0 mrem/hr.

The railroad bay is designated as uncontrolled, or Radiation Zone I, dose rate less than 1.0 mrem/hr. An extremely conservative calculation (again, entire SFP filled with fuel assumed to be cooled only 72 hours, a case that is obviously impossible) shows that the combined dose rate from stored fuel plus fuel in transit will be less than the 1.0 mrem/hr limit. For this assessment, fourteen locations were taken as dose rate points in the railroad bay region.

Calculations were performed to determine if old fuel or no fuel would have to be placed in rack locations nearest the gate slot to the transfer canal to limit the dose rate to a person on the crane work platform, with the transfer canal empty. The area is designated Radiation Zone II, dose rate less than 2.5 mrem/hr. The calculations show that old fuel or no fuel placed in the five rows of Rack B2 closest to the gate slot will limit the dose rate from 72-hour-cooled fuel in all other positions in the pool to less than 1.12 mrem/hr.

The radionuclide concentrations in the pool water are not expected to increase significantly, for they derive principally from the mixing of primary system water with the pool water and the spalling of crud deposits from the spent fuel assemblies as they are moved in the storage pool during refueling operations. Although the overall capacity of the pool is being increased, the movement of fuel during refueling is independent of storage capacity.

Operating experience has shown that there have been negligible concentrations of airborne radioactivity, and no increases are expected as a result of the expanded storage capacity. Area monitors for airborne activities are available in the immediate vicinity of the spent fuel pool.

No increase in radiation exposure to operating personnel is expected; therefore, neither the current health physics program nor the area monitoring system needs to be modified.

## 9.5 Anticipated Exposure During Re-racking

All of the operations involved in re-racking will utilize detailed procedures prepared with full consideration of ALARA principles. Similar operations have been performed in a number of facilities in the past, and there is every reason to believe that re-racking can be safely and efficiently accomplished at the Virgil C. Summer Nuclear Station, with minimum radiation exposure to personnel.

Total occupational exposure for the re-racking operation is estimated to be between 6 and 12 person-rem, as indicated in Table 9.4. While individual task efforts and exposures may differ from those in Table 9.4, the total is believed to be a reasonable estimate for planning purposes. Divers will be used only if necessary, but the estimated person-rem burden includes a figure for their possible exposure.

The existing radiation protection program at V. C. Summer is adequate for the re-racking operations. Where there is a potential for significant airborne activity, continuous air samplers will be in operation. Personnel will wear protective clothing and, if necessary, respiratory protective equipment. Activities will be governed by a Radiation Work Permit and personnel monitoring equipment will be issued to each individual. As a minimum, this will include thermoluminescent dosimeters and electronic dosimeters. Additional personnel monitoring equipment (i.e., extremity badges or alarming dosimeters) may be utilized as required.

Work, personnel traffic, and the movement of equipment will be monitored and controlled to minimize contamination and to assure that exposures are maintained ALARA.

In re-racking, the existing storage racks will be removed, then washed down in preparation for packaging and shipment. Estimates of the person-rem exposures associated with washdown and readying the old racks for shipment is included in Table 9.4. Shipping containers and procedures will conform to Federal DOT regulations and to the requirements of any state through which the shipment may pass, as set forth by the State DOT office.

Table 9.1 RESULTS OF SAS2H-ORIGEN-S/ARP CALCULATIONS  
 FOR RADIONUCLIDES OF IODINE, KRYPTON, AND XENON  
 AT 72 HOURS COOLING TIME

<u>Radionuclide</u>	<u>Curies per mtU</u>
Kr-85	$1.70 \times 10^4$
Kr-85m	$4.65 \times 10^0$
Kr-88	$2.05 \times 10^{-2}$
I-131	$9.61 \times 10^5$
Xe-131m	$1.78 \times 10^4$
I-132	$9.39 \times 10^5$
I-133	$2.31 \times 10^5$
Xe-133	$1.97 \times 10^6$
Xe-133m	$4.43 \times 10^4$
I-135	$1.19 \times 10^3$
Xe-135	$2.57 \times 10^4$
Xe-135m	$1.94 \times 10^2$

Table 9.2 RADIONUCLIDE PROPERTIES USED IN THE  
FUEL HANDLING ACCIDENT ANALYSIS

<u>RADIONUCLIDE</u>	DOSE CONVERSION, <u>REM/CURIE</u>	<u>E<sub>γ</sub> (MEV)</u>	<u>E<sub>β</sub> (MEV)</u>
Iodine-131	1.48 x 10 <sup>6</sup>	----	----
Iodine-132	5.35 x 10 <sup>4</sup>	----	----
Iodine-133	4.0 x 10 <sup>5</sup>	----	----
Iodine-135	1.24 x 10 <sup>5</sup>	----	----
Krypton-85	----	0.002	0.223
Krypton-85m	----	0.151	0.273
Krypton-88	----	1.744	0.933
Xenon-131m	----	0.003	0.142
Xenon-133	----	0.030	0.115
Xenon-133m	----	0.033	0.185
Xenon-135	----	0.246	0.307
Xenon-135m	----	0.422	0.095

Table 9.3 DATA AND ASSUMPTIONS FOR THE EVALUATION  
OF THE FUEL HANDLING ACCIDENT

Core power level, Mw(t)	2958
Fuel enrichment, wt% U	5.0
Fuel burnup, Mwd/MTU	up to 70,000
Specific power, kw/kgU	45.00
Power peaking factor	1.7
Number of failed rods	314
Release to rod gaps	
Iodine-131, %	12
Other iodines, %	10
Krypton-85, %	30
Xenon-133, %	10
Other Xenons, %	10
Iodine composition, %	
Elemental	99.75
Organic	0.25
Pool decontamination factors	
Elemental iodine	133
Organic iodine	1
Noble gases	1
Filter decontamination factors	
Elemental iodine	20
Organic iodine	20
Noble gases	1
$\chi/Q$ , sec/m <sup>3</sup>	$4.08 \times 10^{-4}$
Breathing rate, m <sup>3</sup> /sec	$3.47 \times 10^{-4}$

Table 9.4 PRELIMINARY ESTIMATES OF PERSON-REM EXPOSURES  
DURING RE-RACKING

<u>Step</u>	<u>Number of Personnel</u>	<u>Hours</u>	<u>Estimated Exposure<sup>(1)</sup></u>
Remove empty racks	5	40	0.5 to 1.0
Wash racks	3	10	0.08 to 0.2
Clean and Vacuum Pool	3	25	0.3 to 0.6
Remove underwater appurtenances	4	5	0.4 to 0.8
Partial installation of new rack modules	5	20	0.25 to 0.5
Move fuel to new racks	2	150	0.8 to 1.5
Remove remaining racks	5	120	1.5 to 3.0
Wash racks	3	30	0.2 to 0.4
Install remaining new rack modules	5	35	0.4 to 0.8
Decon and prepare old racks for shipment	4	80	1.0 to 2.0 <sup>(2)</sup>
Total Exposure, person-rem			6 to 12

<sup>(1)</sup> Assumes minimum dose rate of 2-1/2 mrem/hr (expected) to a maximum of 5 mrem/hr except for pool vacuuming operations, which assume 4 to 8 mrem/hr, and possible diving operations, which assume 20 to 40 mrem/hr.

<sup>(2)</sup> Maximum expected exposure, although details of preparation and packaging of old racks for shipment have not yet been determined.

## 10.0 INSTALLATION

### 10.1 Introduction

The installation phase of Virgil C. Summer Nuclear Station (VCSNS) Spent Fuel Pool (SFP) re-rack project will be executed by Holtec International's Field Services Division. Holtec, serving as the installer, is responsible for performance of specialized services, such as underwater diving and welding operations, as necessary. All installation work at VCSNS is performed in compliance with NUREG-0612 (refer to Section 3.0), Holtec Quality Assurance Procedure 19.2, VCSNS project specific procedures, and applicable VCSNS procedures.

Crane and fuel bridge operators are trained in the operation of overhead cranes per the requirements of ANSI/ASME B30.2, and the plant's specific training program. Consistent with the installer's past practices, a videotape aided training session is presented to the installation team, all of whom are required to successfully complete a written examination prior to the commencement of work. Fuel handling bridge operations are performed by VCSNS personnel, who are trained in accordance with VCSNS procedures.

A temporary crane will be used to remove the existing racks and install the new racks. The crane will be designed using CMAA-70 and the AISC manual, to meet the intent of NUREG 0612 through a defense-in-depth approach, (see Section 3.6).

Two rack lifting devices are required: one for handling and installation of the new racks, and one for removal and handling of the existing racks. These lifting devices are designed to engage and disengage on lift points at the bottom of the racks. The lifting devices comply with the provisions of ANSI N14.6-1978 and NUREG-0612, including compliance with the design stress criteria, load testing at a multiplier of maximum working load, and nondestructive examination of critical welds.

Supplemental slings may also be required for removal of the existing racks. These slings will be selected, inspected, and maintained in accordance with ANSI B30.9-1971.

A surveillance and inspection program shall be maintained as part of the installation of the racks. A set of inspection points, which have been proven to eliminate any incidence of rework or erroneous installation in previous rack projects, is implemented by the installer.

Underwater diving operations are required to remove underwater obstructions and the existing racks, to aid in the rack installation by assisting in the positioning of new rack modules, and to verify installation per design. The VCSNS procedures for control of diving and radiological controls for diving operations are utilized. The VCSNS procedures are supplemented by the safe-practices guidance provided by the diving company. These documents describe the precautions and controls for dive operations and were developed utilizing OSHA Standard 29CFR-1910, Subpart T.

Holtec International developed procedures, to be used in conjunction with the VCSNS procedures, which cover the scope of activities for the rack installation effort. Similar procedures have been utilized and successfully implemented by Holtec on previous rack installation projects. These procedures are written to include ALARA practices and provide requirements to assure equipment, personnel, and plant safety. These procedures are reviewed and approved in accordance with VCSNS administrative procedures prior to use on site. The following is a list of the Holtec procedures, used in addition to the VCSNS procedures to implement the installation phase of the project.

A. Installation/Handling/Removal Procedure:

This procedure provides direction for the disassembly and removal of the 11 existing rack modules and the handling/installation of the 12 new high density modules in the Spent Fuel Pool. This procedure delineates the steps necessary to decontaminate an existing fuel rack, engage the existing rack with the lift frame, and remove the rack from the Spent Fuel Pool. It also provides overall direction for the handling and installation of the new maximum density fuel storage rack modules in the SFP. This procedure delineates the steps necessary to receive the new maximum density racks on site, the proper method for unloading and uprighting the racks, staging the racks prior to installation, and installation of the racks. The procedure provides for the installation of rack bearing pads, adjustment of the rack pedestals and verification of the as-built field configuration to ensure compliance with design documents. For the temporary use of a rack in the Cask Pit, this procedure will provide guidance for rack installation and removal, and final placement in the SFP.

B. Receipt Inspection Procedure:

This procedure delineates the steps necessary to perform a thorough receipt inspection of a new rack module after its arrival on site. The receipt inspection includes dimensional measurements, cleanliness inspection, visual weld examination, and verticality measurements.

C. Cleaning Procedure:

This procedure provides for the cleaning of a new rack module, if required. The modules are to meet the requirements of ANSI N45.2.1, Level B, prior to placement in the SFP. Methods and limitations on cleaning materials to be utilized are provided.

D. Pre- and Post-Installation Drag Test Procedure:

These two procedures stipulate the requirements for performing a functional test on a new rack module prior to and following installation. The procedures provide direction for inserting and withdrawing an insertion gage into designated cell locations, and establishes an acceptance criteria in terms of maximum drag force.

E. ALARA Procedure:

Consistent with Holtec International's ALARA Program, this procedure provides guidance to minimize the total man-rem received during the rack installation project, by accounting for time, distance, and shielding. This procedure will be used in conjunction with the VCSNS ALARA program.

F. Liner Inspection Procedure:

In the event that a visual inspection of any submerged portion of the pool liner is deemed necessary, this procedure describes the method to perform such an inspection using an underwater camera and describes the requirements for documenting any observations.

G. Leak Detection Procedure:

This procedure describes the method to test the pool liner for potential leakage using a vacuum box. This procedure may be applied to any suspect area of the liner.

H. Liner Repair and Underwater Welding Procedure:

In the event of a positive leak test result, underwater welding procedures may be implemented which provide for a weld repair, or placement of a stainless steel repair patch, over the area in question. The procedures contain appropriate qualification records documenting relevant variables, parameters, and

limiting conditions. The weld procedure is qualified in accordance with ASME Section XI , or may be qualified to an alternate code accepted by VCSNS and Holtec International.

## 10.2 Rack Arrangement

The reracking process will require fuel shuffling to empty existing racks prior to their removal. Because of the quantity of spent fuel assemblies stored in the pool, a Region 2 style rack must be temporarily located in the Cask Pit and loaded with fuel during the shuffle process. In the latter stages of the reracking, the fuel in the Cask Pit will be moved into the new racks in the SFP, and the Cask Pit rack will be permanently installed in the SFP.

The final rack arrangement allows for a total of 10 Region 2 style and 2 Region 1 style freestanding Holtec racks in the SFP, which provides a total of 1712 storage locations. A schematic plan view depicting the completed configuration of the SFP is shown in Figure 1.1.1.

## 10.3 Rack Interferences

A survey was conducted to identify any objects which would interfere with rack installation or prevent usage of any storage locations. This section discusses existing pool items that would physically interfere with placing the racks into the SFP, present interferences subsequent to reracking, or were considered during the design of the racks. Level and temperature instruments located on the west end of the SFP may interfere with access to a limited number of storage cells after rack installation has been completed. Other obstructions involve existing pedestal bearing pads that were placed along the SFP floor during a previous fuel storage rack installation and the existing pool cooling system sparger piping.

At the west end of the SFP there are two instrument locations containing pool water level instruments and temperature elements. These items will not obstruct rack removal or installation, since the racks can be shifted horizontally to clear these items. These two instrument sets and supports will interfere with access to the fuel storage locations using the fuel handling machine.

The SFP floor liner is covered at a number of locations with bearing plates that were installed during previous rack installation campaigns. Some of these bearing plates may interfere with the placement of the bearing pads for the new storage racks. The as-built locations of these plates has been compared against the locations for the proposed bearing pads to assess possible interferences. Contingencies, such as shimming or bearing pad thickness variations have been considered in the design to integrate the existing plates into the new design configuration, where possible. The adjustable height capability incorporated into the design of the storage rack pedestals provides for small elevation differences at the tops of the bearing pads produced by shimming beneath the pads to produce a level bearing surface. In cases where the existing plates are small and removal is possible, the plates will be removed to preclude any interference.

Existing sparger piping located along the north and south walls will be modified to allow the new high-density racks to be placed closer to the walls. Currently, this piping enters the pool through the walls beneath the water level, turns downward, and extends to an elevation above the top of the racks. This piping will be modified by truncating at the wall, welding a bolted flange, and replacing the downcomer pipe with a bolted on, removable, flanged elbow and piping assembly that terminates at an appropriate elevation to preclude flow induced vibration from damaging the rack cell walls, and to provide adequate cooling flow to the SFP.

#### 10.4 SFP Cooling and Purification

##### 10.4.1 SFP Cooling

The pool cooling system shall be operated in order to maintain the pool water temperature at an acceptable level. It is anticipated that activities, such as bearing pad elevation measurements and cutting piping, may require the temporary shutdown of the Spent Fuel Pool cooling system.

Prior to any shutdown of the Spent Fuel Pool cooling system, the duration to raise the pool bulk coolant temperature to a selected value of  $\leq 120$  °F will be determined. A temperature of  $\leq 120$  °F is chosen such that cooling may be restored to ensure the pool bulk temperature will not exceed 150 °F.

#### 10.4.2 Purification

A portable vacuum system may be employed to remove extraneous debris, reduce general contamination levels prior to diving operations, and to assist in the restoration of SFP clarity following any installation processes.

#### 10.5 Fuel Shuffling

As new high density racks are installed in the SFP, fuel shuffles will be performed in independent phases in order to transfer irradiated assemblies from existing racks into the new racks. This will be completed in a sequence to allow diver access to the next set of racks while maintaining diver exposure ALARA. Fuel movement operations shall be conducted in accordance with VCSNS procedures.

#### 10.6 Removal and Decontamination of Existing Racks and Associated Structures

There are 11 rack modules in the Spent Fuel Pool, all of which are to be removed. Additionally, portions of the coolant system sparger piping, as well as other miscellaneous items in the fuel pool, which will inhibit installation of new rack modules, will be removed from the pool through the use of a diver and underwater cutting tools. (See Section 10.3.)

Prior to removal of any existing structure from the Spent Fuel Pool, a pressure washer or other acceptable cleaning mechanism shall be employed to reduce general contamination levels and to eliminate to the best extent possible any "hot particles" which may be detected. A stainless steel wire brush, or equivalent abrasive tool may be utilized to supplement the removal of discrete high-source particles. These items shall be removed from the pool under dose rate surveillance and placed in an interim storage location to await processing.

Prior to pressure washing and removal of an existing rack, a quality verification shall be performed in order to ensure that no fuel assemblies remain in the module. The interior of each storage location shall be subjected to pressure washing. Upon completion of pressure washing rack internals, the rack will be removed. After rigging is installed between the rack and the temporary crane, the rack shall be lifted a short distance and held stationary for a procedure-defined duration. The rack will then be moved horizontally to the point in the pool designated for its vertical lift and then lifted vertically.

The existing rack will then be lifted slowly to a point just below the pool water surface to allow for any additional pressure washing of the exteriors. Upon completion of pressure washing, the rack shall be removed from the fuel pool under Health Physics dose rate surveillance. The components shall remain over the pool until all significant dripping has abated. The rack shall then be transported along the safe load path to a designated location for any needed wrapping or placement into anti-contamination bags. An appropriate shipping container will arrive on site to remove the existing rack for eventual processing.

#### 10.7 Installation of New Racks

Installation of the new high density racks, supplied by Holtec International, involves the following activities. The racks are delivered in the horizontal position. A new rack module is removed from the shipping trailer using a suitably rated crane, while maintaining the horizontal configuration. The rack is placed on the up-ender and secured. Using two independent overhead hooks, or a single overhead hook and a spreader beam, the module is up-righted into a vertical position.

The new rack lifting device is engaged in the lift points at the bottom of the rack. The rack is then transported to a pre-leveled surface where, after leveling the rack, the appropriate quality control receipt inspection is performed. (See 10.1B & D.)

The SFP floor is inspected and any debris, which may inhibit the installation of bearing pads, is removed. New rack bearing pads are positioned on the floor before the module is lowered into the pool. The new rack module is lifted with the temporary crane and transported along the pre-established safe load path. The rack module is carefully lowered into the SFP.

Elevation readings are taken to confirm that the module is level. In addition, rack-to-rack and rack-to-wall off-set distances are also measured. Adjustments are made as necessary to ensure compliance with design documents. The lifting device is then disengaged and removed from the SFP under Health Physics direction. As directed by procedure, post-installation free path verification is performed using an inspection gage.

## 10.8 Safety, Health Physics, and ALARA Methods

### 10.8.1 Safety

During the installation phase of the SFP re-rack project, personnel safety is of paramount importance, outweighing all other concerns. All work shall be carried out in compliance with applicable approved procedures.

### 10.8.2 Health Physics

Health Physics is carried out per the requirements of the VCSNS Radiation Protection Program.

### 10.8.3 ALARA

The key factors in maintaining project dose As Low As Reasonably Achievable (ALARA) are time, distance, and shielding. These factors are addressed by utilizing many mechanisms with respect to project planning and execution.

## Time

Each member of the project team is trained and provided appropriate education and understanding of critical evolutions. Additionally, daily pre-job briefings are employed to acquaint each team member with the scope of work to be performed and the proper means of executing such tasks. Such pre-planning devices reduce worker time within the radiological controlled area and, therefore, project dose.

## Distance

Remote tooling such as lift fixtures, pneumatic grippers, a support leveling device and a lift rod disengagement device have been developed to execute numerous activities from the SFP surface, where dose rates are relatively low. For those evolutions requiring diving operations, diver movements shall be restricted by an umbilical, which will assist in maintaining a safe distance from irradiated sources. Additional restricting devices may be used as determined necessary by VCSNS. By maximizing the distance between radioactive sources and project personnel, project dose is reduced. Fuel will be shuffled as necessary to ensure safe distances are maintained to satisfy ALARA principles.

## Shielding

During the course of the re-rack project, primary shielding is provided by the water in the Spent Fuel Pool. The amount of water between an individual at the surface (or a diver in the pool) and an irradiated fuel assembly is an essential shield that reduces dose. Additionally, other shielding, may be employed to mitigate dose when work is performed around high dose rate sources. If necessary, additional shielding may be utilized to meet ALARA principles.

### 10.9 Radwaste Material Control

Radioactive waste generated from the rack installation will be controlled in accordance with established VCSNS procedures.

## 11.0 ENVIRONMENTAL COST / BENEFIT ASSESSMENT

### 11.1 Introduction

Article V of the USNRC OT Position Paper [11.1] requires the submittal of a cost/benefit analysis for a fuel storage capacity enhancement. This section provides justification for selecting replacement of the racks in the V.C. Summer Nuclear Station (VCSNS) Spent Fuel Pool (SFP) as the most viable alternative.

### 11.2 Imperative for SFP Rack Replacement

The specific need to increase the limited existing storage capacity of the VCSNS Spent Fuel Pool is based on the continually increasing inventory in the pool, the prudent requirement to maintain full-core offload capability, and a lack of viable economic alternatives.

Based on the current number of stored assemblies and estimated discharge rates, the VCSNS SFP is projected to lose the capacity to discharge one full core following Cycle 17 in the Spring of 2008. The projected loss of storage capacity in the pool would affect the owner's ability to operate the reactor. The owner does not have an existing or planned contractual arrangement for third party fuel storage or fuel reprocessing.

### 11.3 Appraisal of Alternative Options

Adding fuel storage space to the VCSNS SFP is the most viable option for increasing spent fuel storage capacity.

The key considerations in evaluating the alternative options included:

- Safety: Minimize the risk to the public.
- Economy: Minimize capital and O&M expenditures.
- Security: Protection from potential saboteurs, natural phenomena.

- Non-intrusiveness: Minimize required modifications to existing plant systems.
- Maturity: Extent of industry experience with the technology.
- ALARA: Minimize cumulative dose.
- Schedule: Minimize time to implement a plan which will maintain full-core offload capability for the distant future.
- Risk Management: Maximize probability of completing the expansion to support fuel storage needs.

### Rod Consolidation

Rod consolidation has been shown to be a potentially feasible technology. Rod consolidation involves disassembly of one and the disposal of the fuel assembly skeleton outside of the pool (this is considered a 2:1 compaction ratio). The rods are stored in a stainless steel can that has the outer dimensions of a fuel assembly. The can is stored in the spent fuel racks. The top of the can has an end fixture that matches up with the spent fuel handling tool. This permits moving the cans in an easy fashion.

Rod consolidation pilot project campaigns in the past have consisted of underwater tooling that is manipulated by an overhead crane and operated by a maintenance worker. This is a very slow and repetitive process.

The industry experience with rod consolidation has been mixed thus far. The principal advantages of this technology are: the ability to modularize, compatibility with DOE waste management system, moderate cost, no need of additional land and no additional required surveillance. The disadvantages are: potential gap activity release due to rod breakage, potential for increased fuel cladding corrosion due to some of the protective oxide layer being scraped off, potential interference of the (prolonged) consolidation activity which might interfere with ongoing plant operation, and lack of sufficient industry experience. The drawbacks associated with consolidation are expected to diminish in time. However, it is the SCE&G's view that rod consolidation technology has not matured sufficiently to make this a viable option for the present VCSNS SFP limitations.

## On-Site Dry Cask Storage

Dry cask storage is a method of storing spent nuclear fuel in a high capacity container. The cask provides radiation shielding and passive heat dissipation. Typical capacities for PWR fuel range from 21 to 37 assemblies that have been removed from the reactor for at least five years. The casks, once loaded, are then stored outdoors on a seismically qualified concrete pad.

The casks, as presently licensed, are limited to 20-year storage service life. Once the 20 years has expired the cask manufacturer or the utility must recertify the cask or the utility must remove the spent fuel from the container. In the interim, the U.S. DOE has embraced the concept of multi-purpose canisters obsolescing all existing licensed cask designs. Work is also continuing by several companies, including Holtec International, to provide an MPC system that will be capable of long storage, transport, and final disposal in a repository. Holtec International's HI-STAR System which can store up to 24 PWR assemblies is illustrated in Figure 11.1. It is noted that a cask system makes substantial demands on the resources of a plant. For example, the plant must provide for a decontamination facility where the outgoing cask can be decontaminated for release.

There are several plant modifications required to support cask use. Tap-ins must be made to the gaseous waste system and chilled water to support vacuum drying of the spent fuel and piping must be installed to return cask water back to the Spent Fuel Pool/Cask Loading Pit. A seismic concrete pad must be made to store the loaded casks. This pad must have a security fence, surveillance protection, a diesel generator for emergency power and video surveillance for the duration of fuel storage, which may extend beyond the life of the adjacent plant. Finally, the cask park must have facilities to vacuum dry the cask, backfill it with helium, make leak checks, remachine the gasket surfaces if leaks persist, and assemble the cask on-site.

## Other Storage Options

Other options such as Modular Vault Dry Storage and a new Fuel Storage Pool are overly expensive as compared to placing new racks in the SFP. Due to the complexity of implementation, these options could not meet the required schedule for maintaining full-core offload capability.

### 11.3.1 Alternative Option Summary

An estimate of relative costs in 2001 dollars for the aforementioned options is provided in the following:

SFP Rack Expansion:	\$6-8 million
Horizontal Silo:	\$35-45 million
Rod consolidation:	\$25 million
Metal cask (MPC):	\$68-100 million
Modular vault:	\$56 million
New fuel pool:	\$150 million

The above estimates are consistent with estimates by EPRI and others [11.2, 11.3].

To summarize, based on the required short time schedule, the status of the dry spent fuel storage industry, and the storage expansion costs, the most acceptable alternative for increasing the on-site spent fuel storage capacity at VCSNS is expansion of the wet storage capacity. First, there are no commercial independent spent fuel storage facilities operating in the United States. Second, the adoption of the Nuclear Waste Policy Act (NWPA) created a de facto throw-away nuclear fuel cycle. Since the cost of spent fuel reprocessing is not offset by the salvage value of the residual uranium, reprocessing represents an added cost for the nuclear fuel cycle which already includes the NWPA Nuclear Waste Fund fees. In any event, there are no domestic reprocessing facilities. Third, at over \$½ million per day replacement power cost, shutting down VCSNS is many times more expensive than addition of high density racks to the existing SFP.

#### 11.4 Cost Estimate

The plant modification proposed for the VCSNS fuel storage expansion utilizes freestanding, high density, poisoned spent fuel racks in the SFP. The engineering and design is completed for full re-racking of the SFP.

The total capital cost is estimated to be approximately \$8 million as detailed below.

Engineering, design, project management:	\$½ million
Rack fabrication:	\$6 million
Rack installation:	\$1 ½ million

As described in the preceding section, other fuel storage expansion technologies were evaluated prior to deciding on the use of SFP racks. Storage rack capacity expansion provides a cost advantage over other technologies.

#### 11.5 Resource Commitment

The expansion of the VCSNS spent fuel storage capacity via replacement of the racks in the SFP is expected to require the following primary resources:

Stainless steel:	120 tons
Boral neutron absorber:	12 tons, of which 7 tons is Boron Carbide powder and 5 tons are aluminum.

The requirements for stainless steel and aluminum represent a small fraction of total world output of these metals (less than 0.001%). Although the fraction of world production of Boron Carbide required for the fabrication is somewhat higher than that of stainless steel or aluminum, it is unlikely that the commitment of Boron Carbide to this project will affect other alternatives. Experience has shown that the production of Boron Carbide is highly variable, depends upon need, and can easily be expanded to accommodate worldwide needs.

## 11.6 Environmental Considerations

The proposed reracking results in an additional heat load burden to the Spent Fuel Pool Cooling and Cleanup System due to increased spent fuel pool inventory, as discussed in Section 5.0. The maximum bulk pool temperature is conservatively predicted to be limited to 170 F. The peak heat load from the spent fuel pool is less than 41 million Btu/hr, which is a minuscule fraction of the total operating plant heat loss to the environment and is well within the capability of the plant cooling system. Consequently, the short duration of increased heat loading during an outage is not expected to have any significant impact on the environment.

The increased peak bulk pool temperature results in a slightly higher increased pool water evaporation rate for a short period of time. This increase is within the Fuel Handling Building HVAC system capacity and does not necessitate any hardware modifications for the HVAC system. Therefore, the environmental impact resulting from the increased heat loss and water vapor generation at the pool surface is negligible.

References

- [11.1] OT Position Paper for Review and Acceptance of Spent Fuel Storage and Handling Applications, USNRC (April 1978).
- [11.2] Electric Power Research Institute, Report No. NF-3580, May 1984.
- [11.3] "Spent Fuel Storage Options: A Critical Appraisal", Power Generation Technology, Sterling Publishers, pp. 137-140, U.K. (November 1990).

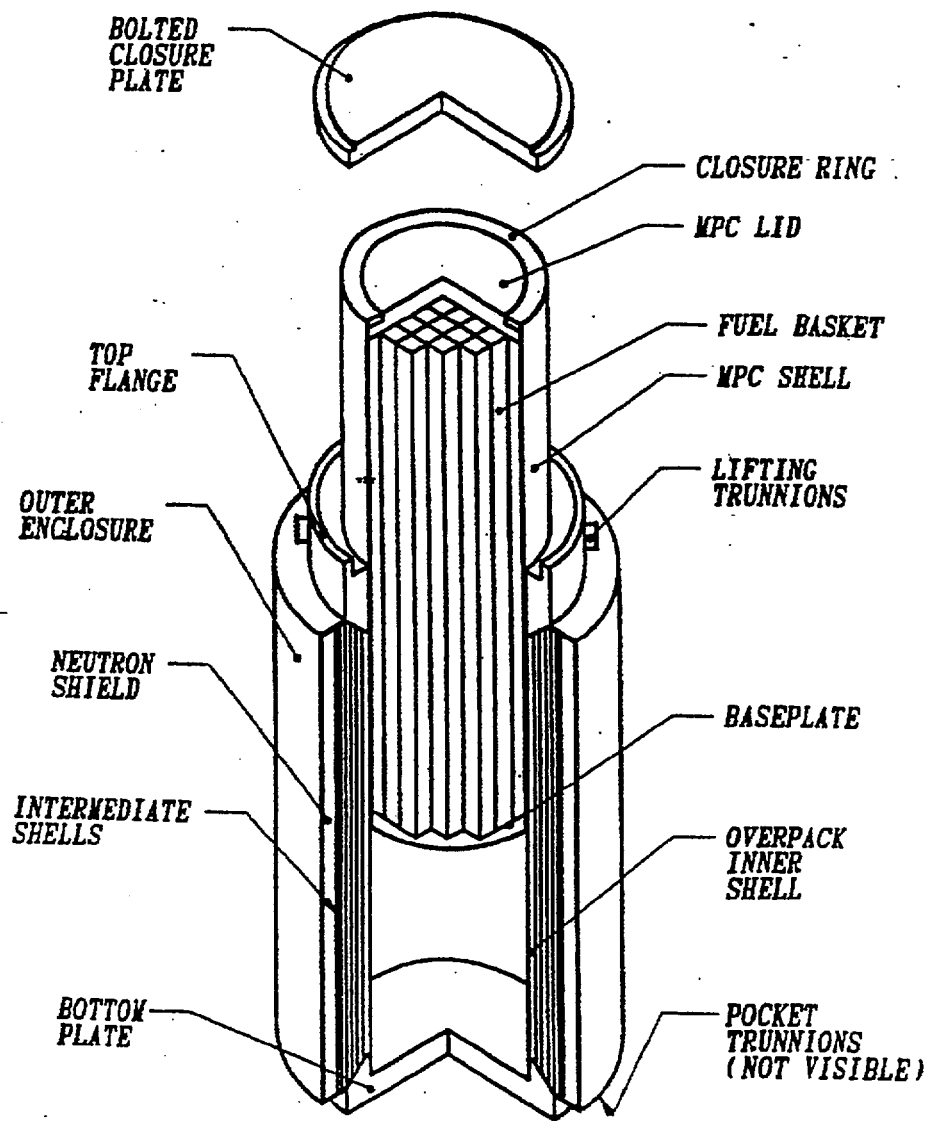


FIGURE 11.1 ; HI-STAR 100 OVERPACK WITH MPC PARTIALLY INSERTED